Characterising the Expression and Transcriptional Regulation of *Peroxidasin* and *Peroxidasin-like* in the Lung During a Cytokine Storm

by

Jamie Fernandez

(1833370)

Dissertation

Submitted in fulfilment of the requirements of the degree

Master of Science

in

Molecular and Cell Biology

in the Faculty of Science, University of the Witwatersrand, Johannesburg, South Africa

Supervisor: Professor Demetra Mavri-Damelin

May 2025

Declaration

I, Jamie Fernandez (1833370), am a student registered for the degree of Master of Science (Dissertation) in the academic year 2024.

I hereby declare the following:

• I am aware that plagiarism (the use of someone else‘s work without their permission and/or without acknowledging the original source) is wrong.

• I confirm that the work submitted for assessment for the above degree is my own unaided work except where explicitly indicated otherwise and acknowledged.

• I have not submitted this work before for any other degree or examination at this or any other University.

• The information used in the thesis has not been obtained by me while employed by, working under the aegis of, any person or organisation other than the University.

• I have followed the required conventions in referencing the thoughts and ideas of others.

• I understand that the University of the Witwatersrand may take disciplinary action against me if there is a belief that this is not my own unaided work or that I have failed to acknowledge the source of the ideas or words in my writing.

Signed  Date: 16/05/2025

Abstract

Peroxidasin (PXDN) and Peroxidasin-like (PXDNL) proteins have recently been shown to have emerging roles in vascular disease. PXDN is secreted into the extracellular matrix (ECM) where it catalyses collagen IV crosslinking and PXDNL is thought to antagonise the function of PXDN. PXDN is predominantly expressed in the cardiovascular system, lung and smooth muscle, while PXDNL expression is found in heart muscle. As these expression patterns correlate with human tissues most affected during SARS-CoV-2 infection, this study aimed to investigate gene expression changes of PXDN and PXDNL under conditions that mimic inflammatory responses. Immunofluorescences microscopy and western botting showed that PXDN and PXDNL expression patterns are altered in response to cytokines (TNF-α, IL-1β, IFN-γ and IL-6) by treating A549 cells with 25 ng/ml of each cytokine for 24 hours, with notable increases in expression in response to IFN-γ and IL-6. Further analysis by chromatin immunoprecipitation (ChIP)-PCR indicated that transcriptional regulation of *PXDN* in the presence of IL-6 and IFN-γ is controlled, at least in part, by STAT3 and by NF-κB in presence of IFN-γ. *PXDNL* is regulated by STAT3 in response to IL-6. These findings indicate that PXDN and PXDNL may be involved in inflammation, and we identified a novel pathway of their transcriptional regulation.

For my father who inspires me

Acknowledgements

The journey of completing this dissertation has been exciting, challenging and empowering. I have learned a lot about myself through this period but more so about the importance of surrounding myself with people whose love and support uplifted me and keep me moving forward.

Firstly, I would like to express my utmost gratitude to my supervisor, Professor Demetra Mavri-Damelin for giving me the opportunity to take on this project that she conceptualised. Her guidance, encouragement and patience was a blessing throughout the duration of this project and I am extremely appreciative for chance to learn from her.

I would like to give thanks to those who helped make this project happen. I thank Dr Tyrone Otgaar for gifting me A549 cells. I thank Dr Aurelie Deroubaix for her assistance in optimising my immunofluorescence microscopy protocol and Dr Deran Reddy for his assistance and training with the Olympus BX63 microscope at the Microscopy and Microanalysis Unit. I am very grateful to the South African Medical Research Council and the Postgraduate Merit Award from the University of the Witwatersrand for funding this research.

One of the greatest outcomes of this degree has been the friendship and bonds formed with my lab mates and I would not have made it this far without their love and encouragement. Thokozile Makhanya and Jemma Falkov taught me the techniques and skills needed for this project with such encouragement and patience and words cannot describe how appreciative I am for their guidance and support. Mistral Sebastian was my rock throughout this journey and I am eternally grateful for her bring so much joy and love into the lab. From late nights in the lab together, to trips to Kara Niches, to making a meme wall together, the memories I've made with her will always be cherished. A huge thank you to my friends in MCB for their support over the years.

I would like to express my gratitude to my colleagues at BioCertica. Balancing work and studies was challenge but their support and patience made this possible. I am so thankful to Gert van Wyk and Arno Smit for the opportunity to work and grow at the company they built and to Dr Edin Hamzic for his guidance in navigating the science world outside of academia.

To my friends who have so lovingly stood at my side through this journey, always offering words of encouragement, a shoulder to cry on and a reason to laugh, I am forever grateful to have them in my life. I am utterly thankful for the grounding and balance of being able to dance

with Hybrid Performing Arts and for the incredible people who inspire me this has bought into my life. I am eternally grateful to John Slabber and Aj van Deemter for empowering me through their unwavering support and believe in my abilities and for all the love and joy they bring into my life.

Lastly, I would not be where I am today if not for the incredible love and support of my family and words cannot describe how grateful I am to them. My father who has worked so hard to give me the opportunity to reach my dreams, my mother who has always believed in me, my sister who has encouraged me so much and fur babies for constant companionship throughout this journey. I am an amalgamation of the greatest people in my life who have built me into the person I am today and I will forever be eternally grateful to them all.

Table of Content

List of Figures

List of Tables

List of Symbols

pg	Picogram
ng	Nanogram
µg	Microgram
mg	Milligram
L	Litre
µl	Microlitre
ml	Millilitre
M	Molar
mM	Millimolar
mm	Millimetre
nm	Nanometre
rpm	Revolutions per minute
℃	Degrees Celsius
kDa	Kilodaltons
A	Amperes
mA	Milliamperes
V	Volts
w/v	Weight per volume
v/v	Volume per volume
xg	Relative centrifugal force

List of Abbreviations

ACE2	Angiotensin-converting enzyme 2
ANOVA	Analysis of variance
ARDS	Acute respiratory distress syndrome
ApoE	Apolipoprotein E
APS	Ammonium persulfate
ASD	Anterior segment dysgenesis
bp	Base pairs
BSA	Bovine serum albumin
CAC	COVID-19-associated coagulopathy
ChIP	Chromatin Immunoprecipitation
CO_2	Carbon dioxide
COVID-19	Coronavirus disease 19
DAPI	4′,6-Diamidino-2-phenylindole
DIC	Disseminated intravascular coagulation
DMEM	Dulbecco's Modified Eagle's Medium
DMSO	Dimethyl sulfoxide
ECM	Extracellular matrix
ECO	Extracellular signal-regulated kinases
EDTA	Ethylenediamineterraacetic acid
EPO	Eosinophil peroxidase
ER	Endoplasmic reticulum
ERGIC	ER-to-Golgi intermediate compartment
ERK1/2	Extracellular signal-regulated protein kinases 1 and 2
ERKs	Extracellular signal-regulated kinases
FAK	Focal adhesion kinase
FBS	Foetal Bovine Serum
FITC	Fluorescein isothiocyanate
GAPDH	Glyceraldehyde-3-phosphate dehydrogenase

gDNA	Genomic DNA
GM-CSF	Granulocyte macrophage-colony stimulating factor
H_2O_2	Hydrogen peroxide
HCl	Hydrochloric acid
HEPES	N-2-hydroxyethylpiperazine-N-2-ethane sulfonic acid
HRP	Horseradish peroxidase
ICAM-1	Intercellular adhesion molecule-1
IFN	Interferon
IgG	Immunoglobulin
IL	Interleukin
IP-10	IFN-γ-inducible protein 10
IRF3	Interferon regulatory factor 3
JAK	Janus kinase
LDL	Low-density lipoprotein
LPO	Lactoperoxidase
Lys	Lysine
MAPKs	Mitogen-activated protein kinases
MCP-1	Monocyte chemoattractant protein-1
MDA5	Melanoma differentiation-associated gene 5
Met	Methionine
MPO	Myeloperoxidase
MTT	3-(4,5-Dimethylthiazol-2-yl)-2,5-Diphenyltetrazolium Bromide
NADPH	Nicotinamide adenine dinucleotide phosphate
NaOH	Sodium hydroxide
NF-κB	Nuclear factor-κB
NLRP3	NACHT-, LRR-, and pyrin domain-containing protein 3
Nox	NADPH oxidase
Nrf2	Nuclear factor erythroid 2-related factor 2
PAMPs	Pathogen associated molecular patterns
PASMCs	Pulmonary artery smooth muscle cells

PBS	Phosphate buffered saline
PCR	Polymerase chain reaction
PMSF	Phenylmethylsulfonyl fluoride
PRRs	Pattern recognition receptors
PVDF	Polyvinylidene fluoride
PXDN	Peroxidasin
PXDNL	Peroxidasin-like
qPCR	Quantitative polymerase chain reaction
RIG-1	Retinoic-acid inducible gene I
RIPA	Radioimmunoprecipitation assay
ROS	Reactive oxygen species
SARS-CoV-2	Severe acute respiratory syndrome coronavirus 2
STAT	Signal transducers and activators of transcription
TAE	Tris-acetate-EDTA
TCA	Trichloroacetic acid
TLR	Toll-like receptor
TEMED	Tetramethylethylenediamine
TGF	Transforming growth factor
TNF	Tumour necrosis factor
TNFR1	TNF type 1 receptors
TNFR2	TNF type 2 receptors
TPO	Thyroid peroxidase
TSS	Transcriptional start site
VPO1	Vascular peroxidase-1
vWf	von Willebrand factor
WHO	World Health Organisation

1. Introduction

1.1. Coronavirus Overview

The December of 2019 saw the first cases of the novel coronavirus, severe acute respiratory syndrome coronavirus 2 (SARS-CoV-2) isolated from patients with pneumonia in Wuhan City, Hubei Province, China (Zhu et al. 2020). As the virus began to spread, the World Health Organisation (WHO) termed the resulting disease coronavirus disease 19 (COVID-19) and declared a pandemic in March 2020 (Cascella et al. 2023). As of May 2023, there have been approximately 687 million reported cases of COVID-19 resulting in almost 6.87 million deaths and the United States and India were most severely affected by the pandemic. In South Africa, just over four million cases of COVID-19 were reported resulting in 102 500 deaths in this time period (www.statista.com).

The coronaviruses belong to the Coronaviridae family of viruses and was named after the Latin term for crown, *corona* because of the appearance given by the spike glycoproteins on the virus envelope, which resembles a crown structure when viewed with an electron microscope. These positive-sense single stranded RNA viruses are common in animals such as bats, camels, horses and avian species but have evolved to cross the animal-human barrier (Sharma, Ahmad Farouk, and Lal 2021). Studies have indicated that the zoonotic transmission of the SARS-CoV-2 virus likely came from bats as a 96.2% similarity of genome sequence was seen between the virus and the SARS-like bat coronavirus, RaTG13 (Andersen et al. 2020). Human-to-human transmission of the SARS-CoV-2 virus is predominantly spread via aerosols, which led to rapid global spread of the virus and outbreaks of several mutant variants such as the Beta and Omicron variants that were first reported in South Africa (Cascella et al. 2023; Sharma, Ahmad Farouk, and Lal 2021).

1.2. Immunopathogenesis in COVID-19

1.2.1. Viral life cycle

The SARS-CoV-2 virus must infect mammalian cell to utilise the cellular machinery to replicate itself. The SARS-CoV-2 virus enters the host cell through the binding of its viral spike glycoprotein with the host's receptor protein angiotensin-converting enzyme 2 (ACE2). Once in the cytoplasm the viral RNA is uncoated (**Figure 1.1**), the viral polymerase is translated from this RNA for replication and transcription of the viral RNA genome. Following the translation of the viral structure proteins, spike proteins, membrane proteins and envelope proteins which localise to the membrane of the endoplasmic reticulum (ER) and transits

through the ER-to-Golgi intermediate compartment (ERGIC). In the cytoplasm, the viral envelope encapsulates the nucleocapsid and viral RNA for virion formation. The newly replicated viral RNA is packaged with nucleocapsid proteins where it is encapsulated with viral structural proteins leading the formation of virions. These virions are then secreted from the cell via exocytosis and is able to infect other cells, increasing the viral load (De Wit et al. 2016). Due to this mechanism of entry, the SARS-CoV-2 virus targets cells that express ACE2, specifically type II pneumocytes in the lungs. Therefore, COVID-19 predominantly affects the respiratory system but can also affect other organs such as the heart, intestine, endothelium and kidney can express ACE2 (Bordallo *et al.*, 2020; Liu *et al.*, 2021). After initial infection, it takes approximately three days before the virus replicates enough for someone to become infectious (Bar-On et al. 2020). In response to viral infection, the innate immune response is activated.

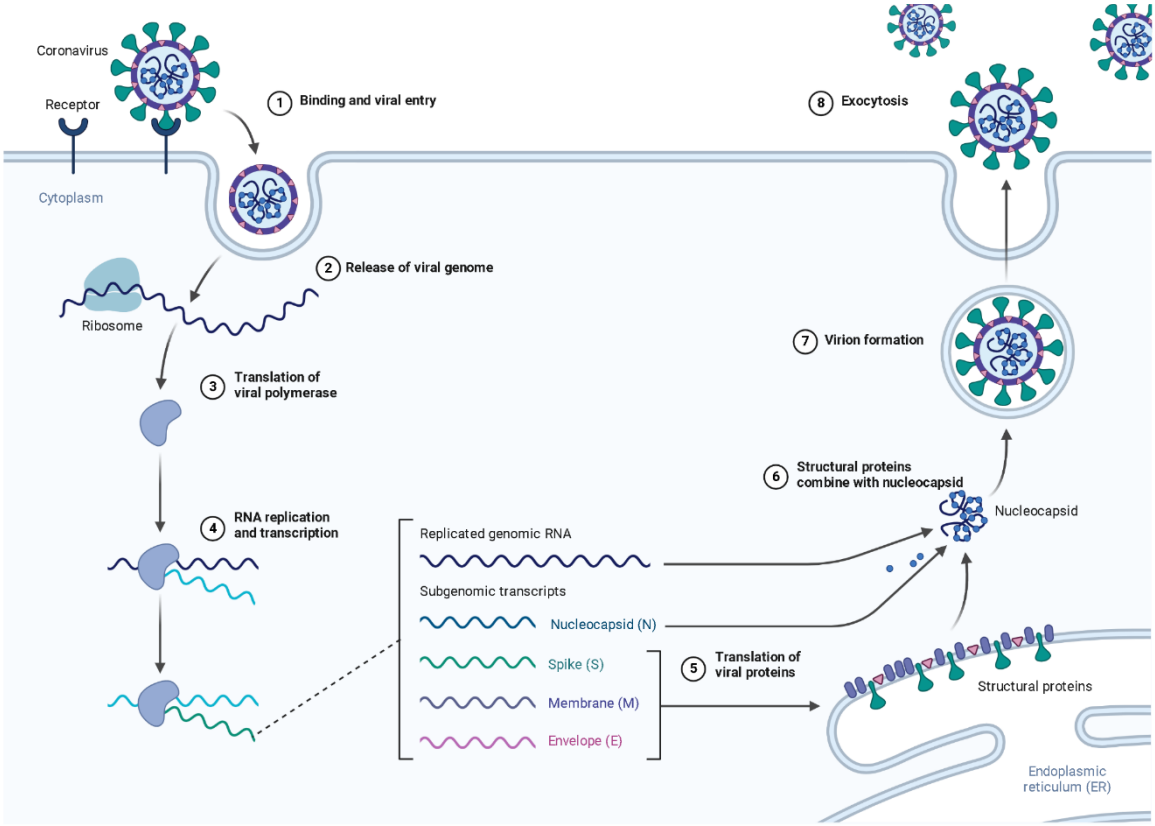

Figure 1.1: Replication cycle of the SARS-CoV-2 virus. *A simplified representation of the coronavirus life cycle showing entry into the cell via the viral spike protein to the ACE2 surface receptor. Upon release of the viral genome, the viral polymerase is translated and utilised for the RNA replication and transcribed of the viral genome. These viral proteins d translated and locate to the membrane of the endoplasmic reticulum before viral assembly with the nucleocapsid. Thereafter, the virus is released from the cell. (Adapted from Guo et al., 2020 and created in BioRender).*

1.2.2. Immune response in COVID-19

The innate immune system is first mechanism for a host to defend against invading pathogens. This is a rapid, non-specific immune reaction that occurs within the first few hours of pathogen entry to minimise the onset of infection by eliminating the invading pathogens quickly before they can multiply further. Cells of the innate immune system such as macrophages, neutrophils, monocytes and natural killer cells are recruited to the site of infection where they produce chemokines and cytokines which trigger signalling cascades (Marshall et al. 2018). Another function of the innate immune system is to stimulate the adaptive immune response, the specific immune response that occurs over days and weeks to target pathogens with more precision (Sapir et al. 2022).

In the early stages of SARS-CoV-2 infection, the innate immune system is crucial for preventing the spread of the virus and minimising the viral load. Innate immune cells such as dendritic cells and macrophages have pattern recognition receptors (PRRs) which bind to distinct molecular structures of invading microbes known as pathogen associated molecular patterns (PAMPs). Subsequently, this binding triggers a pro-inflammatory response by inciting cytokine and chemokine production and intracellular signalling pathways for gene expression (Mogensen 2009). During infection with SARS-CoV-2, toll-like receptor (TLR)-7, melanoma differentiation-associated gene 5 (MDA5) and retinoic-acid inducible gene I (RIG-I) recognise viral RNA and the resulting cascade leads to the activation of the transcription factor pathways of nuclear factor-κB (NF-κB) and interferon regulatory factor (IRF) 3 and 7. These transcriptional pathways lead to the production of pro-inflammatory cytokines for the mediation of further immune response (Y. R. Guo et al. 2020). An adequate and early incitation of this innate immune response contributes to clearing the SARS-CoV-2 virus and as such, could result in patients that are asymptomatic or experience milder symptoms of COVID-19. However, dysregulation of this immune response leads to a the more severe case of COVID-19 that is likely to be deemed as life-threatening (Purbey et al. 2023).

1.2.3. Clinical manifestations of COVID-19

The clinical presentation of COVID-19 has a spectrum of severity from asymptomatic to critical illness. Approximately 18 to 33% of infected patients do not experience any symptoms while most symptomatic patients experience fever, fatigue, myalgia, cough, sore throat, runny nose, and sneezing which are symptoms associated with mild to moderate illness (Cascella et al. 2023). On the other end of the spectrum, severe COVID-19 illness is typically characterised

by oxygen saturation levels below 94% that becomes critical with septic shock, encephalopathy, heart failure, and acute kidney injury, acute respiratory failure and multiple organ dysfunction. Another characteristic marker of critical COVID-19 is acute respiratory distress syndrome (ARDS), a severe onset of respiratory failure and increased risk of mortality. Patients may be more likely to develop more severe COVID-19 if they have comorbidities such as obesity, cardiovascular disease, neoplastic conditions, diabetes mellitus, liver disease, lung disease and kidney disease (Cascella *et al.*, 2023; Yuki, Fujiogi and Koutsogiannaki, 2020). Other indicators for severe COVID-19 are prognostic biomarkers for cytokine storm development include age over 40 years old, male gender, absolute lymphocyte count less than 0.72 $x10^9$/L and elevated plasma interleukin (IL)-6 concentration (greater than 23 pg/ml) (Shcherbak et al. 2021). The ability of the innate immune system to clear the viral load in earlier stages of infection will minimise the duration of the inflammatory response and subsequently results in less severe disease (**Figure 1.2**). An initially low inflammatory response allows the viral load to persist for a longer time which leads to a more extreme inflammatory response. Severe COVID-19 is associated with a dysregulation of the immune system.

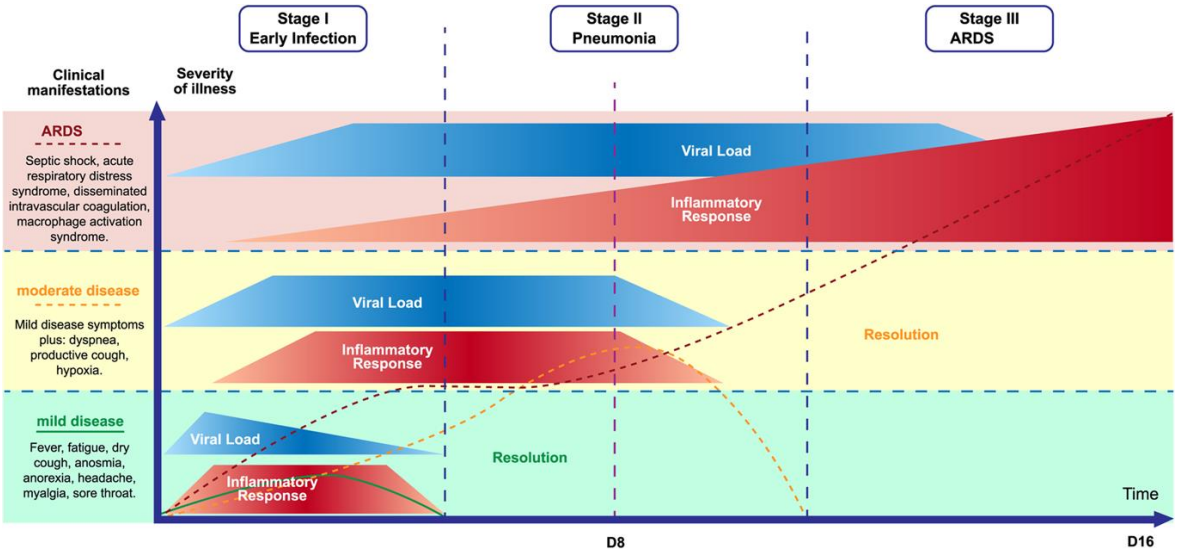

Figure 1.2: Severity levels of COVID-19 illness and timeline of stages. *In mild disease, viral load is cleared quickly and the inflammation response resolves within a few days. In moderate disease, the viral load persists for approximately 8 days and the inflammatory response is proportional. In severe disease, viral load persist past 10 days which causes the inflammatory response increases gradually until reaching the acute respiratory distress syndrome (ARDS) stage where the response is much greater than that of mild and moderate disease cases (Adapted from Bordallo et al., 2020).*

1.3. Cytokine storm

Severe COVID-19 is caused by a dysregulation of the immune system reaction and extreme inflammatory response. This is known as the cytokine storm and is the over production of pro-inflammatory cytokines such as interleukin IL-1β, IL-2, IL-6, interferon (IFN)-γ, monocyte chemoattractant protein-1 (MCP-1), granulocyte macrophage-colony stimulating factor (GM-CSF), tumour necrosis factor (TNF)-α and IFN-γ-inducible protein 10 (IP-10) that leads to an uncontrolled multisystem response (Zanza *et al.*, 2022). Immune cells such as macrophages, neutrophils, natural killer cells and T-lymphocytes produce these cytokines, which go on to trigger the over activation of downstream intracellular signalling cascades including inflammatory-associated transcription factors such as mitogen-associated protein kinases (MAPKs), NF-kB, p38 and extracellular signal-regulated kinases (ERKs). This results in the alteration of gene expression and cell behaviour modification that affects multiple organs that express ACE2 receptors, particularly the lungs that are especially affected in the case of severe COVID-19 (Montazersaheb *et al.*, 2022; Zhang and An, 2007). In clinical studies, it was observed that an inadequate immune response during the initial infection with the virus was likely to lead to a cytokine storm. In such cases, interferons are not produced at the early stage of infection resulting in the inability to clear the infection and allowing for the virus to replicate and accumulate. After some time, the immune system seems to over-correct and so produces a more exaggerated response, hence the cytokine storm (Zanza *et al.*, 2022).

The production of the cytokine storm subsequently leads to multiple clinical manifestations (**Figure 1.3**). Acute lung injury caused by the cytokine storm has pathological effects such as hyaline membrane formation, thrombus formation and diffuse alveolar damage which are characteristic of ARDS and respiratory epithelium damage (Montazersaheb et al. 2022). Other organs that are damaged by cytokine storms include the kidney, liver and brain (Joseph *et al.*, 2020; Li and Fan, 2020; Montazersaheb *et al.*, 2022). Moreover, elevated cytokine levels are associated with the breakdown of vascular endothelium which results in increased blood vessel permeability and subsequent fluid and protein leakage into surrounding tissue. This is known as capillary leak syndrome and contributes to patients developing oedema, hypotension and ARDS. Cytokines are also known to interact with the coagulation system and therefore cytokine storms can cause disseminated intravascular coagulation (DIC), a condition characterised by widespread clotting in small blood vessels which limits blood flow and thus causes tissue ischemia and damage (Mangalmurti and Hunter 2020).

As cytokine storms account for many of the life-threatening complications associated with COVID-19, targeting the reaction and inhibiting this phenomenon is a vital part of treating severe COVID-19. These treatments include anti-inflammatory and immunosuppressive agents such as glucocorticoids which were the standard of care when treating patients during the pandemic. While colchicine, hydroxychloroquine and chloroquine were used to treat COVID-19 patients, subsequent studies on these therapeutic agents have proven to have little to no impact in treating the condition and thus they are no longer recommended. Additionally, cytokine inhibitors, antioxidants and blood purification therapies were also investigated as therapeutic treatments for COVID-19 (Zanza *et al.*, 2022).

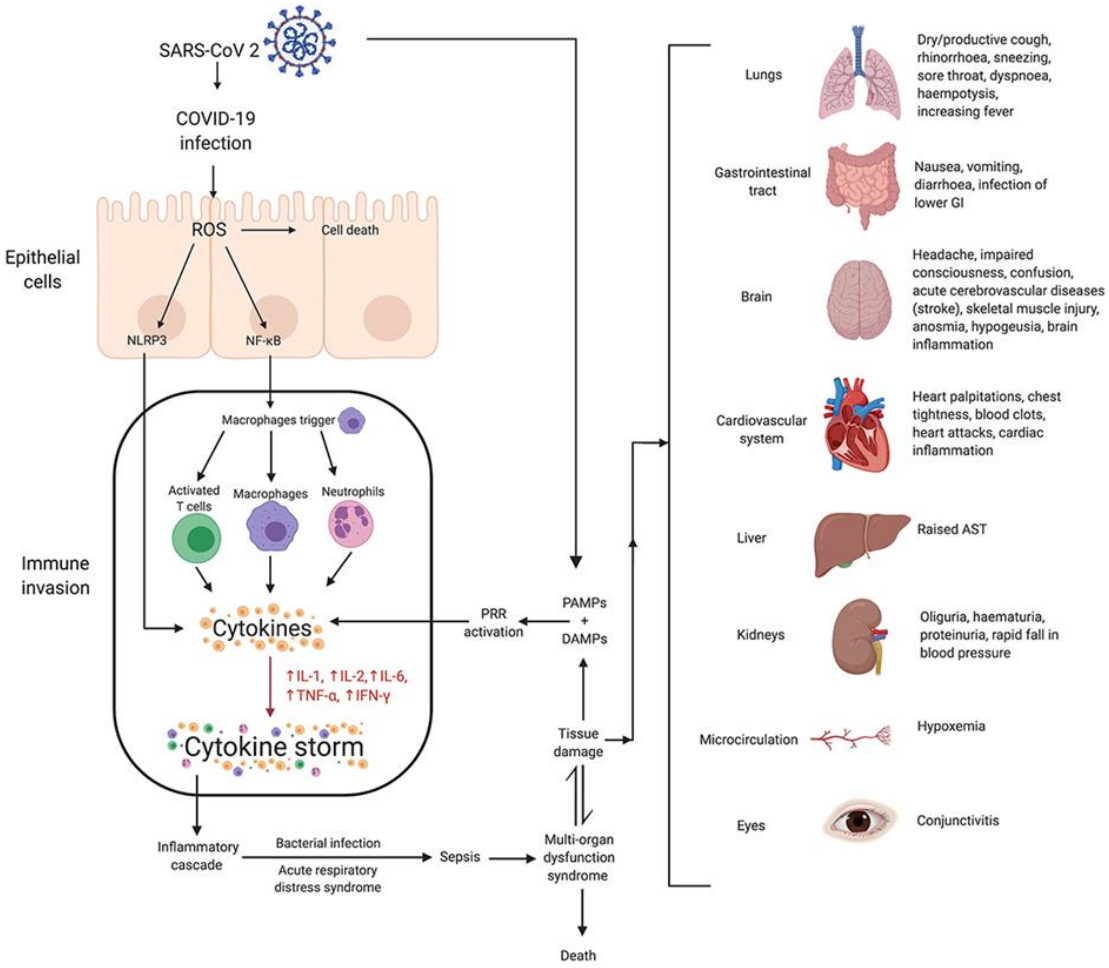

Figure 1.3: Overview of SARS-CoV-2 infection leading to cytokine storm and subsequent organ damage. *This diagram illustrates how SARS-CoV-2 virus leads to elevated reactive oxygen species(ROS) levels and the eventual downstream activation of the cytokine storm through nuclear factor-κB (NF-κB). Tissue damage from the infection leads to the symptoms associated with COVID-19* (Montazersaheb et al. 2022).

The cytokine storm is a very complex phenomena involving many individual components such as key cytokines and transcriptional pathways. Considering the effects of these individual

cytokines creates a much more in depth understanding of disease progression and further potential therapeutic targets.

1.4. Effects of cytokines

While multiple cytokines are elevated in cytokine storms, the effects of certain cytokines are notable in systemic inflammation and makes their expression and pathway activations pivotal in understanding cytokine storms. In the context of COVID-19, TNF-α, IL-6, IL-1β and IFN-γ play prominent roles in the innate immune response of lung tissue and their dysregulation is associated with severe symptoms of COVID-19 (**Figure 1.4**) (Bordallo *et al.*, 2020; Chen *et al.*, 2020; Queiroz *et al.*, 2022). Therefore, these cytokines are prime therapeutic targets to investigate for developing a viable approach to treating COVID-19 (Castelli, Cimini and Ferri, 2020; Fathima, Brundha and Ezhilarasan, 2020).

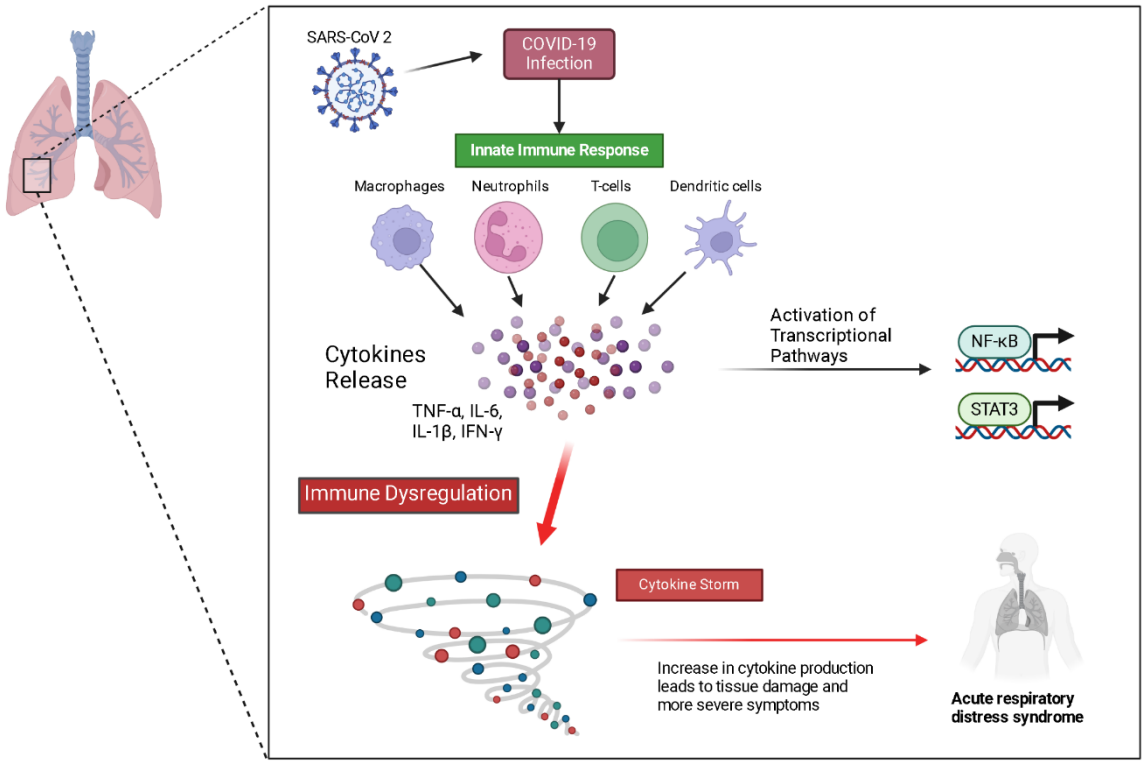

Figure 1.4 Overview immune response and dysregulation of pivotal cytokines during SARS-CoV-2 infection. *The SARS-CoV-2 virus enters the lung and initiates cells of the innate immune cell response which releases cytokines that activate downstream transcriptional pathways such as nuclear factor-κB (NF-κB) and signal transducers and activators of transcription (STAT) 3. The dysregulation of this immune response and subsequent cytokine storm leads to tissue damage and clinical manifestations of severe disease such as acute respiratory distress syndrome (created in BioRender).*

1.4.1. TNF-α

TNF-α has been well established as a prominent regulator in inflammatory response and subsequently contributes to pathogenesis of inflammatory and autoimmune diseases. Following its expression by natural killer cells, T-lymphocytes and macrophages, TNF-α binds to TNF type 1 receptors (TNFR1) which are expressed in all tissue types, such as p55. In addition, TNF-α can also bind to TNF type 2 receptors (TNFR2) such as p75, which are expressed in immune cells. TNF-α binding to its receptor triggers downstream signalling pathways such as the transcriptional activation of NF-κB and intracellular signalling of MAPKs (Jang et al. 2021). High levels of TNF-α were also found in the serum of patients with COVID-19 and is used as a predictor of infection severity and prognosis. It functions within acute and chronic systemic inflammatory response and is able to trigger the production of other cytokines and chemokines that can control cell proliferation and apoptosis simultaneously (Y. Guo et al. 2022). TNF-α mediated inflammation has been associated with lung fibrosis and subsequent complications such as pulmonary oedema, pneumonia and ARDS (Mohd Zawawi et al. 2023). The use of anti-TNF-α treatments to inhibit TNF-α has proven to be associated with a lower risk of hospitalisation and developing more severe COVID-19 in comparison to other therapeutic approaches that target the underlying causes of inflammation (Kokkotis et al. 2022). Additionally, the potential success in targeting TNF-α may be attributed to its effects in initiating the cytokine storm but also to its effects on cell death (Fathima, Brundha, and Ezhilarasan 2020).

1.4.2. IL-1β

Interluekin cytokines play prominent roles in the innate immune response as master regulators of inflammation through binding to the IL-1 receptors. IL-1β is regulated by NF-κB which activates the expression of the intracellular innate immune receptor NACHT-, LRR-, and pyrin domain-containing protein 3 (NLRP3) inflammasome, and the procurer proteins, pro-IL-1β and pro-IL-18. The NLRP3 inflammasome goes on to cause maturation of IL-1β and IL-18 (Liu *et al.*, 2017). The activation mature IL-1β is associated with autoinflammatory diseases such as gout, metabolic syndromes, malignancy and inflammation (acute and chronic) (Gleeson et al. 2022; Kaneko et al. 2019). Moreover, the involvement with the NLRP3 inflammasome pathway leads to COVID-19-associated coagulopathy (CAC) and immunothrombosis (Potere et al. 2023). Immunohistochemical staining of the lungs showed higher production of IL-1β and IL-18 in COVID-19 patients compared to lungs of unaffected individuals (Declercq, De Leeuw, and Lambrecht 2022). IL-1β has also been determined as a crucial cytokine in the

progression of COVID-19 severity and contributes to the development of ARDs especially for individuals who carry specific polymorphisms for the *IL-1 β gene* (Verma et al. 2024).

1.4.3. IFN-γ

Another important cytokine is IFN-γ, a type II interferon and that is predominantly produced by natural killer cells during infection. Through binding of type II interferon receptor, IFN-γ mediates the activation of the JAK/STAT pathway, particularly JAK1/JAK2/STAT1 signalling (Morris, Kershaw and Babon, 2018). In response to viral infection, IFN-γ initiates the differentiation of CD8+T-cells into cytotoxic T-lymphocytes that kill virus-infected cells (Akamatsu et al. 2021). IFN-γ is also involved in amplifying adaptive immune response and triggers anti-microbial activities of macrophages (Mangalmurti and Hunter 2020). Along with TNF-α , IFN-γ has been shown to trigger cell death through the activation of the JAK/STAT1 pathway and the concentration of TNF-α and IFN-γ is proportional to the cell death and therefore a contributing factor to tissue damage in COVID-19 (Fathima, Brundha, and Ezhilarasan 2020). Furthermore, dysregulation of IFN-γ has been associated with long-term respiratory issues following COVID-19 (Li *et al.*, 2024; Soudi *et al.*, 2012).

1.4.4. IL-6

Moreover, IL-6 has both pro-inflammatory and anti-inflammatory properties and is secreted by multiple cell types such as T-cells, macrophages, monocytes, fibroblasts and endothelial cells. IL-6 contributes to the differentiation of B-cells and T-cells as well as their activation and survival. IL-6 plays a vital role in triggering an immune response by targeting leukocytes, eosinophils, basophils and neutrophils (Vatansever and Becer 2020). In the case of a SARS-CoV-2 infection, high levels of IL-6 are correlated with pulmonary inflammation and extensive lung damage. These high levels are also indicative of how a patient may transition from a mild infection to a severe infection (Vatansever and Becer 2020). Additionally, a considerable association has been made between COVID-19 patients with elevated IL-6 levels and higher mortalities (Ragab et al. 2020). Elevated circulating IL-6 has also been correlated with severity of lung injury in COV-19 patients (Chen et al. 2020). Due to the significant role IL-6 has in COVID-19, many have proposed inhibiting this cytokine as a means to treat COVID-19 by hindering the onset of a potentially fatal cytokine storm which may be fatal (Vatansever and Becer 2020; Castelli, Cimini, and Ferri 2020).

1.5. Transcriptional regulation in immune response

Cytokines trigger the activation of multiple transcription pathways but two important pathways in immune response are the NF-κB and JAK/STAT pathways. Both these pathways lead to gene expression changes in cells and contribute to functions of the immune system. However, it is notable that the NF-κB and JAK/STAT pathways do not happen in isolation. Martincuks *et al.* (2017) determined that NF-κB expression has a positive correlation to the levels of STAT3 indicating that NF-κB influences the expression and activation of STAT3. Additionally, the IL-6/JAK/STAT3 pathway in combination with mitogen-activated protein kinases (MAPKs) signalling pathways lead to the activation of NF-κB (Q. Zhou et al. 2023).

1.5.1. NF-κB

NF-κB is a family of inducible transcription factors that play a major role in controlling inflammatory response. The binding of PAMPS to PRR triggers the release of cytokines through the activation of multiple pathways including that of NF-κB (Zhong and Kyriakis 2007). This transcription factor, among others, activate the expression of genes encoding inflammatory cytokines, chemokines and some adhesion molecules (Ragab et al. 2020). In addition, NF-κB regulates multiple aspects of the innate and adaptive immune responses by activating cytokine transcription and inciting the transcription of genes that encode for antimicrobial effectors and regulators of cellular differentiation survival and proliferation (Hayden, West, and Ghosh 2006).

There are five members within the NF-κB family including c-Rel, p52, Rel-B, p50 and Rel-A and two activation pathways of NF-κB transcription. The non-canonical pathway is a more selective response in the adaptive immune system that acts as a supplementary pathway for the canonical pathway. The canonical pathway is more prominently involved in all aspects of immune response and the rapid nuclear translocation of Rel-A and p50 heterodimer in response to signals such as PRR activation and pro-inflammatory cytokines. In this pathway, multi-subunit IκB kinase (IKK) complex phosphorylates IκB complex that sequesters the Rel-A/p50 heterodimer in the cytoplasm. Once phosphorylated, IκB is ubiquitinated and degraded in the proteasome therefore releasing the NF- κB heterodimers and allowing it to enter into the nucleus to activate transcription (Liu *et al.*, 2017; Yu *et al.*, 2020) (**Figure 1.5**).

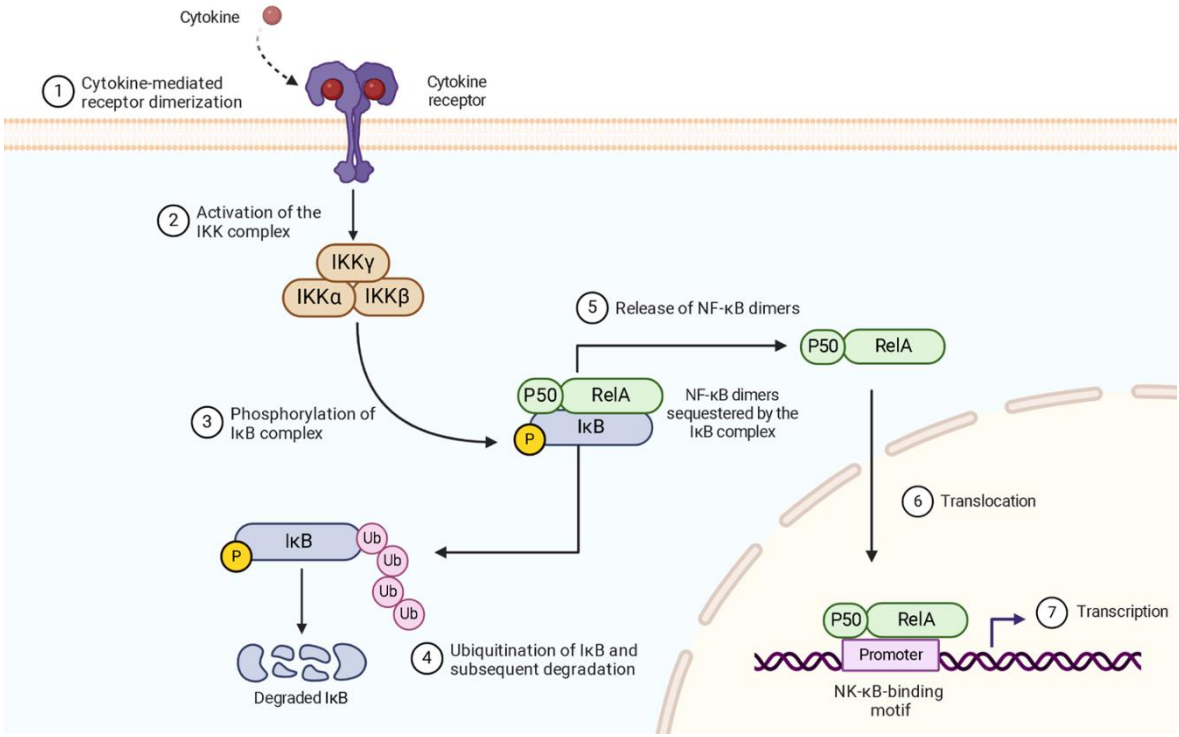

Figure 1.5: The canonical signalling pathway of nuclear factor-κB (NF-κB). *Cytokines mediate dimerization of their receptors to activate the multi-subunit IκB kinase (IKK) complex which in turn phosphorylates the IκB complex and causes its degradation. The Rel-A/p50 heterodimer is released and translocated to the nucleus where it can bind DNA and activate transcription (adapted from Liu et al. (2017) and created in Biorender).*

Due to the prominence of this pathway in immune response, it stands to reason that NF-κB was found to have significant over-activation in SARS-CoV-2 infection. This pathway causes systemic and prolonged inflammatory response such as cytokine storms and thus contributes to the progression of COVID-19 severity (Gudowska-Sawczuk and Mroczko 2022). However, this is not the only transcriptional pathway that is prominent in COVID-19.

1.5.2. JAK/STAT

Another prominent cytokine-mediated transcriptional pathway is the JAK/STAT pathways. While there are multiple JAKs and STATs the general pathway is the same where a cytokine binds to its receptor causing it to dimerise and recruit activated JAKs which then phosphorylate each other and tyrosine residues on the receptor itself. The phosphorylated receptor acts as a docking site for STAT proteins and once they are recruited to the receptor they are phosphorylated by the JAKs. Thereafter, the phosphorylated STATs detach and either

homodimerise or heterodimerise to translocate into the nucleus and binds to specific sequences in the DNA to regulate gene expression (Hu et al. 2021) (**Figure 1.6**).

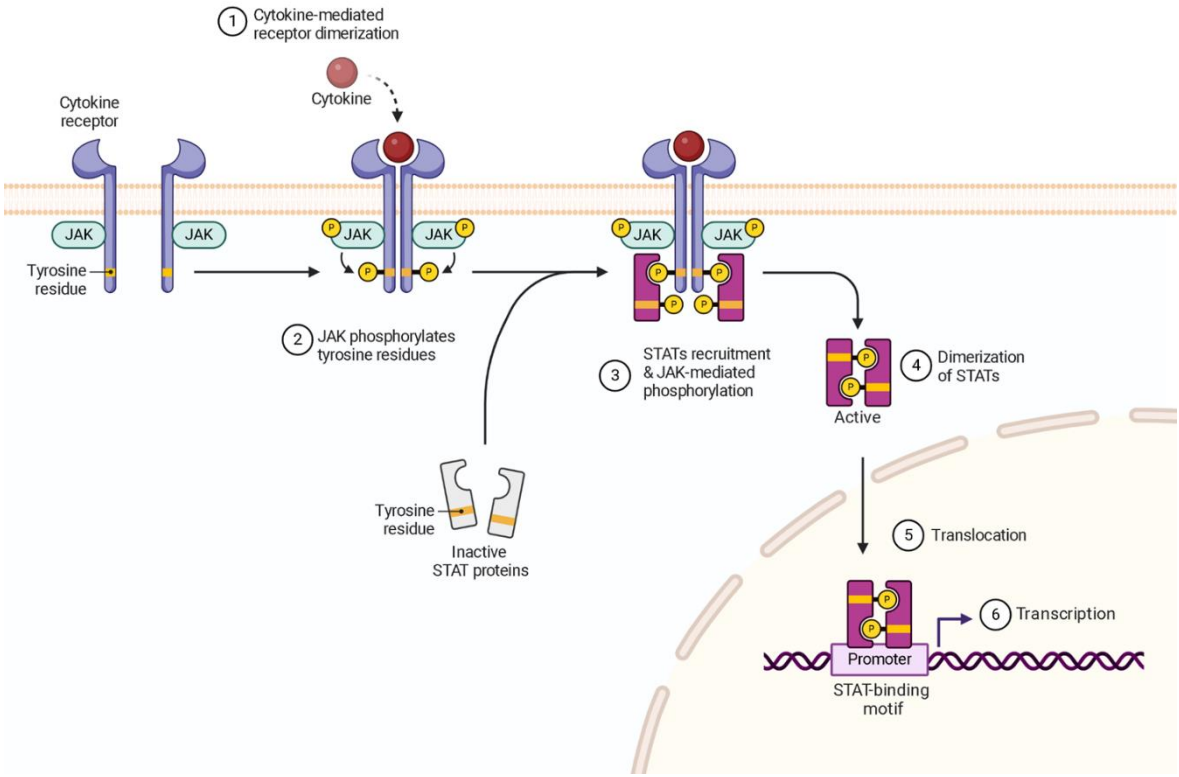

Figure 1.6: The Janus kinase (JAK)/ signal transducers and activators of transcription (STAT) signalling pathway. *Dimerisation of cytokine receptors is mediated upon cytokine binding. This causes the phosphorylation of JAK molecules on the receptors and subsequently recruits STAT molecules. JAK mediates the phosphorylation of the STATs which cause them to dimerise and translocate to the nucleus to activate transcription (adapted from Hu et al. (2021) and created in BioRender) .*

One pathway of interest is the IL-6/JAK/STAT3, where the binding IL-6 binds to the soluble IL-6 receptor glycoprotein 130 resulting in phosphorylation to activate the pathway and as such this pathway contributes to the pathogenesis of COVID-19 (Jafarzadeh, Nemati and Jafarzadeh, 2021). STAT3 was first discovered as part of the IL-6 activated acute phase response factor (APRF) complex, which has a vital role in activating expression of innate immune mediators found in the liver (Hillmer et al. 2016). Additionally, STAT3 has been linked to coagulopathy (bleeding disorder) and lung fibrosis in COVID-19 and therefore has been established as a potential therapeutic target for treating COVID-19. Targeting the IL-6/STAT3 axis could lead to hinder the dysregulation the immune response against SARS-CoV-2 (Jafarzadeh, Nemati and Jafarzadeh, 2021).

These transcriptional pathways regulate the expression of multiple genes in response to cytokines. For our study we looked the potential regulation of peroxidasin (PXDN) and peroxidasin-like (PXDNL) by NF-κB and STAT3 in response to cytokines

1.6. Peroxidase enzymes

The human haem-containing peroxidase enzymes include thyroid peroxidase (TPO), eosinophil peroxidase (EPO), myeloperoxidase (MPO), lactoperoxidase (LPO), and the more recently discovered of these are peroxidasin (PXDN) (previously known as vascular peroxidase-1(VPO1)) and peroxidasin-like (PXDNL). The main physiological function of these enzymes is to catalyse oxidation reactions of substances containing hydrogen peroxide. These enzymes have been noted in thyroid hormone production, host defence and inflammatory response (Cheng and Shi 2022). Of particular interest is the emerging significance of PXDN and PXDNL.

1.6.1. **Structure of PXDN & PXDNL**

As homologues, PXDN and PXDNL have 58% identity and 72% similarity (Péterfi and Geiszt 2014) and share structures that are not present in other peroxidase enzymes, specifically the immunoglobulin (IgG) domain, leucine repeats and von Willbrand factor type C domain (**Figure 1.7**). However, they also lack some structures that are seen in other peroxidase enzymes like the calcium binding epidermal growth factor (EGF)-like domain and transmembrane domain found in TPO (Cheng and Shi 2022). As members of the peroxidase enzyme family, PXDN and PXDNL contain the peroxidase region like the other human peroxidase enzymes. This region is known as the catalytic domain of the enzymes and covalently binds haem. The most significant difference between PXDN and PXDNL is the two amino acid substitution within the catalytic domain. This exchange of glutamine for tryptophan and aspartic acid for glutamic acid results in the lack of peroxidase activity in PXDNL. Both proteins also possess other regions, which make it unique from other peroxidase enzymes and aid in its function as these unique structures predominantly facilitate the protein-protein and protein-ligand binding. PXDN and PXDNL contains five leucine rich repeat region in the N-terminal domain which enables it to bind to laminin in the basement membrane. The IgG loops domain is crucial for the enzyme to form sulfilimine cross-links in its co-locolisation of collagen IV, one of the better understood functions of PXDN. Lastly, the von Willebrand factor (vWf) type C domain also mediates binding in the extracellular matrix (ECM) (Soudi et al. 2012).

.

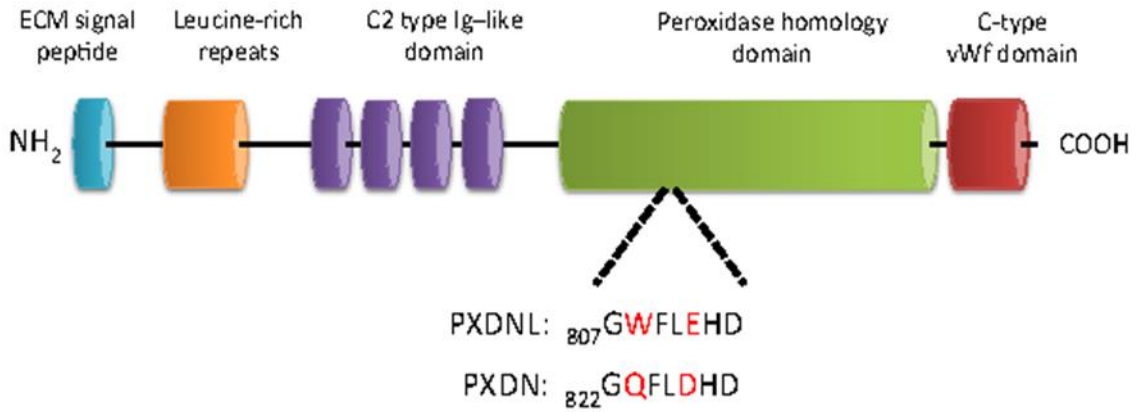

Figure 1.7: Overview of PXDN and PXDNL structure. *Key features of the protein structure are illustrated and the fundamental peptide changes between PXDN and PXDNL are shown including the extracellular matrix (ECM) signal peptide, leucine-rich repeats, immunoglobulin (IgG) loops domain, Peroxidase domain and the von Willebrand factor (vWf) type C domain (adapted from Péterfi and Geiszt, 2014).*

1.6.2. PXDN

In recent years, evidence has highlighted the importance of PXDN as its physiological roles have been implemented in multiple systems and linked to numerous conditions. PXDN is expressed from the VPO1 gene located on chromosome 2p25 next to TPO and contain 25 exons and 22 introns (Cheng and Shi 2022). Expression analysis shows that PXDN is present in many tissue types including skeletal muscle, eye, kidney, pancreas, heart, brain, liver, lung, and placenta but is notably highly expressed in the cardiovascular system (Cheng and Shi 2022). PXDN is also seen in many cell types within these different organs including fibroblasts, epithelial cells and endothelial cells (Péterfi and Geiszt, 2014). Although the human orthologue has been characterised, PXDN was initial described in *Drosophila melanogaster* (Nelson et al. 1994).

The fundamental function of PXDN is to catalyse the oxidation of substrates by hydrogen peroxide (H_2O_2) for the formation of hypohalous acids. PXDN has multiple functions in the ECM and basement membrane formation. PXDN is important for the cross-linking of collagen IV to stabilise it in the formation of basement membranes. PXDN utilises H_2O_2 to oxidise bromide to hypobromous acid (HOBr), which is important for the collagen IV sulfilimine cross-link formation (**Figure 1.8**) (Bhave et al. 2012). Moreover, three conserved cysteine residues in the PXDN protein allow for oligomerisation of PXDN into a trimeric complex to provide a unique structure-function relationship that optimises collagen IV crosslinking (Lázár

et al. 2015). This would implicate PXDN in the architecture and alteration of the matrix and its stiffness and could therefore affect cell movement (Lampi and Reinhart-King 2018).

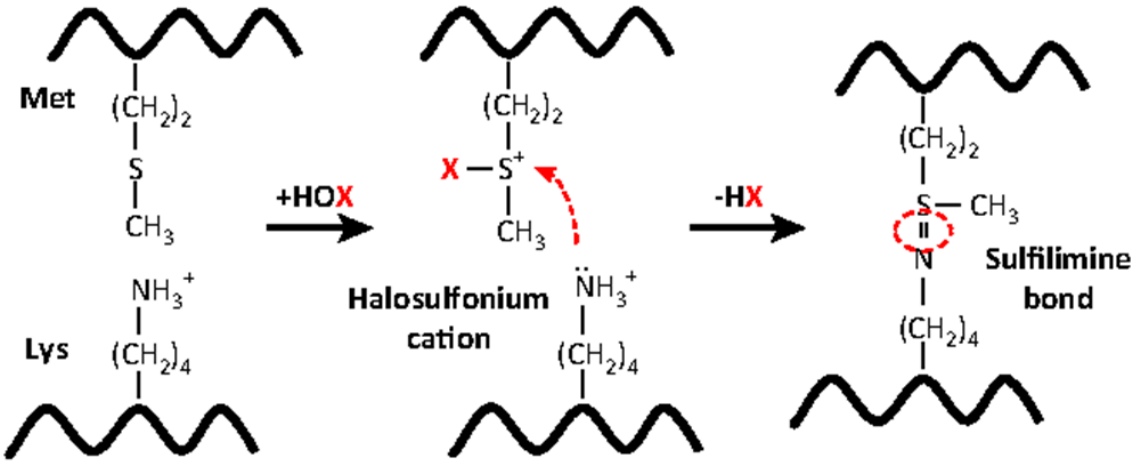

Figure 1.8: Chemical reaction of sulfilimine bond formation catalysed by PXDN. *The crosslinking of methionine (met) and lysine (lys) via a halosulfomium cation intermediate form via the reaction between the hypohalide and the sulfur atom resulting in the sulfilimine bond (adapted from Colon, Page-McCaw and Bhave (2017)).*

In addition to collagen IV cross-linking, PXDN oxidises reactions to form tyrosine crosslinks (H. Li et al. 2012) and similarly to MPO, PXDN also functions to oxidise lipids. Specifically, PXDN oxidises apolipoprotein E (ApoE) and low-density lipoprotein (LDL) in the presence of H_2O_2 and chlorine which suggest a role of PXDN in atherosclerosis development (Y. Yang et al. 2013; Tang et al. 2015). Further catalytic roles of PXDN are seen in oxidative stress as it catalyses the oxidation of various reactive oxygen species (ROS). Research shows that knockdown of PXDN increases oxidative stress, gluconeogenesis, mitochondrial dysfunction and increased apoptosis. PXDN is also involved in nicotinamide adenine dinucleotide phosphate (NADPH) oxidase (NOX) enzyme signalling that mediates oxidative stress. Additionally, the role of PXDN in oxidative stress is further emphasised through its regulation by the transcription factor nuclear factor erythroid 2-related factor 2 (Nrf2), a known regulator of antioxidant response (Hanmer and Mavri-Damelin 2018). In prostate cancer, PXDN's ability to inhibit oxidative stress promotes a decrease in apoptosis thus facilitating the progression of cancer (Dougan et al. 2019).

Moreover, PXDN has two mechanisms of defence in host immunity. Shi *et al.* (2018) have determined that key structural features of the PXDN protein, the immunoglobulin domain and five leucine-rich repeats, enable it to bind to liposaccharides in the membranes of gram-negative bacteria in the lung. This in combination with the ability of PXDN to form hypohalous

acids that mediate bactericidal activity, aid in host immune defence against bacterial infection (Shi *et al.*, 2018). Since PXDN possesses many integral functions, dysregulation of PXDN expression is often associated with in diseases.

Mutations in PXDN have been associated with anterior segment dysgenesis (ASD) disorders such as, microphthalmia, developmental glaucoma, congenital cataract and corneal opacity, which are disorders that affect eye development (Khan *et al.*, 2011; Choi *et al.*, 2015). Furthermore, overexpression of PXDN in ovarian cancer results in a poor prognosis as it supports the tumour through the promotion of proliferation, invasion and migration (Zheng and Liang 2018). PXDN also has implications in regulated kinases such as extracellular signal-regulated protein kinases 1 and 2 (ERK1/2), protein kinase B and focal adhesion kinase (FAK) that leads to the promotion of angiogenesis for the development of cancer (Medfai et al. 2019). As a mediator of the ECM, PXDN has been identified as having a role in the progression of solid cancers as aberrant collagen IV networks in the tumour microenvironment are correlated to increased PXDN expression (Wyllie, Panagopoulos, and Cox 2023). The functionality of PXDN to alter ECM structure is seen tissue fibrosis when secreted by myofibroblasts (Péterfi *et al.*, 2009). Additionally, PXDN overexpression in the heart leads to myocardial ischemic-reperfusion injury via the NOX mediated pathway and inhibiting PXDN protects the myocardium from this tissue injury (Zhang *et al.*, 2012). PXDN regulates cardiac fibrosis and function during remodelling following myocardial infarction (Z. Liu et al. 2019). Moreover, hypoxia is induced by a pathway mediated by NOX4, PXDN, hypochlorous acid production and NF-κB in pulmonary arteries. This PXDN-mediated hypoxia promotes proliferation, apoptosis resistance, and migration of pulmonary artery smooth muscle cells (PASMCs) (You et al. 2018).

1.6.3. PXDNL

PXDNL is a protein that is highly homologous to PXDN and has been found to be highly expressed in the heart (Péterfi *et al.*, 2014), although the functions of PXDNL are not well-established especially given its lack of catalytic function (Péterfi *et al.*, 2014). However, there is some research that suggests PXDNL has a role to play in the ECM since it shares the same structural feature that allow PXDN to interact in the ECM such as the IgG loops domain and von Willebrand factor type C domain (**Figure 1.7**) (Papageorgiou and Heymans 2014). In addition, PXDNL forms a complex with PXDN acting as a functional antagonist and rendering PXDN catalytically inactive (Péterfi *et al.*, 2014). The role of PXDNL in disease is also poorly

understood but high expression of PXDNL has been observed in failing myocardium which is potentially induced by angiotensin II, a known mediator of cardiac remodelling. It has been extrapolated that expression of PXDNL is evident in failing heart muscle where it may associate, and subsequently antagonise PXDN function leading to disorganization of ECM in heart tissue and subsequent decline in tissue function (Péterfi *et al.*, 2014). On the other hand, Papageorgiou and Heymans (2014) have theorised that increased PXDNL expression in heart failure may be a compensatory mechanism to increase ECM stability but may also contribute to increasing cardiac stiffening. Beyond potential roles in the cardiovascular system, PXDNL has been established a putative prognostic biomarker in breast cancer (Y. Li et al. 2019) and bladder carcinoma (Lu et al. 2023).

Although PXDN and PXDNL have not yet been characterised as part of an immune response, they are expressed in tissue that is notably associated with immune response particularly in the case of COVID-19 such as pulmonary, cardiac and vascular tissues. Additionally, the function and subsequent dysfunction of PXDN and PXDNL is associated with characteristic features of clinical manifestations of COVID-19 following and aberrant immune response such as a cytokine storm. Thus, investigation of putative cytokine-mediated regulation of PXDN and PXDNL could implicate these proteins as contributors to disease progression and subsequently suggest their potential as therapeutic targets and biomarkers of severe COVID-19.

1.7. Aim and Objectives

1.7.1. **Aim:**

To characterise the expression of *PXDN* and *PXDNL* in lung cells and determine the transcriptional regulation underlying this expression in response to cytokines.

1.7.2. **Objectives:**

1.7.2.1. Characterise the expression of proteins in lung epithelial cells (A549s) in response to cytokines .

i. Quantify protein expression of PXDN and PXDNL through western blotting in untreated versus cells treated with TNF-α. IL-1β, IFN-γ and IL-6 for 24 hours.

ii. Observe the cellular localisation of expression of PXDN and PXDNL proteins with immunofluorescence in untreated versus cells treated with TNF-α. IL-1β, IFN-γ and IL-6 for 24 hours.

iii. Quantify protein expression of STAT3 and NF-κB through western blotting in untreated versus cells treated with TNF-α. IL-1β, IFN-γ and IL-6for 3 hours.

iv. Observe the cellular localisation of expression of STAT3 and NF-κB proteins with immunofluorescence in untreated versus cells treated with TNF-α. IL-1β, IFN-γ and IL-6 for 24 hours.

v. Compare expression patterns for treated and untreated cells and assess the differences with statistical methods.

1.7.2.2. To determine whether *PXDN* and *PXDNL* are transcriptionally regulated bySTAT3 and NF-κB in response to cytokines.

i. Determine potential binding sites for STAT3 and NF-κb in the promotor regions of PXDN and PXDNL using JASPAR and ChIP-seq data.

ii. Determine if STAT3 and NF-κb are able to bind to the promotor regions of PXDN and PXDNL by assessing DNA-protein interactions using Chromatin immunoprecipitation-PCR when untreated and treated with IFN-γ and IL-6.

2. Materials and Methods

2.1. Reagents

Cell culture reagents were purchased from ThermoFisher Scientific (Waltham, Massachusetts, USA) and other reagents were purchased from Merck (Darmstadt, Germany) unless otherwise stated.

2.2. Cell Culture

The A549 epithelial lung carcinoma cell line were used in this study and were kindly gifted from Dr Tyrone Otgaar (School of Molecular and Cell Biology, University of the Witwatersrand, Johannesburg). Cells were be cultured in Dulbecco's Modified Eagle's Medium (DMEM) nutrient mixture F12 supplemented with 10% Foetal Bovine Serum (FBS) (v/v), 1% penicillin and streptomycin (v/v) and 1% N-2-hydroxyethylpiperazine-N-2-ethane sulfonic acid (HEPES) (v/v). Cells were incubated with a 5% CO_2 atmosphere and at a temperature of 37˚C.

For routine maintenance, once the cells reached approximately 80% confluence, they were sub-cultured by discarding the culture medium and rinsing the cell layer with 2 ml of 1X phosphate buffered saline (1X PBS, pH 7.4) there times. Cells were then detached with 1 ml 0.25% Trypsin: ethylenediaminetetraacetic acid (EDTA) diluted in 1 ml 1X PBS and incubated at 37˚C for 6 minutes. The Trypsin: EDTA was neutralised with 2 ml of fresh culture medium and cells were physically detached with gently pipetting. Thereafter, 700 µl of cell suspension was added to 8 ml of fresh culture medium and allowed to grow for two to three days in a 10 mm cell culture dish.

When required for experiments, cells were counted by mixing 10 µl of the trypsinised cells with 10 µl of 0.2% Trypan blue in 1X PBS (w/v), then pipetting the mixture under a glass coverslip on a haemocytometer. Live cells were counted to calculate the concentration of the cells and the volume required to seed or to collect the desired number of cells.

2.3. Treatments

Throughout this study, A549 cells were treated with cytokines, specifically TNF-α (cat# SRP3177), IL-1β (cat# IL038), IFN-γ (cat# I17001) and IL-6 (cat# H7416). The cytokines were reconstituted in double distilled water to a stock concentration of 100 µg/ml. Thereafter, stocks

were diluted with culture medium as described above but without FBS (serum-free medium) to make the required working concentrations. When cells were treated with cytokines, the culture medium was removed, cells washed with 1X PBS three times and then cultured in serum-free medium with the treatment to ensure that the FBS did not interfere with the treatment process. The effects of these cytokines were investigated individually; therefore, when preparing the treatment samples, the cells were treated with either TNF-α, IL-1β, IFN-γ or IL-6 and an untreated sample was also prepared in the same manner but without the addition of any cytokines.

2.4. MTT Cell Proliferation Assay

Prior to downstream assays, the survival and proliferation of the cells when being treated with cytokines was determined with a 3-(4,5-Dimethylthiazol-2-yl)-2,5-Diphenyltetrazolium Bromide (MTT) assay. Cell metabolic activity causes the reduction of MTT to formazan crystals which is quantifiable through the colorimetric changes from yellow to purple in this reaction (Riss et al. 2016).

Cells were counted as described in section 2.2 and seeded in 96-well flat bottom plate at a density of 1 x10^4 cells per well and incubated for 24 hours at 37˚C and 5% CO_2 in fresh culture medium to a final volume of 100 µl. Medium was then removed and the cells gently rinsed with 1X PBS before adding 100 µl of the cytokine treatments in working concentrations prepared as described in section 2.3 and incubated for 24 hours 37˚C and 5% CO_2. Working concentrations of the cytokines were 1, 3, 6, 12 and 25 ng/ml and each treatment condition was performed in triplicate. These concentrations were chosen as they reflected the concentrations of cytokine treatments used in various cell culture based studies (Boost *et al.,* 2008; Corbière *et al.,* 2011; Eda *et al.,* 2011; Gopallawa *et al.,*2021; Mitchell *et al.,*1994; Stringer and Kobzik, 2010; Yeh *et al.,* 2007).

After 24 hours, the medium containing the cytokines was removed and 100 µl of 0.5 mg/ml MTT in serum free medium (w/v) was added to each well and incubated at 37˚C for 2.5 hours. Following this, 80 µl of the MTT solution was removed from each well with great care taken to avoid disturbing the formazan crystals. The crystals were then solubilised with 100 µl dimethyl sulfoxide (DMSO) and incubated for five minutes at 37˚C followed by shaking the plate for 25 minutes at room temperature in the dark. The absorbance was measured at a

wavelength of 570 nm on the Multiskan GO microplate reader spectrophotometer using Multiskan GO 3.2 software (ThermoFisher Scientific).

2.5. Western Blot

Western blotting or immunoblotting is a useful technique for the quantification of proteins. Proteins in cell lysates are separated with sodium dodecyl sulfate–polyacrylamide gel electrophoresis (SDS-PAGE), a form of electrophoresis in which a protein is denatured and given a negative charge by the SDS before being electrophoresed on a polyacrylamide gel using an electric field. Due to the negative charge created by SDS, the protein will run from the negative electrode to the positive electrode to separate proteins based on size from large to small. These proteins are then transferred onto a nitrocellulose or polyvinyl membrane. Immunodetection of the protein of interest is done with a primary antibody and a corresponding secondary antibody-enzyme conjugate which causes a quantifiable reaction (Mahmood and Yang 2012). For the purposes of this study, western blotting was used to quantify the protein expression of PXDN, PXDNL, STAT3, NF-κB and ICAM-1 in response to the cytokine treatments.

2.5.1. Preparation of cells and lysis

Cells were seeded in 100 mm culture plates, cultured for 48 hours until 80% confluent and then treated with 25 ng/ml of each cytokine as described in 2.3 for 24 hours. Cells were harvested by washing three times in cold 1X PBS on ice and collected by scraping in 1 ml of 1X PBS. The cells were pelleted by centrifugation at 6 700 xg for 10 minutes at 4˚C and the PBS was discarded. The pellet was re-suspended in 1X radioimmunoprecipitation assay (RIPA) buffer (50 mM tris-HCl, pH 8.0, 150 mM NaCl, 0.1% SDS, 1% Triton X-100, 0.5% sodium deoxycholate in distilled water) with protease inhibitors (10 μM leupeptin and 1 mM phenylmethylsulfonyl fluoride (PMSF)) and lysis was completed by rotating the sample for one hour at 4˚C. Protein in cell lysate was collect in the supernatant following centrifugation at 9 660 xg for five minutes at 4˚C. This was stored at -80˚C until further use.

2.5.2. Bramhall assay

Protein quantification was performed using the Bramhall assay (Bramhall et al. 1969). Whatman filter paper was prepared by soaking in distilled water for 20 minutes prior to soaking in increasing concentrations of ethanol, 95% (v/v) then 100% (v/v) for five minutes each and thereafter 100% acetone (v/v) for five minutes. Once dried, the Whitman filter paper was

blotted with 1 mg/ml of bovine serum albumin (BSA) dissolved in lysis buffer standard in a series of volumes (1, 3, 6, 12, 16 and 20 µl) and 2 µl of each sample obtained in 2.4.1. Once the protein was dried it was fixed by incubating the filter paper in 7.5% trichloroacetic acid (TCA) for 45 minutes. The protein was then stained by incubating the Whitman filter paper in Coomassie brilliant blue (3 mM Coomassie blue, 50% methanol, 10% acetic acid) for one hour and then in destain solution (10 % methanol and 12 % glacial acetic acid) for one hour. Thereafter, the Whitman filter paper was dried again and then each of the blue protein spots were cut out and placed in 5 ml of elution buffer (66 % methanol and 1 % of 25 % ammonium solution) in separate tubes and incubated for two hours in the dark. Thereafter, 160 µl of the eluted Coomassie blue stain was transferred to a 96 well plate in triplicate and quantified with by measuring absorbance at 595 nm on the Multiskan GO microplate reader using Multiskan GO 3.2 software (ThermoFisher Scientific). A linear standard curve of protein concentration (µg/µl) vs. absorbance (relative absorbance units) was plotted in Microsoft Excel using the BSA standards and was used to calculate the protein concentration of the samples. The protein concentrations were used to calculate the volume of each sample required to ensure equal protein quantity was loaded for each untreated and treated samples.

2.5.3. SDS-PAGE

SDS-PAGE gels were prepared according to recipes described in **Table 2.1** and cast using the Mini-PROTEAN® Tetra Cell system (Bio-Rad Laboratories; Hercules, California, USA). The percentage of the resolving gel used was dependent on the size of the protein of interest such that proteins with smaller molecular weights were electrophoresed on higher percentage gels and larger molecular weights were electrophoresed on lower percentage gels (**Table 2.1**). PXDN and PXDNL were electrophoresed on 8% gels; ICAM-1, STAT3 and NF-κB on 10% gels and β-actin on 12% gels. Protein samples were prepared by being mixed with 2X protein loading buffer (4% SDS, 120 mM Tris-HCl pH 6.8, 20% glycerol, 0.2% bromophenol blue, 50 mM EDTA, 2% β-mercaptoethanol) and heated to 70°C for 10 minutes in a water bath to denature the proteins. Thereafter the protein samples were loaded into the wells of the gels and the PageRuler™ Plus Pre-stain Protein Ladder, 10 to 250 kDa (ThermoFisher Scientific) was used as a molecular weight marker. The gels were electrophoresed in running buffer (0.1% SDS, 192 mM glycine, 25 mM Tris, pH 8.8) at 80V until the dye front reached the end of the stacking gel, then the voltage was increased to 100V for the protein to move through the resolving gel. SDS-PAGE was done with the Mini-PROTEAN® Electrophoresis System (Bio-Rad Laboratories).

Table 2.1: Reagents required for making SDS-PAGE gels.

	Resolving gel			**Stacking gel**
Reagent	**8%**	**10%**	**12%**	**5%**
Distilled water	4.6 ml	4 ml	3.3 ml	3.4 ml
29:1 Acrylamide /Bisacrylamide	2.7 ml	3.3 ml	4.0 ml	830 µl
1M Tris-HCl pH 6.8				630 µl
1.5M Tris-HCl pH 8.8	2.5 ml	2.5 ml	2.5 ml	
10% SDS (w/v)	100 µl	100 µl	100 µl	50 µl
10% Ammonium persulfate (APS) (w/v)	100 µl	100 µl	100 µl	50 µl
Tetramethylethylenediamine (TEMED)	6 µl	5 µl	4 µL	4 µl

2.5.4. Electroblotting

Following SDS-PAGE, the now separated proteins were transferred to a membrane for immunodetection. For larger proteins of interest such as PXDN and PXDNL, a wet transfer was done on nitrocellulose membrane while smaller proteins of interest underwent a dry transfer on polyvinylidene fluoride (PVDF) membrane. For the wet transfer, the gels from the SDS-PAGE, nitrocellulose membrane and filter paper were submerged in transfer buffer (25 mM Tris, 20% methanol, 192 mM glycine, pH 8.3) to allowed for equilibration of the gel and to remove any residual SDS from the gels. Excess gel such as the stacking gel and dye front were removed and the nitrocellulose membrane was cut to the size of the gel. The transfer sandwich was assembled in the following order: cathode; sponge; filter paper; gel; nitrocellulose membrane; filter paper; sponge; anode. The proteins were transferred for three hours at 300 mA using the Mini Trans-Blot Cell system (Bio-Rad Laboratories). As heat is generated in the transfer process, this was done in a 4˚C cold room with ice packs and cold transfer buffer in the tank, which was changed periodically. The dry transfer was carried out using the Trans-Blot Turbo Transfer System (Bio-Rad Laboratories). The transfer sandwich was assembled from the bottom up in the following order: anode; PVDF membrane (which

was activated by briefly submerging in 100% methanol); SDS-PAGE gel; cathode. All components were kept damp with transfer buffer and all bubbles between the layers were removed. The transfer was run to 1.0A with constant 25V for 30 minutes.

2.5.5. Blocking and antibody binding

Prior to immunodetection, the non-specific regions of membranes were blocked by incubating membranes in 5% BSA in 1X Tris-buffered saline with Tween-20 (TBST) (20 mM Tris, 150 mM NaCl, pH 7.6, 0.1% Tween-20) (w/v) at room temperature for one hour on a shaker at 40 rpm. Membranes were then washed three times in cold 1X TBST for five minutes at room temperature on a shaker at 100 rpm. Thereafter, the membranes were incubated with primary antibody (**Table 2.2**) diluted in 5% BSA in 1X TBST to a (1:1000) and left overnight at 4˚C on a shaker at 40 rpm. The membranes were washed five times with cold 1X TBST for five minutes, then incubated with the corresponding horseradish peroxidase (HRP)-conjugated secondary antibodies (**Table 2.2**) diluted in 5% BSA in 1X TBST (1:2000) at room temperature in the dark for one hour. The membranes were then washed five times with cold 1X TBST for five minutes in the dark.

2.5.6. Chemiluminescence band detection and quantification

Chemiluminescence substrate (SuperSignal West Pico, ThermoFisher Scientific) was used to detect the proteins, which were imaged on Gel Doc XR+ Gel Documentation System (Bio-Rad Laboratories). Densitometry was performed using Image Lab Software version 6.1 (Bio-Rad Laboratories).

Table 2.2: Primary and secondary antibodies used in western blotting.

Protein target	Primary Antibody	Secondary Antibody
PXDN	PXDN rabbit monoclonal antibody cat# NBP 3-05251 (Novus Biologicals; Littleton, Colorado)	Goat anti-rabbit IgG HRP cat# 70745 (Cell Signalling Technology; Danvers, Massachusetts)
PXDNL	PXDNL goat polyclonal antibody cat# sc-98093 (Santa Cruz Biotechnology; Dallas, Texas)	Mouse anti-goat IgG HRP cat# sc-2354 (Santa Cruz Biotechnology)
ICAM-1	CD54/ICAM-1 mouse monoclonal antibody cat# VF27-516 (Cell Signalling Technology)	Horse anti-mouse IgG HRP cat# 70765 (Cell Signalling Technology)
NF-κB	NF-κB p65 XP rabbit monoclonal antibody cat# D14E12 (Cell Signalling Technology)	Goat anti-rabbit IgG HRP cat# 70745 (Cell Signalling Technology)
STAT3	STAT3 rabbit monoclonal antibody cat# D3Z2G (Cell Signalling Technology)	Goat anti-rabbit IgG HRP cat# 70745 (Cell Signalling Technology)
β-actin	B-actin rabbit monoclonal antibody cat# D6A8 (Cell Signalling Technology)	Goat anti-rabbit IgG HRP cat# 70745 (Cell Signalling Technology)

2.6. Immunofluorescence microscope

In addition to quantifying protein expression, the cellular localisation of PXDN, PXDNL, ICAM-1, STAT3 and NF-κB was determined through immunofluorescence microscopy. For this technique, cells were fixed to a glass coverslip and the cell membranes were permeabilised. The proteins of interest were detected with specific primary antibodies and probed with a corresponding fluorescent antibody and observed with a fluorescent microscope (Im et al. 2019). If the cytokine treatments have an effect on the expression of these proteins they should localise to where they function. Due to the function of PXDN and PXDNL, these proteins localise to the ECM following their expression and ICAM-1 is a cell surface protein. On the

other hand, as transcription factors, STAT3 and NF-κB localise to the nucleus when activated in order to effect gene expression changes.

Cells were seeded on glass cover slips placed into the wells of a 6 well plate and cultured for 48 hours to grow to 80% confluency before being treated with 25 ng/ml of each cytokine as described in section 2.3. Samples prepared for the localisation of PXDN, PXDNL and ICAM-1 were treated for 24 hours to allow for enough time for these larger proteins to be translated and exported to the ECM. Samples prepared for the localisation of STAT3 and NF-κB were treated for three hours, as nuclear localisation is a shorter process. The media was removed and cells were washed once with cold 1X PBS. Cells were fixed to the cover slips with 2 ml of 3% formaldehyde in 1X PBS (v/v) and incubated for 15 minutes at room temperature. The formaldehyde was removed, and cells were washed three times with cold 1X PBS. To permeabilise cells, 2 ml of 0.025% Triton X-100 in 1XPBS (v/v) was added to the wells for 7 minutes at room temperature. Cells were washed three times with cold 1X PBS and 2 ml of 0.5% BSA in 1X PBS (w/v) was added to the wells for one hour at room temperature to block non-specific binding in preparation for immunodetection. Following three washes with cold 1X PBS, cells were incubated with primary antibody (**Table 2.3**) diluted in 0.5% BSA in 1X PBS (1:50) for one hour at 37˚C. Cells were washed three times with cold 1X PBS before being incubated with secondary fluorescein isothiocyanate (FITC)-conjugated antibody (**Table 2.3**) diluted in 0.5% BSA in 1X PBS (1:200) for one hour at 37˚C. In order to counterstain the nuclei, cell were washed three times with cold 1X PBS and incubated with 0.1 µl/ml 4′,6-diamidino-2-phenylindole (DAPI) in 1X PBS (v/v) for five minutes at room temperature in the dark. DAPI binds to double stranded DNA by associating with the adenine-thymine clusters in the minor groove and due to displacement of water molecules causes a fluorescence enhancement. Following a further three washes with cold 1X PBS, the coverslips were mounted onto a microscope slide with Invitrogen ProLong™ Gold antifade reagent (ThermoFisher Scientific) and allowed to cure for 45 minutes in the dark. Slides were viewed on an Olympus BX63 OFM microscope (Olympus - Life Science Solutions; Waltham, Massachusetts, USA) and the images were processed using ImageJ Software version 1.53.

Table 2.3: Primary and secondary antibodies used in immunofluorescence microscopy.

Protein target	Primary Antibody	Secondary Antibody
PXDN	PXDN mouse monoclonal antibody cat# sc-293408 (Santa Cruz Biotechnology)	Goat anti-mouse IgG FITC cat# A10530 (ThermoFisher Scientific)
PXDNL	PXDNL goat polyclonal antibody cat# sc-98093 (Santa Cruz Biotechnology)	Mouse anti-goat IgG FITC cat# sc-2356 (Santa Cruz Biotechnology)
ICAM-1	CD54/ICAM-1 mouse monoclonal antibody cat# VF27-516 (Cell Signalling Technology)	Goat anti-mouse IgG FITC cat# A10530 (ThermoFisher Scientific)
NF-κB	NF-κB p65 XP rabbit monoclonal antibody cat# D14E12 (Cell Signalling Technology)	Mouse anti-rabbit IgG FITC cat# sc-2359 (Santa Cruz Biotechnology)
STAT3	STAT3 rabbit monoclonal antibody cat# D3Z2G (Cell Signalling Technology)	Mouse anti-rabbit IgG FITC cat# sc-2359 (Santa Cruz Biotechnology)
β-actin	B-actin rabbit monoclonal antibody cat# D6A8 (Cell Signalling Technology)	Mouse anti-rabbit IgG FITC cat# sc-2359 (Santa Cruz Biotechnology)

2.7. Bioinformatics analysis

STAT3 and Rel-A (NF-κB) putative binding sites in the promoter regions of *PXDN* and *PXDNL* were detected using JASPAR (https://jaspar.elixir.no/), an open-access database for determining transcription factor binding sites (Castro-Mondragon et al. 2022). Matrix profiles for STAT3 (matrix profile: MA0144.2) and Rel-A (matrix profile: MA0107.1) were used to search for the corresponding binding motifs in regions of 2000 base pairs (bp) upstream of the transcription start sites of the *PXDN* and *PXDNL* genes and these sequences were extracted from the NCBI Ensembl genome browser database (https://www.ensembl.org/index.html) (PXDN: ENSG00000130508 and PXDNL: ENSG00000147485). The relative profile score threshold which determines the sensitivity and specificity of the binding motif match was set to 80% as this is the default recommended threshold for JASPAR.

2.8. Primer Design

Following the establishment of the putative binding sites as described in section 2.6, primer pairs were designed using the NCBI Primer-BLAST tool (Ye et al. 2012) to amplify across these regions and isolate the binding sites in subsequent ChIP-PCR. As there were numerous binding sites across both promoter regions most primer pair amplicons contained multiple sites; however, primers were designed in such a way that no binding sites were included in the overlap regions of the primer amplicons. These primer oligonucleotide sequences were synthesised by Inqaba Biotechnical Industries (Pretoria, South Africa) and reconstituted in Tris-EDTA (TE) buffer (10 mM Tris, 1 mM EDTA, pH 7.5) to stock concentrations of 100 µM and working aliquots of 10 µM were prepared with by diluting the stocks with nuclease-free water. The annealing temperatures were optimised with genomic DNA (gDNA) for template DNA in PCR and amplicons electrophoresed on agarose gels.

2.9. Genomic DNA extraction

Genomic DNA was extracted to be used in optimisation of primer annealing temperatures and for to be used in as a positive control for PCR. DNA was extracted using a column-based method with the GeneJET Genomic DNA Purification Kit (ThermoFisher Scientific) as per the manufacturers' instructions. A549 cells were cultured to 80% confluency as described in section 2.2 before the culture media was removed and cells were washed three times with 1X PBS. Cells were detached by scraping the plate in 500 µl of 1X PBS and pelleted in a microcentrufuge tube by centrifuging at 420 xg for five minutes. After removing the supernatant, the cell pellet was resuspended in 200 µl of 1X PBS with 20 µl of proteinase K solution, vortexed and 200 µl of lysis solution was added and mixed by with pipetting and vortexing. The sample was incubated at 56˚C for 10 minutes with occasional vortexing and 20 µl of RNase A solution was added before incubating at room temperature for a further 10 minutes. 400 µl of 50% molecular grade ethanol in distilled water (v/v) was mixed into the sample and this prepared lysate was transferred into the GeneJet Column was inserted in a collection tube and centrifuged for one minute at 7 400 xg. After discarding the flow through from the collection tube, 500 µl of wash buffer 1 was added to the column and centrifuged for one minute at 7 400 xg. The above was repeated with wash buffer 2 and centrifuged at 11 300 xg for three minutes. The column was placed in a 1.5 ml microcentrifuge tube and 200 µl of autoclaved and filter sterilised double distilled water was added to the column and incubated at room temperature for two minutes before eluting the DNA by centrifuging at 7 400 xg for

one minute. To increase the DNA yield, the eluted DNA sample was placed back on the column, incubated for two more minutes at room temperature and centrifuged again at 7 400 xg for one minute. The quality and quantity of the extracted gDNA was assessed with NanoDrop One/One^{C} Microvolume UV-Vis Spectrophotometer (ThermoFisher Scientific) at 260 nm and 280 nm. The sample was diluted to a concentration of 20 ng/µl and stored at -20˚C.

2.10. Polymerase Chain Reaction (PCR)

PCR was carried out with HotStart *Taq* DNA Polymerase (New England Biolabs; Ipswich, Massachusetts, USA) and the reaction was set up according to **Table 2.4** to make up a final reaction volume of 25 µl. The PCR amplification was done on a T100 Thermal Cycler (Bio-Rad Laboratories) under the conditioned stipulated in **Table 2.5** and PCR samples were kept at 4˚C until agarose gel electrophoresis was performed.

Table 2.4: Reaction setup for PCR.

Reagent	**Volume (µl)**
HotStart *Taq* polymerase master mix	12.5
Forward primer (10 µM)	1
Reverse primer (10 µM)	1
Template DNA (20 ng/µl)	5
Double distilled water	5.5

Table 2.5: Thermocycling conditions for PCR.

Step	**Temperature (˚C)**	**Duration (minutes)**	**Cycles**
Initial denaturation	94	0.5	1
Denaturation	94	0.5	40
Annealing	53 - 60	1	
Extension	68	1	
Final extension	68	5	1
Hold	4	∞	

2.11. Agarose Gel Electrophoresis

1.7% agarose gels in 1X Tris-acetate-EDTA (TAE) buffer (40 mM Tris, 0.1% glacial acetic acid, 0.2% 0.5 M EDTA, pH 8.0) (w/v) were prepared by sufficiently heating agarose powder in the buffer until dissolved. Gels were stained with ethidium bromide (1 µl of 10 mg/ml stock per 1 ml of agarose gel) and cast. 10 µl of the DNA sample was loaded into the well and 5 µl of Quick-Load 100 bp ladder (New England Biolabs) was loaded to assess band size. The agarose gels were electrophoresed at 90 V for 30 minutes in 1X TAE buffer and imaged on the Gel Doc XR+ Gel Documentation System (Bio-Rad Laboratories) and any necessary densitometry was performed using Image Lab Software version 6.1 (Bio-Rad Laboratories).

2.12. Chromatin Immunoprecipitation (ChIP) - PCR

ChIP-PCR was used to identify if there is binding of STAT3 and NF-κB in the promoter regions of the *PXDN* and *PXDNL* genes. For this study, the *ICAM-1* promoter region served as a positive and negative control for binding of STAT3 and NF-κB as established binding and non-binding have been established Kesanakurti *et al.*, (2012). The procedure of ChIP involves cross-linking proteins to the DNA and then fragmenting the DNA. The protein attached to the DNA is immunoprecipitation with a specific antibody to isolate those fragments of DNA. The protein-DNA cross-links are then reversed and the DNA is isolated to be used as input for end-point PCR (Haring et al. 2007).

ChIP was performed using the High Sensitivity ChIP kit (Abcam; Cambridge, United Kingdom) according to the manufacturer's instructions. All reagents were supplied in the kit with the exception of PBS, formaldehyde, cell culture medium, glycine, ethanol, antibodies of interest (STAT3, NF-κB and ICAM-1) and those in the DNA purification kit.

2.12.1. Sample preparation

The A549 cells were cultured for 48 hours to reach 80% confluency prior to being treated with 25 ng/ml of IFN-γ and IL-6 for three hours as stated in section 2.3. Cells were then trypsinised and counted (as described in section 2.2) so that approximately $5x10^4$ cells were collected in a 1.5 ml microfuge tube and pelleted at 68 xg for five minutes then washed with 1X PBS and pelleted again. Cells were then cross-linked with 1% formaldehyde in culture medium (as prepared in section 2.2) at room temperature for 10 minutes while shaking at 100 rpm. The formaldehyde was quenched with 1.25 M glycine in a 1:9 ratio of glycine to formaldehyde and mixed thoroughly. Cells were then pelleted by centrifuging at 68 xg for five minutes. The

supernatant was removed and the cells were washed with cold 1X PBS and cells pelleted again at 68 xg for five minutes. Cells were lysed by resuspending the pellet in lysis buffer with protease inhibitor cocktail and incubated on ice for 10 minutes. The samples were vortexed vigorously for 10 seconds and then centrifuge at 600 xg for five minutes to pellet the nucleus. This pellete was resuspended in ChIP Buffer containing protease inhibitor solution and incubated on ice for 10 minutes with occasional vortexing. The chromatin was then sheared by sonication with the Q55 Sonicator (Qsonica; Newtown, Connecticut) set to 50% amplitude for 10 seconds, then the sample was left on ice for 30 seconds to cool, sonicated for a further 10 seconds and placed back on ice. The chromatin was then collected by centrifuging at 9 660 xg at 4˚C for 10 minutes and collecting the supernatant. The chromatin sample was stored at -80˚C until further use.

2.12.2. Sample Confirmation and Input Preparation

Before proceeding to the ChIP assay, a sample of the chromatin prepared in in section 2.11.1 above was taken to assess that the size of the sheared chromatin was ideal (between 300 and 800 bp). To reverse the crosslinks of this chromatin sample, 25 µl of chromatin was mixed with 25 µl of DNA release buffer with added proteinase K in a 0.2 ml PCR tube and incubated at 60˚C for 30 minutes and then at 95˚C for 10 minutes to inactivate the enzyme. The sample was briefly spun down at maximum speed and the supernatant containing the chromatin was collected and transferred to a new 0.2 ml PCR tube. The collected chromatin was then electrophoresed on a 1.7% agarose gel with 6X loading dye (New England Biolabs) as described in section 2.10. This chromatin sample with reversed crosslinks was purified with the GeneJET PCR purification kit (ThermoFisher Scientific) to be used as the input control in the end-point PCR. The chromatin sample was mixed with binding buffer in a 1:1 ratio and 800 µl of the mixture was transferred to a GeneJET purification column and centrifuged at 11 300 xg for one minute. After discarding the flow-through, the column was washed with 700 µl of the wash buffer and centrifuged at 11 300 xg for one minute. The column was placed into a 1.5 ml microcentrifuge tube and 50 µl of autoclaved and filter sterilised double distilled water was added to the column and incubated for two minutes at room temperature before eluting the DNA by centrifuging at 11 300 xg for one minute. To increase the DNA yield, the eluted DNA sample was placed back on the column and the elution process was repeated.

2.12.3. ChIP Assay procedure

Wells were prepared by adding 50 µl of antibody buffer and 2 µl of antibody to the wells, which were incubated at room temperature with 100 rpms shaking for 90 minutes. The antibodies used in the ChIP assay were the STAT3, NF-κB and ICAM-1 primary antibodies described in **Table 2.2** and **Table 2.3** and the control antibodies supplied by kit (RNA polymerase II for a positive control and non-immune IgG for a negative control). Thereafter, the antibody solutions were removed and the wells were washed with 150 µL of ChIP buffer before adding the ChIP reaction. This reaction contained 50 µl of ChIP buffer containing protease inhibitor cocktail; 38 µl of chromatin sample prepared in section 2.11.1; 2 µl of enrichment enhancer reagent and 10 µl of blocker solution and was left to incubate for three hours at room temperature with shaking at 100 rpm. Thereafter the reaction solution was discarded and the wells were washed with 200 µl of wash buffer with two minutes of shaking at 100 rpm, repeated four times. A final wash was done with DNA release buffer before the crosslinks were reversed.

2.12.4. Reversal of Cross-Links, Release and Purification of DNA

A solution of 1 µl of RNase A to 40 µl of DNA release buffer was added to each well and incubated for 30 minutes at 42˚C then 2 µl of proteinase K was added and the wells were incubated for a further 45 minutes at 60˚C. The DNA solution was then transferred to 0.2 ml PCR tubes and incubated for a final 15 minutes at 95˚C. To purify the DNA, the DNA solution was mixed with 200 µl of DNA binding solution and added to a F-spin column in a F-collection tube (supplied by the assay kit) and centrifuged at 9 660 xg for 30 seconds. The column was then washed with 200 µl of 90% ethanol and centrifuged at 9 660 xg for 30 seconds three times with the last centrifugation for one minute. The column was transferred to a 1.5 ml microcentrifuge tube and 35 µl of DNA elution buffer was added to the column, incubated for two minutes at room temperature and centrifuged at 9 660 xg for 30 seconds. The eluted DNA was placed back on the column, incubated for two minutes at room temperature and centrifuged at 9 660 xg for 30 seconds to increase the DNA yield. This DNA was not diluted to standardise the concentration across the samples because the amount of DNA immunoprecipitated corresponds to the level of binding. In other words if there is more DNA-protein binding, a greater yield of DNA would be immunoprecipitated to be used as template DNA in end-point PCR which would result in higher band intensity on the agarose gel. The eluted DNA was stored at -20˚C until used in end-point PCR.

2.12.5. End-Point PCR and Electrophoresis

To confirm that the assay was successful, PCR was performed using the Glyceraldehyde-3-phosphate dehydrogenase (GAPDH) primers supplied in the kit on the DNA immunoprecipitated with the positive control and the negative control antibodies. PCR was carried out as described in section 2.9 and the subsequent agarose gel electrophoresis was done as described in section 2.10.

Thereafter, end-point PCR was done using the primer sets designed in section 2.7 to amplify regions across the *PXDN* and *PXDNL* promoters and the control primers that amplify regions in the *ICAM-1* promoter established by Kesanakurti *et al.*(2012). In order to conserve the immunoprecipitated DNA, the volume of template DNA in the PCR reaction was reduced to 2 µl and the volume of water was increased to 8.5 µl to keep the final reaction volume at 25 µl otherwise PCR was done as described in section 2.9. Thereafter, agarose gel electrophoresis was done as described in section 2.10.

2.13. Statistical Analysis

Data obtained from the MTT assay was analysed using an analysis of variance (ANOVA) test and data obtained from western blotting densitometry was analysed using a two-tailed paired Student's t-test. P-values less than 0.05 were considered significant. Experiments were performed in triplicate and outliers were determined using a Grubbs' test and subsequently removed from the data. Data analysis was perform using MATLAB R2024b (version 24.2.0.27122019) and graphs were plotted in Microsoft Excel.

3. Results

3.1. Cytokines have no detrimental effect on proliferation and viability of A549 cells

Before any experimental analysis using the cytokines could be done, it was necessary to first establish how the A549 cells respond to the cytokines, therefore an MTT assay was performed to assess the viability of cells in response to cytokines (**Figure 3.1**). Statistical analysis with ANOVA test showed that there was no significant difference in absorbance between the varying concentrations of each cytokine. From this assay, together with a consensus from the literature, it was decided that a concentration of 25 ng/ml would be used for the downstream experiments.

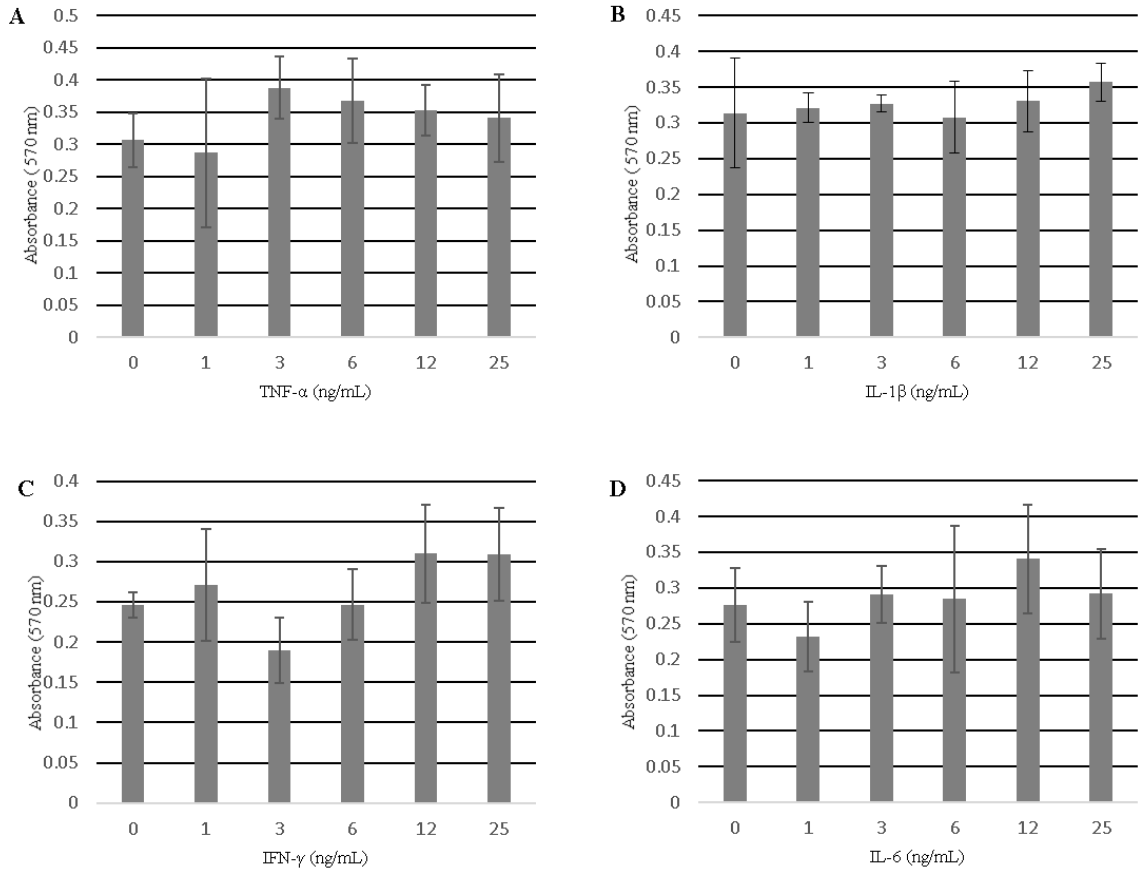

Figure 3.1: Proliferation and viability of A549s are not significantly affected by cytokines. *Treatments with cytokines for 24 hours led to some fluctuation in absorbance showing variability in cell viability but no p-values were significant in comparison to the untreated control for each concentration of (A) TNF-α, (B) with IL-1β, (C) IFN-γ and (D) IL-6.*

3.2. Expression of PXDN and PXDNL increase in response to IFN-γ and IL-6

A549 cells were treated with 25 ng/ml of each cytokine for 24 hours then western blotting was used as a semi-quantitative method to determine protein expression of PXDN and PXDNL, while immunofluorescence microscopy was used to determine localisation of PXDN and PXDNL. **Figure 3.2.1** shows that for PXDN expression, there were small decreases of approximately 20% in response to TNF-α and by 27% in response to IL-1β when compared to the untreated sample, however, expression increased by 16% and 86% in response to IFN-γ and IL-6 respectively. Unfortunately, the untreated band for PXDN was not highly visible in this representative image. When compared to untreated cells, PXDNL expression increased in response to all cytokines by 5% for TNF-α, 31% for IL-1β, 46% for IFN-γ and 20% for IL-6. However, PXDNL in response to IL-6, had a significantly high outlier (as determined with a Grubbs test) which was removed and thus n=2 for this sample.

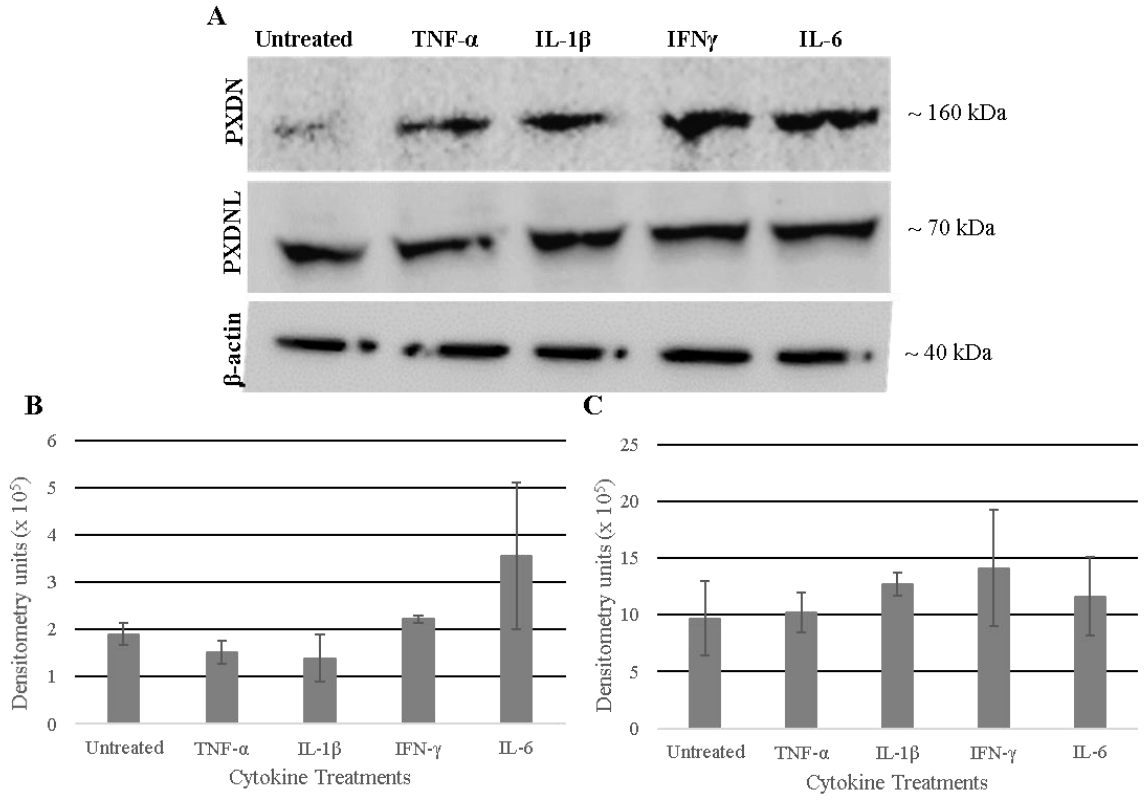

Figure 3.2: Western blot quantification of PXDN and PXDNL showed increased response to IFN-γ and IL-6 treatments. *A549s cells were treated with 25 ng/ml of either TNF-α, IL-1β, IFN-γ or IL-6 for 24 hours. (A) Shows PXDN bands at roughly 160 kDa, PXDNL bands at roughly 70 kDa and β -actin bands at approximately 40 kDa. (B) Quantification of PXDN showed a decrease in response to TNF-α and IL-1β and an increase to IFN-γ and IL-6. (C) Quantification of PXDNL showed an increase in response to TNF-α, IL-1β, IFN-γ and IL-6 (n=3±SD, n=2 for IL-6).*

Similar trends of protein expression were observed with immunofluorescence microscopy (**Figure 3.3** and **Figure 3.4**) when compared to the protein quantification in **Figure 3.2.** A visual increase of PXDN expression is seen with treatment of IFN-γ and IL-6 (**Figure 3.3**). However, the localisation of PXDN appears more concentrated around the nuclei (counter-stained with DAPI), especially in IFN-γ and IL-6 treated samples with some brighter regions of the green fluorescence overlaying some nuclei. Furthermore, an increase in PXDNL expression was seen in response to IFN-γ (**Figure 3.4**). Although PXDNL is also partially concentrated around the nuclei, there is more localisation to the space surrounding the nuclei and between cells, which is most prominent in the IFN-γ treated sample.

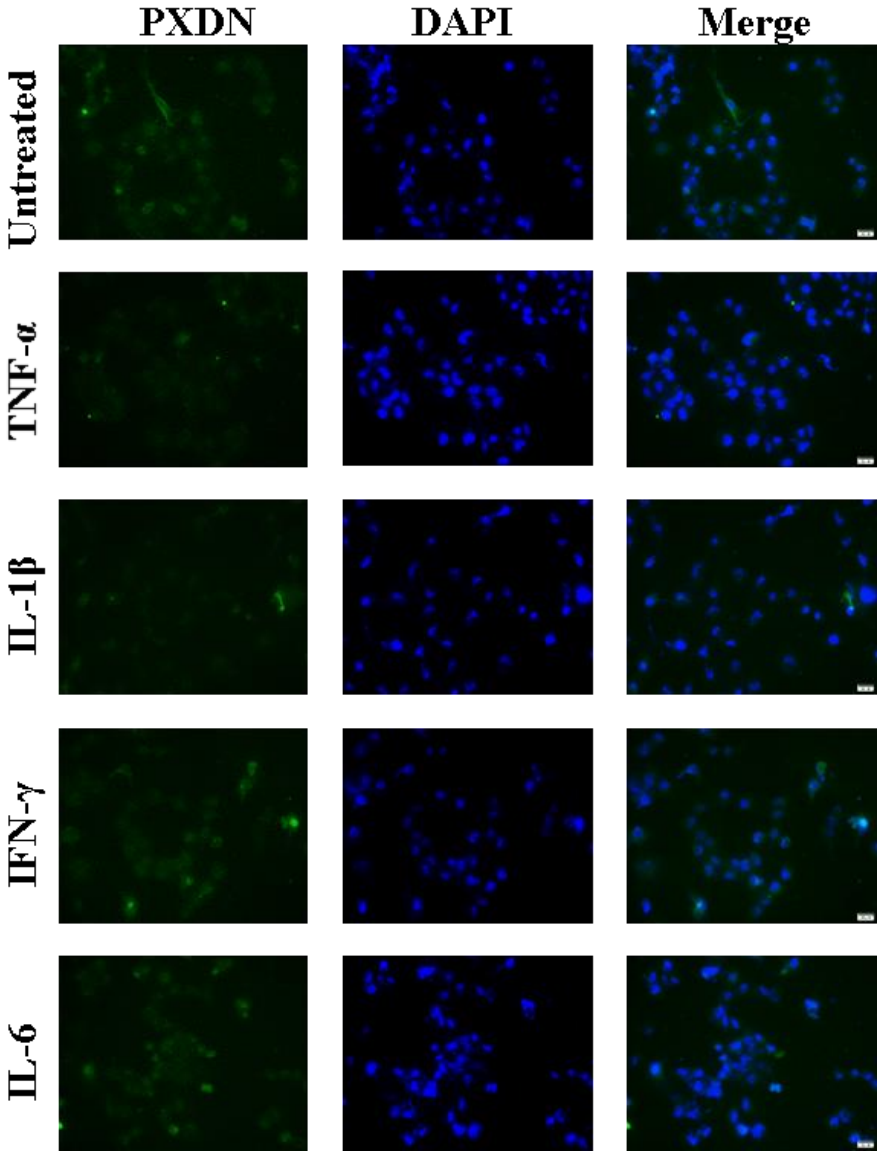

Figure 3.3: Immunofluorescence microscope showed PXDN expression and localisation in response to cytokine treatment. *Cells were treated with 25 ng/ml of either TNF-α, IL-1β, IFN-γ or IL-6 for 24 hours. FITC-conjugated secondary antibody was used to determine expression visualised at 40x magnification (scale bar = 20 μm). Detection of PXDN with high fluorescence intensity around the nuclei in IFN-γ and IL-6 treated cells.*

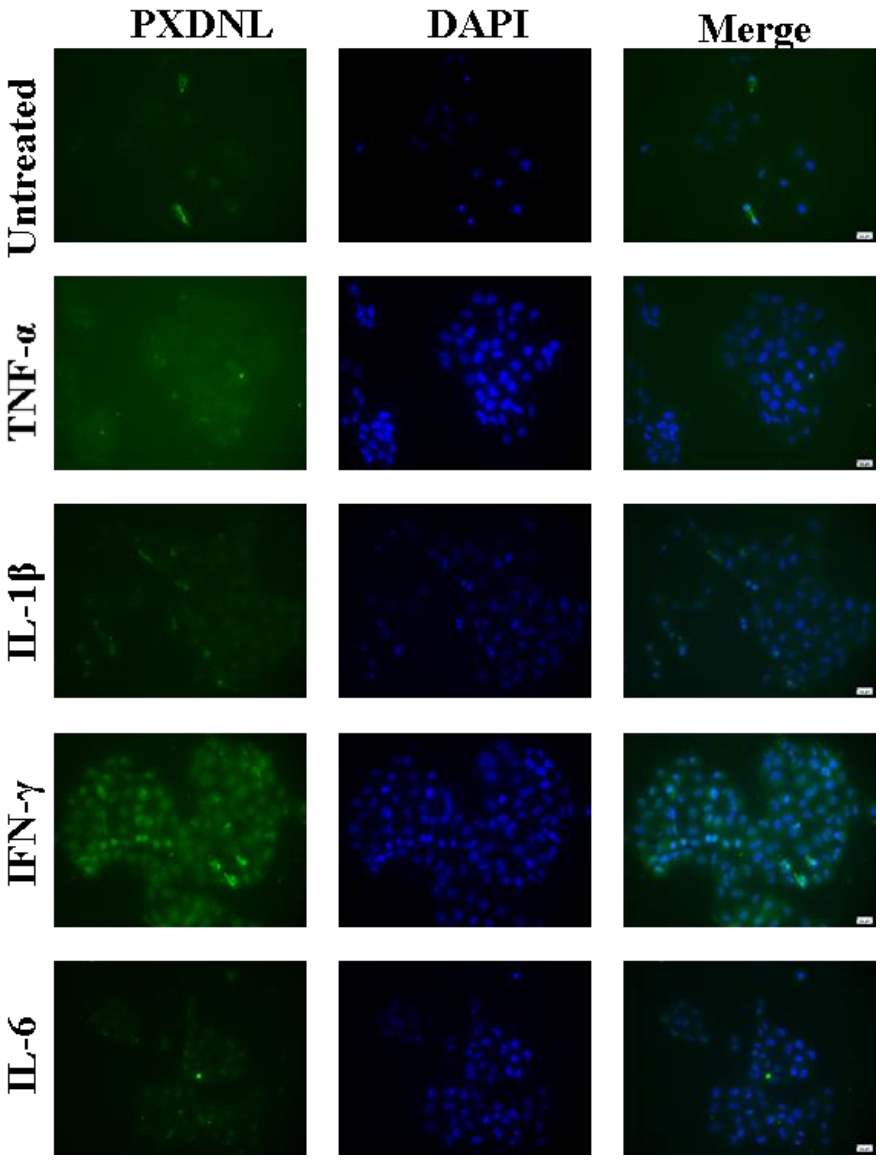

Figure 3.4: Immunofluorescence microscope showed PXDNL expression and localisation in response to cytokine treatment. *Cells were treated with 25 ng/ml of either TNF-α, IL-1β, IFN-γ or IL-6 for 24 hours. FITC-conjugated secondary antibody was used to determine expression visualised at 40x magnification (scale bar = 20 μm). Detection of PXDNL with high fluorescence intensity in IFN-γ treated cells.*

3.3. Cytokines cause nuclear translocation of NF-κB and STAT3 in A549 cells

In order to assess the expression patterns and nuclear localisation of transcription factors NF-κB and STAT3. A549 cells were treated with 25 ng/ml of each cytokine for three hours before quantification with western blotting and detection with immunofluorescence microscopy.

Western blotting results for NF-κB and STAT3 showed that in comparison to untreated samples, treatment with TNF-α, IL-1β and IFN-γ decreased detection of NF-κB by 35%, 37%

and 29% respectively and decreased detection of STAT3 by 26%, 45% and 22% respectively **(Figure 3.5**). However, IL-6 caused almost no change in NF-κB detection (increase of 2%) and an insignificant 28% increase in STAT3 detection, when compared to untreated samples.

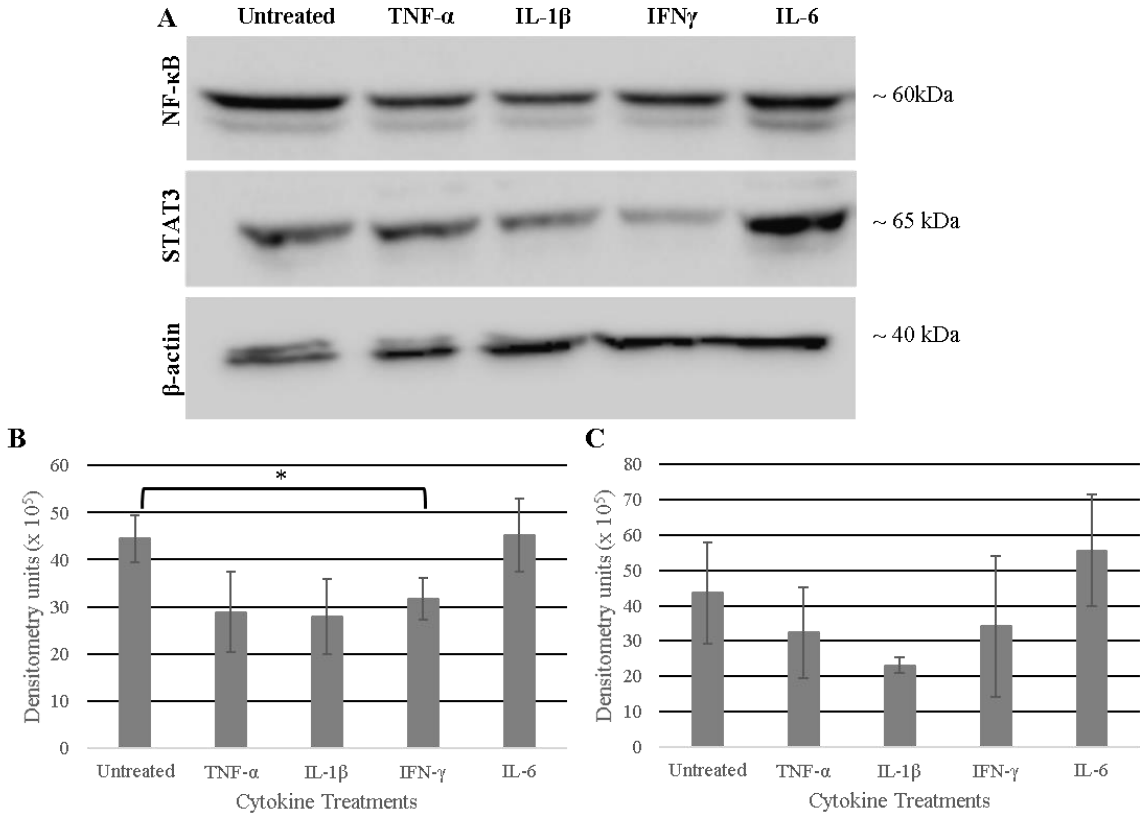

Figure 3.5: Western blot quantification of NF-κB and STAT3 response to treatment with cytokines. *A549s cells were treated with 25 ng/ml of either TNF-α, IL-1β, IFN-γ or IL-6 for 3 hours. (A) Shows STAT3 bands at roughly 65 kDa, NF-κB bands at roughly 60 kDa and β -actin bands at approximately 40 kDa. (B) Quantification of NF-κB showed a decrease in response to TNF-α, IL-1β and IFN-γ and no change to IL-6. (C) Quantification of STAT3 showed a decrease in response to TNF-α, IL-1β and IFN-γ and an increase to IL-6.*

For visualisation of NF-κB and STAT3 in A549 cells following treatment with cytokines, there was clear detection of these proteins both in untreated and treated samples. For both NF-κB (**Figure 3.6**) and STAT3 (**Figure 3.7**), concentration of green FITC fluorescence is seen around and overlaying with the DAPI stained nuclei as expected for transcription factors that have translocated to the nucleus. In **Figure 3.6**, NF-κB, the fluorescence intensity appeared greater in treated cells as compared to the untreated cells with overall higher fluorescence in cells treated with IL-1β and IFN-γ particular in the nuclei. In **Figure 3.7**, STAT3, the fluorescence intensity appeared to be greater with more highly concentrated regions that overlap with the

nuclei in the treated cells compared to the untreated cells especially in those treated with TNF-α and IFN-γ and in a few cells treated with IL-6.

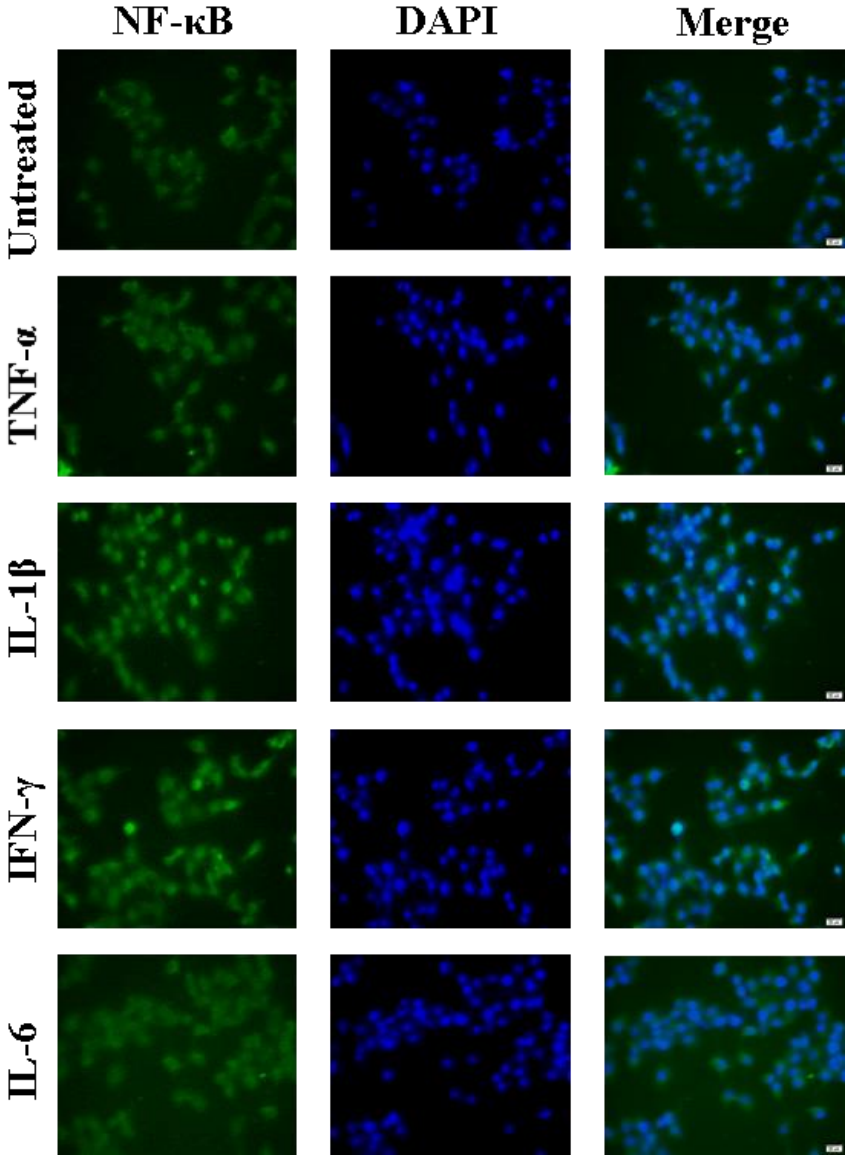

Figure 3.6: Immunofluorescence microscope showed NF-κB localise to the nuclei. *Cells were treated with 25 ng/ml of either TNF-α, IL-1β, IFN-γ or IL-6 for 3 hours. FITC-conjugated secondary antibody was used to determine expression visualised at 40x magnification (scale bar = 20 μm). (A) Detection of NF-κB concentrated in and around the nuclei in all treatments.*

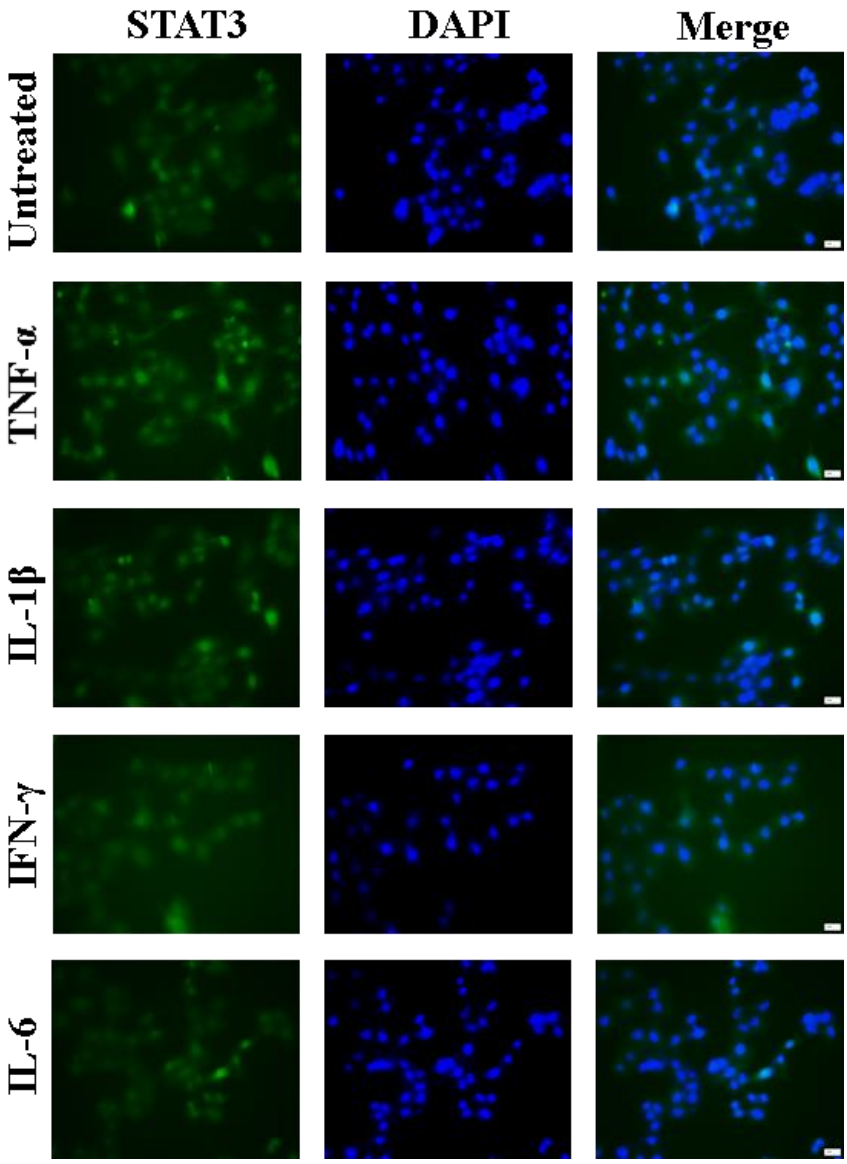

Figure 3.7: Immunofluorescence microscope showed STAT3 localise to the nuclei. *Cells were treated with 25 ng/ml of either TNF-α, IL-1β, IFN-γ or IL-6 for 3 hours. FITC-conjugated secondary antibody was used to determine expression visualised at 40x magnification (scale bar = 20 μm). Detection of STAT3 concentrated to the nuclei for all treatments.*

3.4. ICAM-1 protein is expressed in A549s in response to cytokines

As mentioned in section 2.11, regions within the *ICAM-1* promoter region have been shown to bind STAT3 and NF-κB and these can therefore serve as positive control regions for downstream ChIP-PCR analysis. Therefore, the expression of ICAM-1 in A549 in response to cytokines had to first be established to ensure that this protein could be used as a viable control. Cells were treated with 25 ng/ml of each cytokine for 24 hours and the expression of ICAM-1 assessed with western blotting and immunofluorescence microscopy.

Western blotting results in **Figure 3.8** A and B showed that in comparison to untreated cells, ICAM-1 expression is increased by 158% in response to TNF-α, 1121% in response to IL-1β, 218% in response to IFN-γ and 23% in response to IL-6. The expression of ICAM-1 as visualised through immunofluorescence microscopy was most prominent in response to IL-1β and IFN-γ as shown in **Figure 3.8** C.

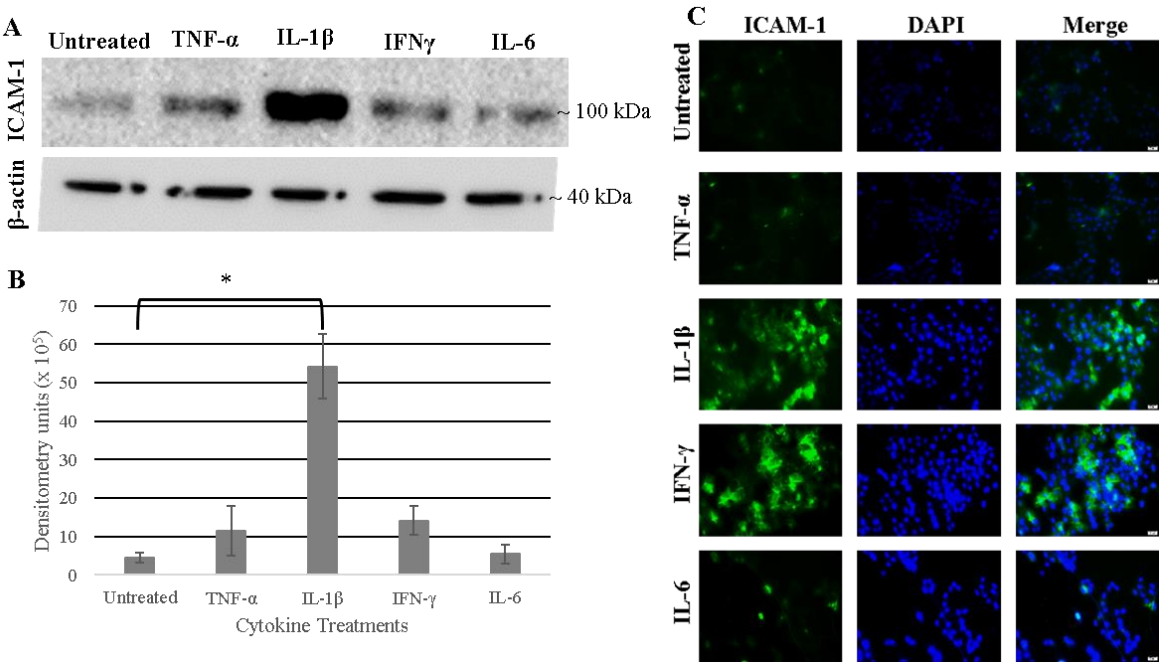

Figure 3.8: Expression of ICAM-1 in A549 cells in response to treatment cytokines. *A549s cells were treated with 25 ng/ml of either TNF-α, IL-1β, IFN-γ or IL-6 for 24 hours. (A) Western blots of ICAM-1 show bands at roughly 100 kDa, and β-actin bands at approximately 40 kDa. (B) Quantification of western blots shows ICAM-1 is present in A549s and significantly increased in response to IL-1β.(C) Immunofluorescence microscopy at visualised 40x magnification shows increased ICAM-1 expression in response to IL-1β and IFN-γ treatment (scale bar = 20 μm).*

3.5. Putative binding sites for NF-κB and STAT3 found in the promoter regions of *PXDN* and *PXDNL*

Once expression patterns of PXDN, PXDNL, NF-κB, STAT3 and ICAM-1 had been characterised in A549 cells, the potential underlying mechanisms of transcriptional regulation of PXDN and PXDNL by STAT3 and NF-κB were investigated.

The promoter regions of *PXDN* and *PXDNL* were explored for putative binding sites of NF-κB and STAT3. The binding profile logos of Rel-A (a subunit of NF- κB) and STAT3 as determined by the bioinformatics tool JASPAR, are seen in **Figure 3.9**. The Rel-A binding motif has prominent guanine bases in the beginning of the motif and thymine and cytosine at

the end of the motif. STAT3 is fairly rich in thymine and guanine and has a characteristic double adenine at the end of the binding motif.

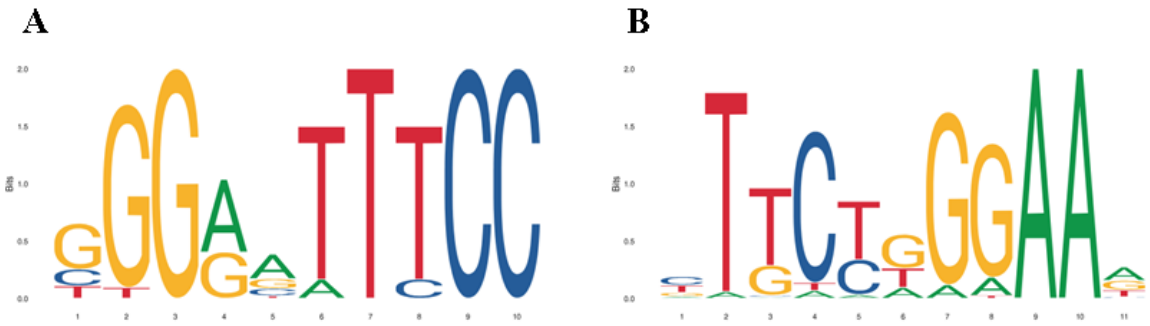

Figure 3.9: Binding motif structures of Rel-A and STAT3. *(A) The binding motif of Rel-A with a matrix length of 10 nucleotides. (B) The binding motif of STAT3 with a matrix length of 11 nucleotides.*

Following the JASPAR search of 2000 bp up stream of the transcriptional start sites of both *PXDN* and *PXDNL* genes, multiple putative binding sites were found. Both NF- κB (Rel-A) and STAT3 sites were found in the *PXDN* promoter region and only STAT3 sites were found in the *PXDNL* promoter region, which are listed in **Table 3.1** and **Table 3.2**. JASPAR calculates the score of each putative binding site such that it considers the length of the matrix, probability of observing the sequence based position frequency matrices compared to the frequencies described by the background model. For the purpose of this study, the binding sites were ranked and labelled on a scale from highest to lowest binding affinity score (column labelled 'Score') with each site in numerical ascending order such that "1" has the highest binding affinity score. Additionally, the location of the binding sites relative to the transcriptional start site (TSS) within the promoter regions is summarised in **Figure 3.10** and **Figure 3.11**. Thereafter, the primer-BLAST tool was used to design primer pairs to isolate sections of the promoter regions to be used in ChIP-PCR and the amplicon size and annealing temperatures were established.

The 2000 bp *PXDN* promoter region was divided into five sections (A to E) that encompassed the three putative Rel-A (NF-κB) sites and 13 putative STAT3 binding sites that were discovered in the promoter region. All Rel-A sites are located in the PXDN-C amplicon region while the STAT3 sites were spread through-out the promoter region with two sites in *PXDN-A*, one site in *PXDN-B*, three sites in *PXDN-C*, six sites in *PXDN-D* and one site in *PXDN-E*.

Table 3.1: Rel-A (NF-κB) and STAT3 binding sites in the *PXDN* promoter.

Binding Site number	Predicted Sequence (5′-3′)	Strand	Score	Amplicon section
NF-κB-1	GGGGGTTCCC	Positive	11.08	*PXDN-C*
NF-κB-2	GGGGGGTTCC	Positive	9.55	*PXDN-C*
NF-κB-3	TGGGGTTTGC	Positive	7.82	*PXDN-C*
STAT3-1	TTTTTTGGAAC	Positive	8.23	*PXDN-D*
STAT3-2	CTGCAGGAAAG	Positive	8.08	*PXDN-B*
STAT3-3	CAGCCTGGAAT	Negative	8.01	*PXDN-C*
STAT3-4	GTTCCAAAAAA	Negative	6.68	*PXDN-D*
STAT3-5	CAGTTGGGAAA	Negative	6.32	*PXDN-D*
STAT3-6	GTGCATAGAAT	Positive	4.86	*PXDN-A*
STAT3-7	GTCACTGGAAT	Positive	3.48	*PXDN-A*
STAT3-8	TTTCCTCAAAA	Positive	2.97	*PXDN-D*
STAT3-9	GCGCCTGGAAT	Positive	2.50	*PXDN-D*
STAT3-10	CTCCTGGGACA	Negative	2.20	*PXDN-C*
STAT3-11	TTTTGAGGAAA	Negative	2.19	*PXDN-D*
STAT3-12	CAGCTGGGACG	Positive	0.83	*PXDN-E*
STAT3-13	GACTTTGGAAA	Negative	0.40	*PXDN-C*

The position of these binding sites can be seen in **Figure 3.10** relative to the section (A to E) in which they are positioned. As primers were designed to isolate these sections, the annealing temperatures of the *PXDN* primer pairs were determined (**Table 3.1**) and the sizes of these amplicons were confirmed with PCR and agarose gel electrophoresis, which showed successful amplification for each primer set with no non-specific amplification (**Figure 3.11**).

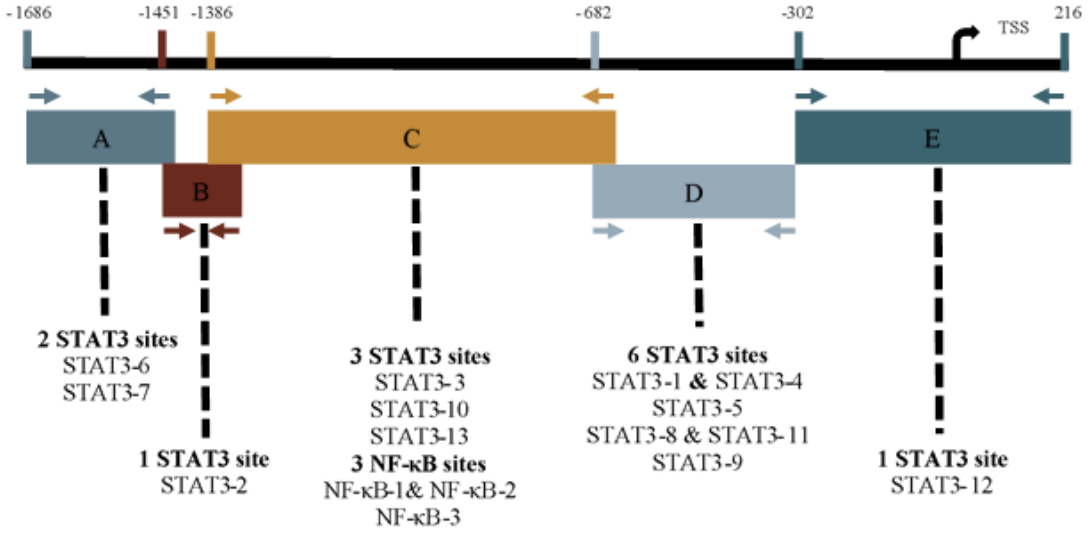

Figure 3.10: Diagram showing putative binding sites for NF-κB and STAT3 in the *PXDN* promoter region. *All three NF-κB sites are located in primer region C and sites 1 and 2 overlap. There are a total of 13 STAT3 sites but sites 1 and 4 overlap and sites 8 and 11 overlap.*

Table 3.2: Primer pairs used for ChIP-PCR of *PXDN* promoter.

Primer Pair	Primer sequences	Annealing Temperature (˚C)	Amplicon size (bp)
PXDN-A	Forward Primer: 5′- CGGCATCCGGAGTGTGAAA-3′ Reverse Primer: 5′ - TATCCACCCTCTACAGCGGA-3′	59	279
PXDN-B	Forward Primer: 5′- ATGGAATCCGGAGTGTGAGC -3′ Reverse Primer: 5′- ACCTAACCCAGCCTTGGAAC -3′	58	150
PXDN-C	Forward Primer: 5′- ATCTGGAATGTCAGCGGGAG -3′ Reverse Primer: 5′- GGTCCTGTGTGGAGTCCTTG -3′	58	767
PXDN-D	Forward Primer: 5′- CACTGAAGGCCGCGAGAATC -3′ Reverse Primer: 5′- TGCGCTCACTACGGGTTTTT -3′	59	380
PXDN-E	Forward Primer: 5′- AAAAAACCCGTAGTGAGCGCA -3′ Reverse Primer: 5′- CAGATGCATGCAGCGCAC -3′	53	539

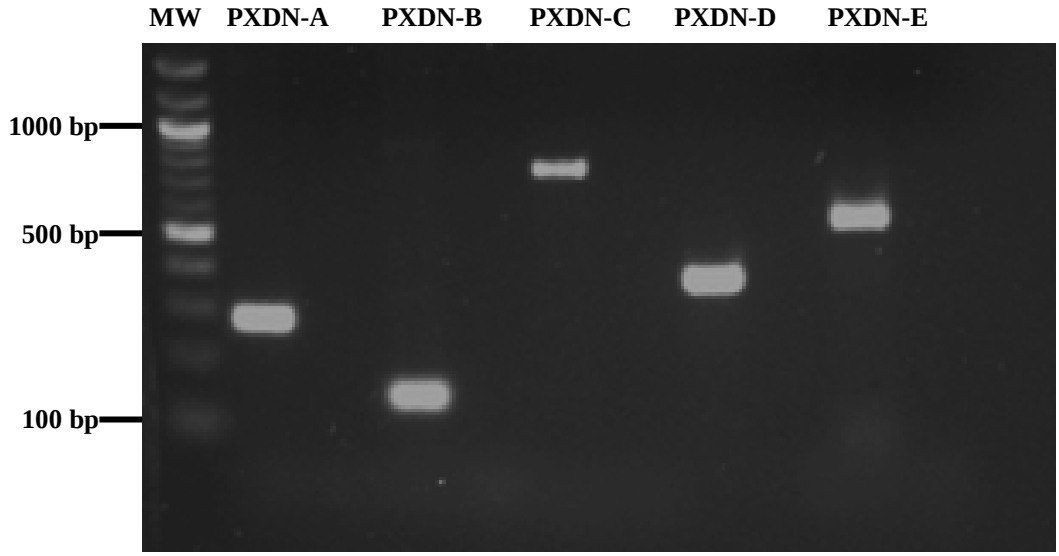

Figure 3.11: Amplicons of the primer pairs designed to amplify across the *PXDN* promoter. *Following PCR, the amplicons were electrophoresed on a 1.7% agarose gel with a 100 bp molecular weight ladder to confirm the amplicon sizes. The PXDN-A band is seen just below the 300 bp marker, the PXDN-B band is seen between the 100 bp and 200 bp markers, the PXDN-C is seen near the 800 bp marker, the PXDN-D band is seen just below the 400 bp marker and the PXDN-E band is seen just above the 500 bp marker, in line with their expected amplicon lengths.*

The *PXDNL* promoter region was divided into four sections (A to D) and 36 putative STAT3 binding sides were discovered in the promoter region and no NF-κB sites were detected. *PXDNL-A* section contains 9 putative, *PXDNL-B* contained 11 putative sites, *PXDNL-C* contained 13 putative sites and *PXDNL-D* contained one putative site.

Table 3.3: STAT3 binding sites *PXDNL* promoter.

Binding Site number	Predicted Sequence (5′-3′)	Strand	Score	Amplicon section
STAT3-1	CTTCAGGGAAA	Positive	12.82	*PXDNL-C*
STAT3-2	ATTTTGGAAAA	Positive	7.52	*PXDNL-C*
STAT3-3	TTGTTTGAAAA	Positive	7.22	*PXDNL-B*
STAT3-4	TTTACAGAAAA	Negative	7.02	*PXDNL-A*
STAT3-5	GTTTTAGAAAG	Positive	6.35	*PXDNL-C*
STAT3-6	TTTAAAGGAAT	Positive	5.77	*PXDNL-B*
STAT3-7	GTGTCTGAAAA	Negative	5.55	*PXDNL-B*
STAT3-8	TTTTCTGTAAA	Positive	5.31	*PXDNL-A*
STAT3-9	AATTTTGGAAA	Positive	4.75	*PXDNL-C*
STAT3-10	TTTCTGTAAAA	Positive	4.52	*PXDNL-A*
STAT3-11	TTGATGAAAAA	Negative	4.37	*PXDNL-C*
STAT3-12	TAGTTTGGAAT	Positive	4.32	*PXDNL-C*
STAT3-13	GCTCTAGGAAG	Negative	4.27	*PXDNL-C*
STAT3-14	CTGATGAAAAG	Positive	4.10	*PXDNL-C*
STAT3-15	CTGCCTAAAAC	Positive	4.05	*PXDNL-C*
STAT3-16	GTGCTGGGATT	Negative	4.01	*PXDNL-A*
STAT3-17	CTGTTTAAAAA	Positive	3.81	*PXDNL-B*
STAT3-18	CTTTTGGCAAA	Negative	3.52	*PXDNL-B*
STAT3-19	TTGAATGAAAA	Negative	3.30	*PXDNL-A*
STAT3-20	TATCTGGTAAC	Negative	3.03	*PXDNL-C*
STAT3-21	GAACCTGGAAG	Positive	2.95	*PXDNL-A*
STAT3-22	ATGCTTAAAAC	Negative	2.66	*PXDNL-C*
STAT3-23	GATCTAAAAAA	Negative	2.60	*PXDNL-B*
STAT3-24	ATTATAAAAAA	Negative	2.22	*PXDNL-A*
STAT3-25	GTGGTGGAAAG	Negative	1.75	*PXDNL-D*
STAT3-26	CATCTGGGATT	Positive	1.73	*PXDNL-B*
STAT3-27	GTTAAAAGAAG	Positive	1.65	*PXDNL-C*
STAT3-28	GTTCATGGAGA	Positive	1.63	*PXDNL-B*
STAT3-29	TTTTTTATAAT	Positive	1.44	*PXDNL-A*
STAT3-30	TTGCATTGAAA	Positive	1.31	*PXDNL-C*
STAT3-31	TTTATTGGTAT	Positive	1.27	*PXDNL-B*
STAT3-32	CTTTCTAAAAC	Negative	1.22	*PXDNL-C*
STAT3-33	GTAATAGAAAA	Negative	1.09	*PXDNL-B*
STAT3-34	TTTAATAAAAA	Negative	1.03	*PXDNL-C*
STAT3-35	TTGTTGGGATT	Positive	0.75	*PXDNL-B*
STAT3-36	ATTTTGGGGAG	Negative	0.68	*PXDNL-B*
STAT3-37	TTACAGAAAAA	Negative	0.35	*PXDNL-A*
STAT3-38	CATTCTGTAAG	Negative	0.22	*PXDNL-B*

These sites can be seen in **Table 3.3** and their positions visualised in **Figure 3.12**. The *PXDNL* primers were designed, annealing temperatures determined (**Table 3.4**) and the sizes of these amplicons were confirmed with PCR and agarose gel electrophoresis, which showed successful amplification for each primer set with no non-specific amplification (**Figure 3.13**).

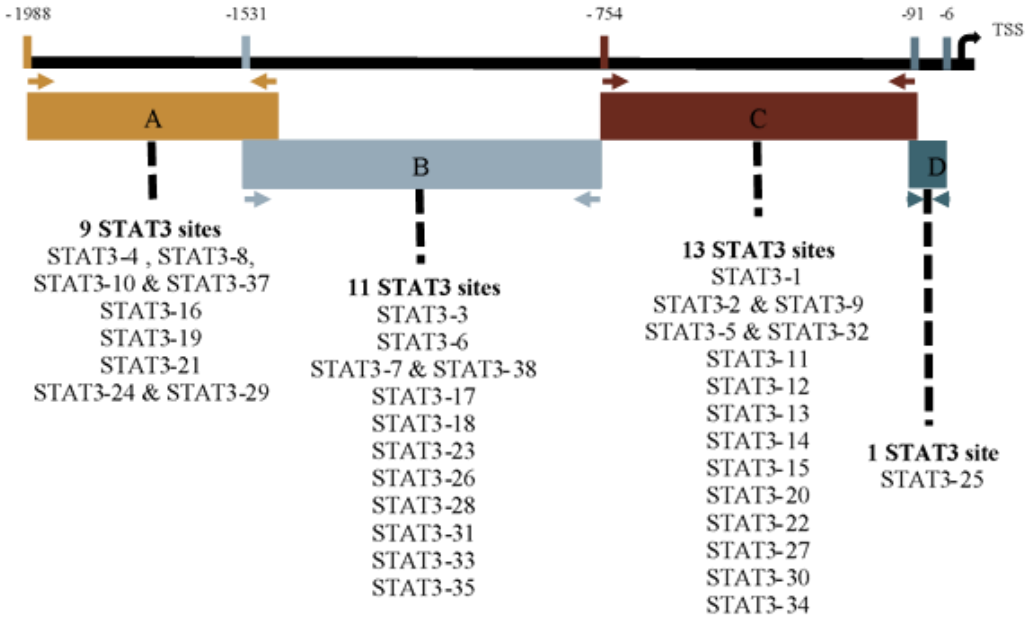

Figure 3.12: Diagram showing putative binding sites for STAT3 in the *PXDNL* promoter region. *There are a total of 38 STAT3 sites in total. In region A, sites 4, 8, 10 and 37 overlap and sites 24 and 29 overlap. In region B, sites 7 and 38 overlap and in region C sites 2 and 9 overlap and sites 5 and 32 overlap.*

Table 3.4: Primer pairs used for ChIP-PCR of *PXDNL* promoter.

Primer Pair	**Primer sequences**	**Annealing Temperature (˚C)**	**Amplicon size (bp)**
PXDNL-A	Forward Primer: 5′- ATGCCTTGCAGTTCTTAGTCC -3′ Reverse Primer: 5′- AAGGCAAGACATGCGGTTCTA -3′	59	562
PXDNL-B	Forward Primer: 5′- ATTCGAACTGAAAACAAGGCACA -3′ Reverse Primer: 5′- TCGTTGAGGACGTGTCTGAA -3′	60	797
PXDNL-C	Forward Primer: 5′- TTCAGACACGTCCTCAACGA -3′ Reverse Primer: 5′- GACACCCCTCTGACCAATCC -3′	58	709
PXDNL-D	Forward Primer: 5′- GCCCTGTAATGTGATATCCCTCC -3′ Reverse Primer: 5′- GTTTGGGAGCCGTGGTGGAA -3′	59	85

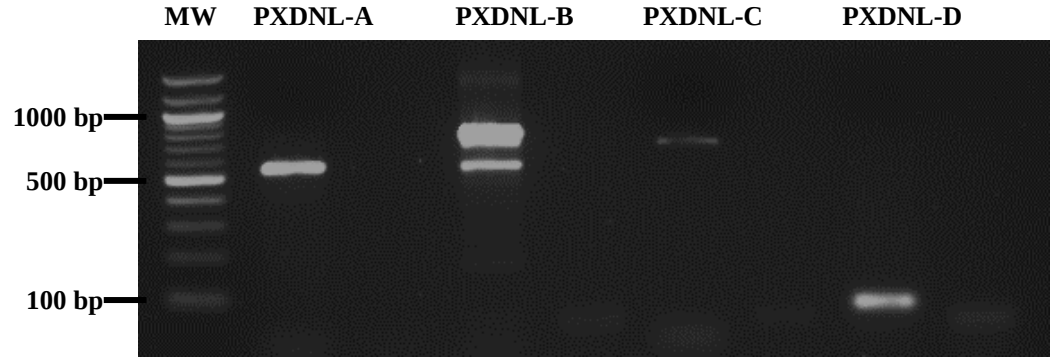

Figure 3.13: Amplicons of the primer pairs designed to amplify across the *PXDNL* promoter. *Following PCR, the amplicons were electrophoresed on a 1.7% agarose gel with a 100 bp molecular weight ladder to confirm the amplicon sizes. The PXDNL-A band is seen just below the 600 bp marker, two PXDNL-B bands are seen with the more prominent band showing at roughly the 800 bp marker while the other band at 600 bp is likely non-specific binding. The PXDNL-C is seen near the 700pb marker, and the PXDNL-D band is seen just below the 100 bp marker, in line with their expected amplicon lengths.*

Furthermore, the ICAM-1 promoter was used as a positive control STAT3 and NF-κB binding (Kesanakurti *et al.*, 2012). Primers were designed to amplify across regions with STAT3 and NF-κB binding sites (**Table 5.5**) and a site that contains no binding sites in the *ICAM-1* promoter region used as positive and negative controls. The sizes of these amplicons were confirmed with PCR and agarose gel electrophoresis, which showed successful amplification for each primer set with no non-specific amplification (**Figure 3.14**).

Table 3.5: Primer pairs used for ChIP-PCR of *ICAM-1* promoter.

Primer Pair	Primer sequences	Annealing Temperature (˚C)	Amplicon size (bp)
ICAM-1 NF-κB Positive	Forward Primer: 5′- CAGGATTTTCCCAGGCCTT -3′ Reverse Primer: 5′- CTCGGTCATTCCCAAGGAA -3′	60	158
ICAM-1 STAT3 Positive	Forward Primer: 5′- TAGCCCCTCCTTCCCATAA -3′ Reverse Primer: 5′- TGAGTCGGGGTGGGGATT -3′	60	121
ICAM-1 Negative	Forward Primer: 5′- AGCAAACACCCGCTCATAT -3′ Reverse Primer: 5′- ACTGAGGCAGCTAGCTTGGA -3′	60	214

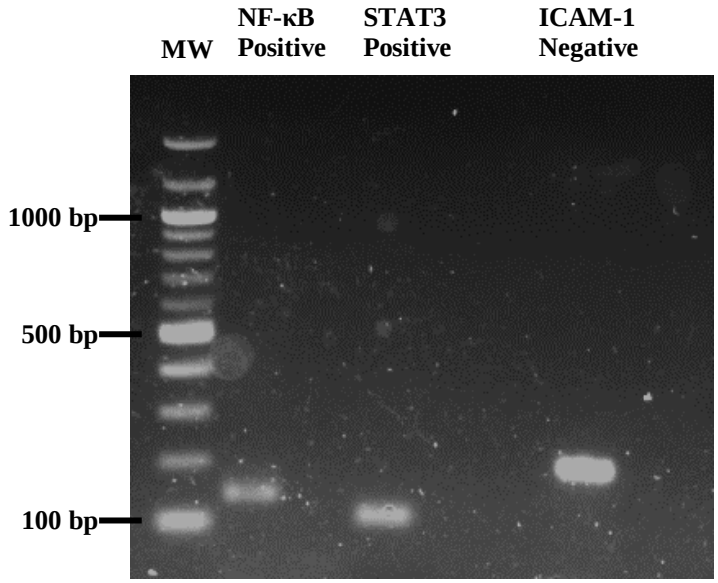

Figure 3.14: Amplicons of the primer pairs designed to amplify across the *ICAM-1* promoter. *Following PCR, the amplicons were electrophoresed on a 1.7% agarose gel with a 100 bp molecular weight ladder to confirm the amplicon sizes. The NF-κB positive band is seen between the 100 bp and 200 bp markers, the STAT3 positive band is seen just above the 100 bp marker and the ICAM-1 negative band is seen at roughly the 200 bp marker.*

3.6. *PXDN* promoter region contains NF-κB and STAT3 binding sites and *PXDNL* promoter region contains STAT3 binding sites

The final objective was to investigate the if PXDN and PXDNL expression is under the control of the STAT3 and NF-κB transcriptional pathways in response to cytokines. After characterising expression patterns of PXDN, PXDNL, STAT3 and NF-κB it was determined that IFN-γ and IL-6 had the greatest effect on increasing expression patterns and therefore these were the treatments used for ChIP-PCR.

Following treatment with 25 ng/ml of IFN-γ and IL-6 for three hours, proteins were cross-linked to DNA with formaldehyde and thereafter the DNA was isolated and sheared with sonication. A sample of the fragmented DNA was electrophoresed on a 1.7% agarose gel after reversing the DNA-protein crosslinks so determine that the fragment size was between 300 bp and 800 bp.

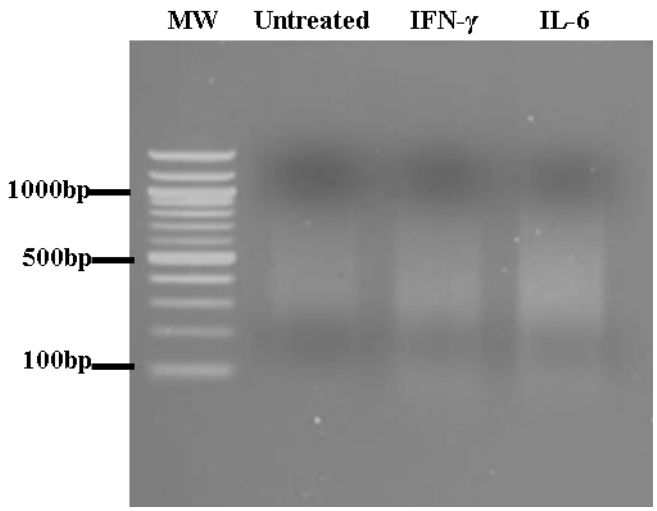

Figure 3.15: Fragmentation of samples with sonication. *Fragmented DNA from untreated, IFN-γ and IL-6 samples following sonication between 300 bp and 800 bp in size.*

Additionally, to ensure that the assay procedure was accurate, DNA was immunoprecipitated with an anti-RNA polymerase II antibody (positive control) and a non-immune IgG antibody (negative control) and this DNA was PCR amplified with GAPDH primers. As a band was present in the positive control and not in the negative control, it was established that the assay procedure was successful.

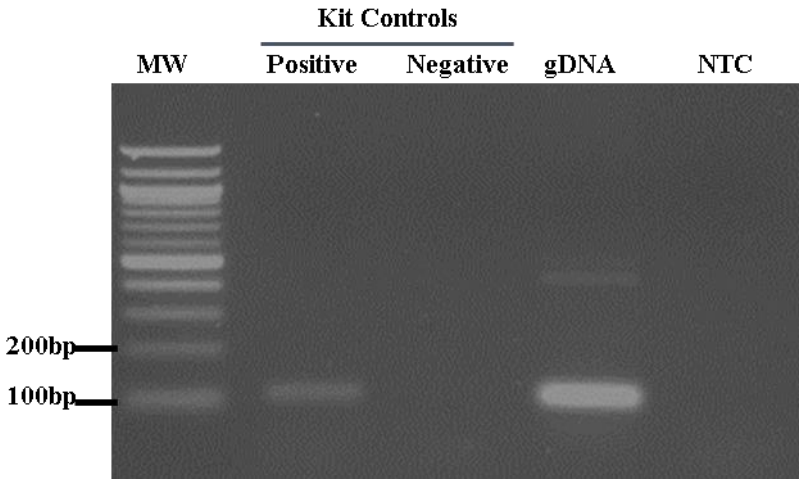

Figure 3.16: ChIP assay controls. *DNA immunoprecipitated with anti-RNA polymerase II antibody (positive control) and DNA immunoprecipitated with non-immune IgG (negative control), genomic DNA and a non-template control underwent PCR with GAPDH primers. A band is present in the positive control.*

Following the ChIP assay, end-point PCR was done with STAT3 and NF-κB immunoprecipitated DNA to establish protein-DNA binding. As it is possible that DNA can bind non-specifically to the wells, DNA extracted from the non-immune IgG control was used

as a background control to account for this non-specific binding. Therefore, densitometry analysis of the experimental bands and the IgG band was done and the volume of densitometry of the IgG band subtracted from the experimental bands to establish if there was binding above background. Additionally, purified sonicated DNA was used as input controls for PCR to establish if there are highly susceptible break points within the amplicons that could lead to no amplification. Lastly, PCR controls included gDNA and a no template control (NTC) to establish the integrity of the of the PCR process.

Following the ChIP assay using anti-NFkB and STAT3 antibodies, end-point PCR was done with immunoprecipitated DNA to establish transcription factor-DNA binding. First, in the PXDN promoter, we looked at the STAT3 binding sites with anti-STAT3 immunoprecipitated DNA, following densitometry analysis, the densitometry of the IgG bands were subtracted from the experimental bands. In assessing STAT3 binding in section *PXDN-A*, bands corresponding to the correct amplicon size (279 bp) were detected in **Figure 3.17A**, with bands across the experimental samples and IgG control. Densitometry analysis showed the untreated sample showed volume above the background but not for the IFN-γ and IL-6 treated samples. In **Figure 3.17B**, bands with a size of 150 bp (the amplicon size of *PXDN-B)* were detected. The densitometry of the IgG band was not greater than that of the experimental samples indicating bands above background and the untreated sample had 1181% and 1032% greater densitometry volume than the IFN-γ and IL-6 samples. In amplification of the *PXDN-C* section in **Figure 3.17C**, bands of the amplicon size (767 bp) were detected. Only the untreated and IL-6 samples showed densitometry volume above background and the densitometry of the untreated sample is 316% greater than IL-6. In **Figure 3.17D**, no bands of 380 bp were detected for the amplification of the *PXDN-D* sections despite bands being seen for the input controls. For section *PXDN-E* (**Figure 3.17E)**, no bands corresponding to 539 bp were detected in the experimental samples, IgG or input controls (except for a very faint band from IL-6 sample) indicating that amplification of this section was not successful in the ChIP-PCR assay.

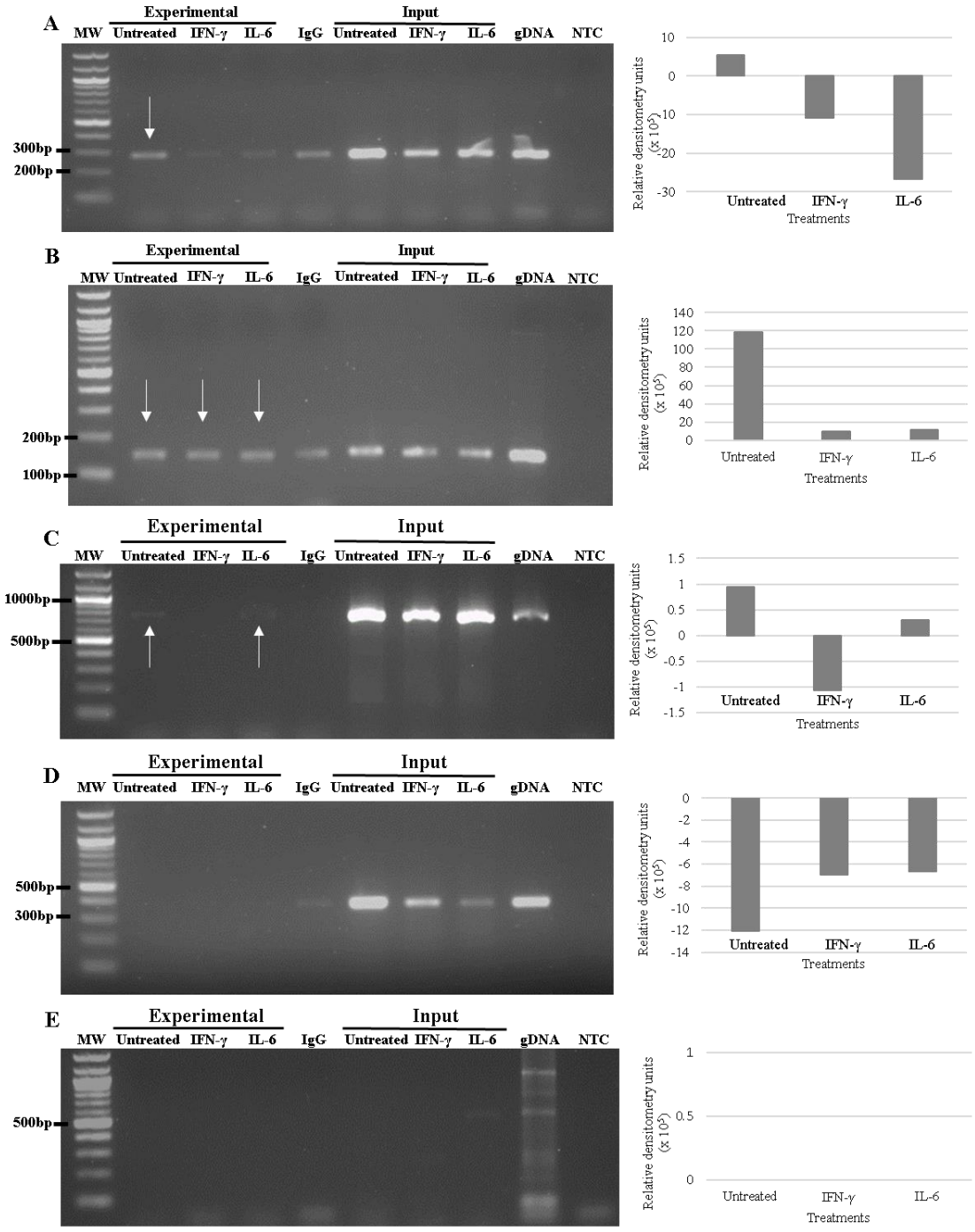

Figure 3.17: ChIP-PCR amplification of the *PXDN* promotor region for STAT3 binding sites. *Cells were untreated, treated with 25 ng/ml of IFN-γ or Il-6 for 3 hours before ChIP was performed and the extracted DNA and that of the necessary controls were subjected to end-point PCR and electrophoresed on 1.7% agarose gels. Positive bars on the graphs indicate binding above background. (A) PCR amplification of PXDN-A primers showing a band above background for the untreated sample. (B) PCR amplification of PXDN-B primers showing binding above background for untreated, IFN-γ and IL-6 samples. (C) PCR amplification of PXDN-C primers showing binding above background for untreated and IL-6 samples. (D) PCR amplification of PXDN-D primers showing no binding above background for any of the experimental samples. (E) PCR amplification of PXDN-5 primers with no distinguishable bands in the experiment samples, IgG sample or input samples except for a slight band for IL-6 input sample.*

Next, in the PXDN promoter we looked at the potential NF-κB sites found in the *PXDN*-C region and ChIP DNA that had been precipitated with the Rel-A antibody was subjected to PCR with the *PXDN*-C primers. The results showed bands corresponding to the amplicon size of 767 bp. Densitometry analysis showed bands above background in the untreated and IFN-γ samples but not the IL-6 treated sample and the untreated sample had greater densitometry volume (432%) than the IFN-γ sample.

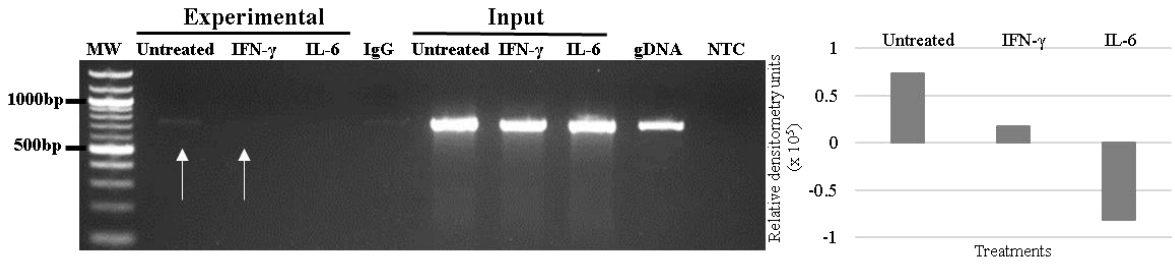

Figure 3.18: ChIP –PCR of the *PXDN* promotor region searching for NF-κB binding sites in *PXDN*-C region. *Cells were untreated, treated with 25 ng/ml of IFN-γ or Il-6 for 3 hours before ChIP was performed and the extracted DNA and that of the necessary controls were subjected to end-point PCR and electrophoresed on 1.7% agarose gels. Positive bars on the graphs indicate binding above background. PCR amplification of PXDN-C primers showing a band above background for the untreated sample and IFN-γ sample.*

For the *PXDNL* promoter, PCR was performed on DNA immunoprecipitated with the STAT3 antibody and the densitometry volume of bands in the subsequent agarose gel electrophoresis were measured and assessed. In **Figure 3.19A** bands of the *PXDNL-A* amplicon (562 bp) were detected and densitometry analysis showed that the densitometry volume of the only band from the IL-6 treated sample was greater than that of the IgG control band. In **Figure 3.19B** had no detection of bands corresponding to the *PXDNL-B* amplicon (797 bp) were detected in the experimental samples or the IgG control. In amplification of the *PXDNL-C* section in **Figure 3.19C**, bands of the amplicon size (709 bp) were detected. Only the IL-6 treated sample showed densitometry volume above background and the densitometry. In **Figure 3.19D**, no bands of 85 bp above background were detected for the amplification of the *PXDNL-D* sections despite bands being seen for the input controls.

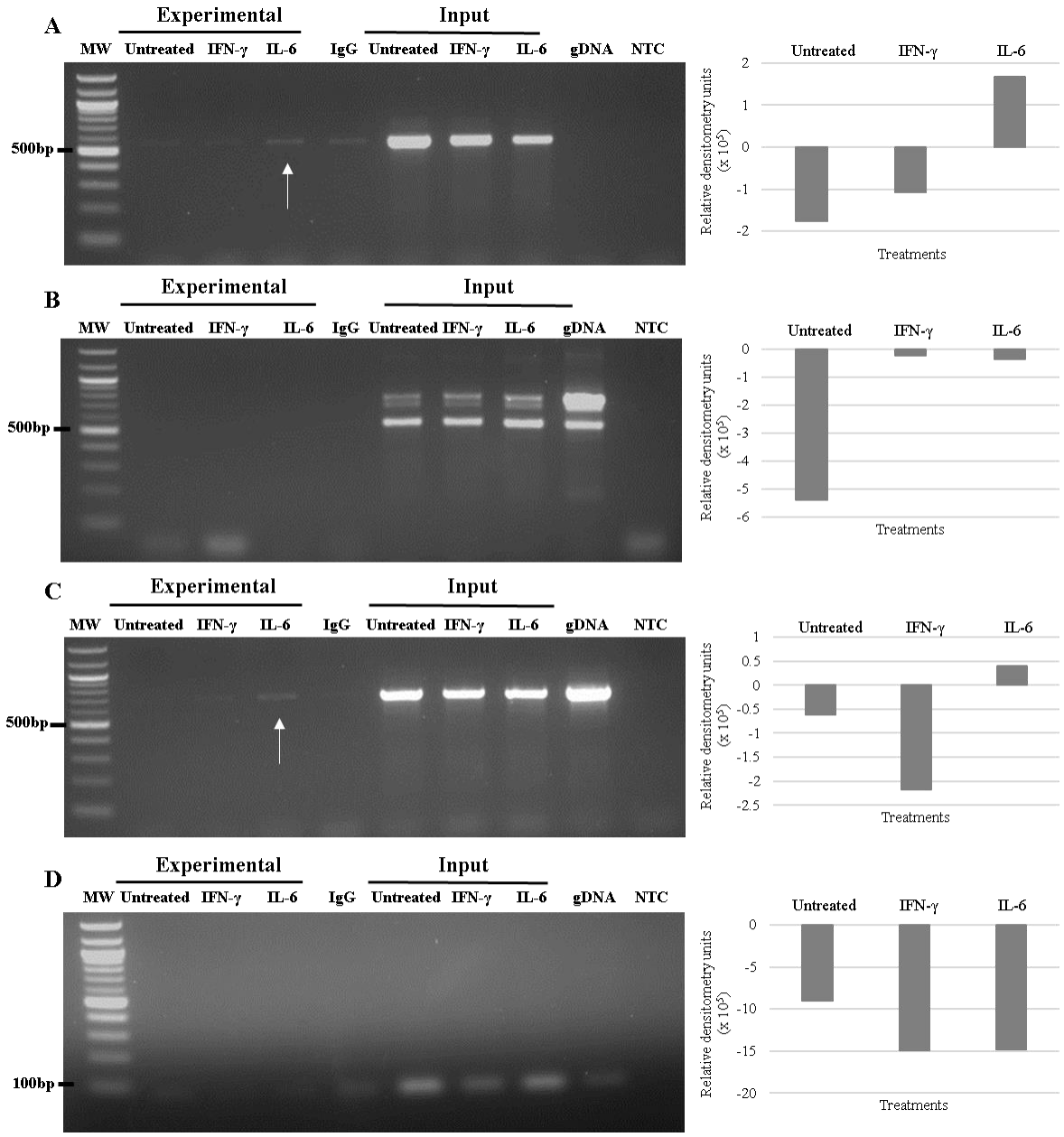

Figure 3.19: ChIP –PCR of the *PXDNL* promotor region searching for STAT3 binding sites. *Cells were untreated, treated with 25 ng/ml of IFN-γ or Il-6 for 3 hours before ChIP was performed and the extracted DNA and that of the necessary controls were subjected to end-point PCR and electrophoresed on 1.7% agarose gels. Positive bars on the graphs indicate binding above background. (A) PCR amplification of PXDNL-A primers showing a band above background for the IL-6 sample. (B) PCR amplification of PXDNL-B primers showing no bands of 797 bp and therefore no binding above background for untreated, IFN-γ and IL-6 samples. (C) PCR amplification of PXDNL-C primers showing binding above background for the IL-6 sample. (D) PCR amplification of PXDN-D primers showing no prominent bands at 85 bp and therefore no binding above background for any of the experimental samples.*

Finally, controls for STAT3 and NF-κB binding in the *ICAM-1* promoter region were performed using primer pairs in **Table 3.5** and analysed with gel electrophoresis and densitometry measurement of the bands. As seen in **Figure 3.20A**, no bands of 158 bp were detected for the amplification of the *ICAM-1 NF-κB positive* sections for PCR with NF-κB immunoprecipitated DNA despite bands being seen for the input controls. In amplification of the *ICAM-1 negative* section in **Figure 3.20B**, bands of the amplicon size (214 bp) were detected. Only the untreated and IL-6 samples showed densitometry volume above background. In **Figure 3.20C**, bands of *ICAM-1 STAT3 positive* amplicon (121 bp) were detected but upon densitometry analysis it was seen that the experimental bands (untreated, IFN-γ treated and IL-6 treated) did not have densitometry volumes greater than the IgG control band. In **Figure 3.20D**, bands with a size of 214 bp (the amplicon size of *ICAM-1 negative* control) were detected. The densitometry of the IgG band was not greater than that of the experimental samples indicating bands above background.

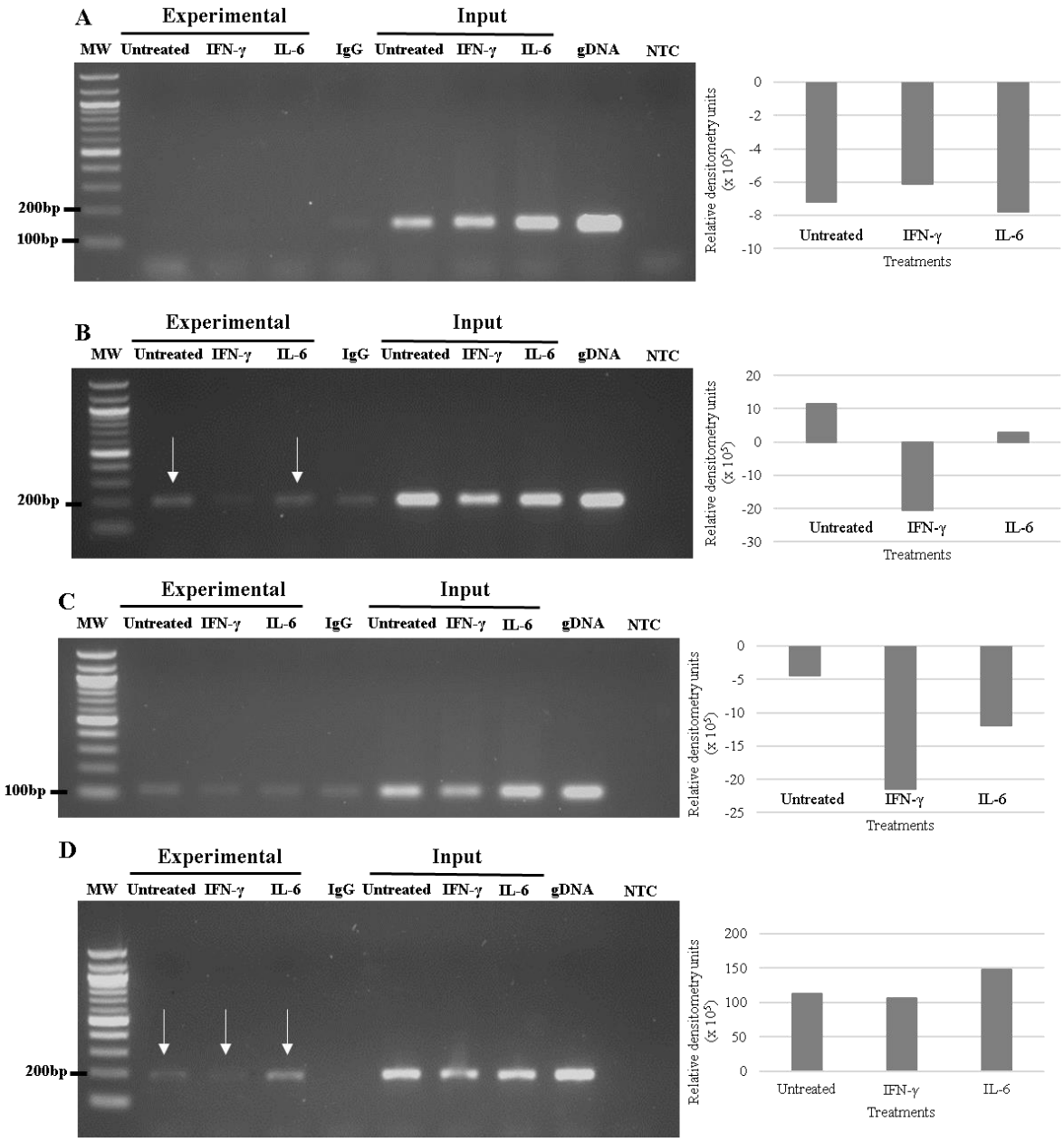

Figure 3.20: ChIP –PCR of the *ICAM-1* promotor region searching for NF-κB and STAT3 binding sites. *Cells were untreated, treated with 25 ng/ml of IFN-γ or Il-6 for 3 hours before ChIP was performed and the extracted DNA and that of the necessary controls were subjected to end-point PCR and electrophoresed on 1.7% agarose gels. Positive bars on the graphs indicate binding above background. (A) PCR amplification of ICAM-1 NF-κB positive primers on DNA immunoprecipitated with NF-κB antibody showing no binding above background. (B) PCR amplification of ICAM-1 negative primers on DNA immunoprecipitated with NF-κB antibody showing binding above background for untreated and IL-6 samples. (C) PCR amplification of ICAM-1 STAT3 positive primers on DNA immunoprecipitated with STAT3 antibody showing no bands above background. (D) PCR amplification of ICAM-1 negative primers on DNA immunoprecipitated with STAT3 antibody showing binding above background for untreated, IFN-γ and IL-6 samples.*

4. Discussion

COVID-19 is the disease caused by the SARS-CoV-2 virus that caused a global pandemic in 2020 (Cascella et al. 2023). Clinical reports of COVID-19 vary with some patients being mildly affected and other patients expressing severe and life-threating complications such as ARDS, a complex condition that compromises the respiratory system (Cascella et al. 2023). The cause of severe COVID-19 can be linked to an over exaggerated response by the immune system where pro-inflammatory cytokines such as TFN-α, IL-1β, IFN-γ and IL-6 are over produced and that lead to changes in the expression and organisation of the lung ECM (Bordallo et al. 2020). This response, called the cytokine storm, leads to the dysregulation of transcriptional pathways such as NF-κB and STAT3, which can regulate the expression of such ECM proteins, amongst their involvement in many other pathways (Zanza *et al.*, 2022).

In tissues that are most affected by COVID-19 such as the lung and vasculature, PXDN and PXDNL are expressed. The functions of PXDN are greatly associated with the ECM such as its ability to cross-link collagen IV to stabilise the formation of basement membranes (Bhave et al. 2012). Additionally, PXDN has important roles in oxidative stress, which leads to cell and tissue damage such as ischemic reperfusion injury and fibrosis (Cheng and Shi 2022). Furthermore, as PXDNL has been proposed as a regulator of PXDN and shares functional protein domains, this would suggest that PXDNL and PXDN have overlapping physiological functions in the ECM (Péterfi *et al.*, 2014), although little is known about the functions of PXDNL in the lung. Therefore, aberrant changes to the expression of PXDN and PXDNL could lead to alternations of the ECM structure, which may contribute to the complications, and symptoms of COVID-19.

Having first established, using MTT assay, that the cytokines do not negatively affect the A549 cells, they were then used to look at whether the treatments modified PXDN and PXDNL expression. From the data obtained through western blotting (**Figure 3.1**), these cytokines appear to have an effect on the expression of these proteins. PXDN expression is decreased by TNF-α and IL-1β and trends towards increased by IFN-γ and IL-6, while PXDNL expression is slightly elevated in response to TNF-α and highly elevated in response to IFN-γ.

The protein extraction method involved scraping the cells from the plate and pelleting them, could have led to loss of the ECM in the sampling process. For better analysis of PXDN and PXDNL secretion into the ECM, an alternative method may be to isolate proteins from the culture media as was done in previous studies evaluating PXDN expression (Péterfi *et al.*,

2009). As PXDN and PXDNL localise to the ECM, it was not possible to tell if these protein were therefore being excluded from the protein lysate. However, if the protein lysate, was composed predominantly of cellular proteins, it is reasonable to question if the expression of PXDN and PXDNL detected in this assay was actually indicative of the quantity of these proteins still within the cytoplasm if they had not yet been exported to the ECM. Unfortunately, despite notable trends seen in western blotting, high variability in the triplicate repeats led to no statistical significance found between treatments and the untreated control. immunofluorescence microscopy served as an additional layer of examination of these expression patterns. Considering the corresponding immunofluorescence microscopy images of PXDN and PXDNL expression (**Figure 3.2**), there is a tendency for the fluorescence to localise around the counter-stained nucleus, which likely indicates that the proteins were localised within the cell and had not yet been secreted the ECM. In a study by Péterfi *et al.* (2009), the level of PXDN were measured in the ECM of human pulmonary fibroblasts following a 72 hour treatment period with transforming growth factor (TGF)-β1 and therefore it is possible that a 24 hour period did not allow for sufficient time for the proteins to be expressed and transported into the ECM. Although, in previous studies, 24 hour treatments were sufficient to detect PXDN (Hanmer and Mavri-Damelin 2018); therefore, the results obtained in this study may be cell and condition specific for cytokines and lung.

Moreover, the molecular weight of PXDNL is calculated to be 164 kDa as the full-length protein contains 1463 amino acids; however, in this western blot analysis, a very prominent PXDNL band of 70 kDa was continuously detected despite multiple attempts at that the technique. Upon further research, multiple isoforms of PXDNL that arise from alternative splicing have been noted in NCBI databases. The anti-PXDNL primary antibody used was raised against a peptide mapping near the N-terminus of the PXDNL protein. Following a NCBI BLAST inquiry, it was found that only a computationally predicted isoform, probable oxidoreductase PXDNL isoform X6 [Homo sapiens] (accession number: XP_047277325) has the conserved N-terminus region of the canonical sequence and has a molecular weight close to 70 kDa as this isoform consists of 747 amino acids (Appendix: **Figure E**). Unfortunately, the protein functions of this isoform are unknown and therefore it is not clear as to why lung cells would express the isoform rather than the full-length protein. We also considered that since PXDN and PXDNL are isoforms, the anti-PXDNL antibody might have detected a potential isoform of PXDN however; these isoforms tend to be larger and likely would not be detected at 70 kDa. Although the specificity of the anti-PXDNL antibody for detecting

canonical PXDNL was questionable, unfortunately, this was the only anti-PXDNL antibody commercially available at the time of experimentation. The antibody was also discontinued from production by the manufacturer part way through this study, and as such hindered the number of attempts of experiments that could be done during the optimisation processes and repeating of experiments.

Next, we characterised the expression patterns of NF-κB (Rel-A) and STAT3 in response to cytokines in A549 cells. For this, cells were treated for three hours with the cytokines as transcription factors require less time to translocate to the nucleus (Swift and Coruzzi 2016). From western blot analysis TNF-α, IL-1β and IFN-γ treatments caused decreased detection of both NF-κB and STAT3 while IL-6 caused a slight increase of both transcription factors. However, these patterns do not correlate with the corresponding immunofluorescence microscopy images as fluorescence appeared greater in treated cells compared to untreated and was concentrated to the DAPI counter-stained nuclei suggesting that the transcription factors translocate to the nucleus in response to the cytokines. The discrepancies in western blotting expression trends and trends observed in immunofluorescence microscopy could be explained by the dimerisation process required to activate transcription such that the NF-κB complex in the heterodimer of Rel-A and p50 and STAT3 homodimerises or heterodimerises with other STAT proteins. In the denaturation of proteins during western blotting, non-covalent bonds that hold protein complexes together will dissociate but protein complexes that are formed with stronger bonds may remain fully or partially intact and therefore will be detected at a higher molecular weight in western blotting (Bass et al. 2016). Using a 2X protein loading buffer with 4% SDS and 2% β-mercaptoethanol and heating at 70˚C may not have been sufficient in fully reducing the hydrogen in the Rel-A/p50 heterodimer (Kumar et al. 2021) and disulphide bonds in STAT3 dimers (L. Li and Shaw 2004). We extrapolated that the dimer forms of the activated transcription factors were excluded from detection in this western blot as the larger protein complexes were likely not transferred with the dry transfer method. Therefore, there may be a misrepresentation of expression levels detected for NF-κB and STAT3 in the western blots.

Once expression patterns had been established, it was decided that treatments with IFN-γ and IL-6 would be used in the ChIP-PCR assay because the expression levels of both PXDN and PXDNL showed a trend in increased in response to these treatments, and NF-κB and STAT3 also showed a response to the treatments. Bioinformatics assessment revealed putative binding sites for STAT3 across both *PXDN* and *PXDNL* promoters and putative binding sites for NF-κB in the *PXDN* promoter region. The promoter regions were divided into sections with primer

pairs to amplify across putative binding sites. Through ChIP-PCR analysis, the binding of the transcription factor to the was indicated by the presence of a band in the subsequence gel electrophoresis.

Upon assessment of STAT3 binding to the *PXDN* promoter, the sections that showed presence of binding somewhat correlated to the binding affinities of the putative binding sites. Slight binding was present in the *PXDN-A* section without treatment, which corresponds to the putative sites *PXDN-STAT3-6* and *PXDN-STAT3-7* and although these sites have lower predicted binding affinities. For section *PXDN-B*, that contained a putative binding site with the second highest binding affinity score, the ChIP-PCR analysis showed that STAT3 binding was detected in untreated cells, with weaker binding in IFN-γ and IL-6 treatment cells. For *PXDN-C*, STAT3 binding was seen in untreated cells and with IL-6 treatment; this is likely to indicate the putative *PXDN-STAT3-3* site which has the highest affinity binding score of all sites in this particular section (*PXDN-STAT3-10* and *PXDN-STAT3-13*). Although it was expected that the putative binding site with the highest affinity would show binding, there is no indication of STAT3 binding in section *PXDN-D* although it is possible that binding of STAT3 to this site could be induced by a different treatment or in different cell type. Unfortunately, binding potential could not be determined in *PXDN-E* as no substantial bands were detected. Although there is a very faint band in the IL-6 input control, the other controls showed no amplification and a band of the required size was seen in the gDNA control. This would indicate that the lack of amplification in the inputs is due to this amplicon section being susceptible to breakage during sonication resulting in failure of the polymerase to amplify across the region. Therefore, the absence of bands in the experimental samples does not indicated no binding of STAT3 in the *PXDN-E* section but rather an inability to detect potential binding. However, as only *PXDN-STAT3-12* is located in this section and since the binding affinity of this site is very low, the chance of binding in this region is unlikely.

We then looked at NF-κB binding to the *PXDN* promoter – all three predicted sites were very close to each other in *PXDN-C* section. ChIP-PCR data showed binding without treatment and in response to IFN-γ, but not IL-6.

Analysis of the *PXDNL* promoter region showed STAT3 binding in response to IL-6 for regions *PXDNL-A* (which contains 9 putative binding sites) and *PXDNL-C* (which contains 13 putative binding sites including *PXDNL-STAT3-1* and *PXDNL-STAT3-2*). As no binding is

observed in untreated cells, this would indicate that IL-6 induces binding of STAT3 to the *PXDNL* promoter.

Table 4.1: Summary of binding in the *PXDN* promoter region

	STAT3						NF-κB
	A	**B**	**C**	**D**	**E**		**C**
Untreated							
IFN-γ							
IL-6							

**Dark grey indicates higher levels of binding, light grey indicates lower binding and white indicates no binding.*

Table 4.2: Summary of binding in the *PXDNL* promoter region

	STAT3			
	A	**B**	**C**	**D**
Untreated				
IFN-γ				
IL-6				

**Light grey indicates lower binding and white indicates no binding.*

Binding of these transcription factors was expected due to the sheer number of predicted binding sites that were found in the PXDN and PXDNL promoter regions, especially for STAT3. However, as cytokines induce STAT3 and NF-κB pathways, we expected to find greater binding in IFN-γ and IL-6 treated cells compared to the untreated cells; however, this was not the case in the *PXDN* promoter. This may be reflective of the cancerous nature of the A549 cells as lung cancers have constitutively active STAT3 (Schütz et al. 2015) and NF-κB

(Saitoh et al. 2010), which would explain why binding was seen in untreated cells. However, cytokines (including IFN-γ and IL-6) do induce the activation of STAT3 and NF-κB in lung cancer (Hopewell et al. 2013; Dutta et al. 2015). PXDN is expressed in A549s without stimulation by cytokines therefore STAT3 and NF-κB could maintain basal levels of PXDN while greater binding effects could be seen with higher concentrations of the cytokine treatments or a combination of the treatments. Based on these findings, the increase in PXDN expression in response to IFN-γ is likely through the NF-κB pathway while the STAT3 pathway likely causes the increase in PXDN expression via IL-6. However, NF-κB and STAT3 are known to trigger other transcriptional pathways and therefore there may be a greater transcriptional network responsible for this PXDN expression in response to treatments (Hayden, West and Ghosh, 2006; Jafarzadeh, Nemati and Jafarzadeh, 2021). For PXDNL, the increased expression in response to IFN-γ may not be related to activation by STAT3, as it would appear that STAT3 binding was not induced by IFN-γ. An alternative could be through STAT1 activation that is also triggered by IFNy (Visan, 2015; Morris, Kershaw and Babon, 2018; Lv *et al.*, 2024). A preliminary scan for STAT1 binding in the *PXDNL* promoter region, revealed 23 putative binding sites (Appendix: **Table E**) which could indicate the potential of the STAT1 signalling pathway to upregulate *PXDNL* in the presence of IFN-γ. The presence of the STAT1 putative binding sites could also cause the formation of STAT1-STAT3 heterodimers in response to IL-6, which co-activates both STAT3 and STAT1 (Wang et al. 2023). However, although we were able to quantify data from end-point PCR, quantitative PCR (qPCR) would provide a more comprehensive assessment of the degree of binding between untreated and treated samples.

For ChIP-PCR, regions of the ICAM-1 promoter region were used to establish positive and negative binding control for NF-κB and STAT3 as previously established by ChIP-PCR (Kesanakurti *et al.*, 2012). Unfortunately, the regions established to be positive controls for NF-κB and STAT3 did not show binding while the region established as the negative control showed binding of both transcription factors. When these regions were searched for putative binding sites, five putative Rel-A binding sites with were found in the *ICAM-1 NF-κB positive* region (Appendix: **Table F-1**) and two putative STAT3 binding sites were found in the *ICAM-1 STAT3 positive* region (Appendix: **Table F-2**). Additionally, while no Rel-A putative binding sites were found in the *ICAM-1 negative* region, a more general binding region for NF-κB was identified along with two STAT3 binding sites (Appendix: **Table F-3**). The binding results of this study do not correlate with those found in the original study, which could be due to

differences in cell types and treatments as these sites were established in glioma xenograft cells following treatment with ionizing radiation. However, multiple other studies using various other methods have established regulation of ICAM-1 by NF-κB (Holden et al. 2004; Tamanini et al. 2003; Xue et al. 2009) and STAT3 (X. P. Yang et al. 2005; Wei et al. 2018; Han et al. 2016), which validates the use of this promoter to serve as a control for investigating binding of these transcription factors. Although this needs further refining and validation in our model.

Further investigation would be required to establish that STAT3 and NF-κB are responsible for the expression of PXDN and PXDNL in A549 cells in response to cytokines by assessing the full functionality of these transcriptional pathways. To account for the dimeric nature of these transcription factors, it would need to be established if there are any putative binding sites for other STAT transcription factors (most likely STAT1) and putative binding sites for p50 in the PXDN and PXDNL promoter regions which can be assessed with bioinformatics tools and ChIP-PCR. Based on these findings, regions that include sites for both monomers in the STAT heterodimer or homodimers and the NF-κB heterodimer (Rel-A and p50) would be cloned into a vector to be used for luciferase report assays.

This study was done *in vitro* and while cell culture serves as a useful model for study, there is limitations as to how representative it is of the organ. As cell growth in culture must be maintained by passaging, it limited the period over which the treatments could take place and the concentration and combination of cytokines had to be minimised to reduce toxicity in cell culture therefore characterised expression of PXDN and PXDNL may not be reflective of expression patterns observed in the clinical pathogenesis of COVID-19. Therefore, further consideration for PXDN and PXDNL expression could include modifying concentrations and combinations of cytokines to mimic those observed in clinical observations of the disease, as well as the time for secretion into the ECM and accumulation of the proteins especially within the context of a disease-like state. Cytokine storms and inflammatory responses are an amalgamation of cytokines and thus numerous downstream pathways are activated simultaneously. However, for the purpose of this study, cytokines were studied individually to investigate the specific pathways of activation. However, transcriptional regulation may be altered due to crosstalk between cytokines activating pathways such as the heterodimerisation of STAT1 and STAT3 when co-activation of IFN-γ and IL-6 (Qi et al. 2013).

Furthermore, this study was carried out using lung carcinoma cells (A549) as the model. It must be considered that A549 cells are derived from a carcinoma and the cancerous nature of

these cells may have contributed to the results of this study as *PXDN* and *PXDNL* are upregulated in cancers (Wyllie, Panagopoulos, and Cox 2023). However, as these cells are epithelial in origin, they gave an advantage of being more predictive of the lung structure, which was beneficial for the purposed of this study. An approach for future work could characterise PXDN and PXDNL expression patterns in myofibroblast cells as PXDN has been seen to be expressed by these cells (Péterfi *et al.*, 2009).

To contextualise the finding of this study, it must be questioned why PXDN and PXDNL would be expressed in parallel with an immune response. The role of PXDN in host immunity is a highly plausible explanation for PXDN to be regulated by immune response networks and with particular relevance to this study is the contribution of PXDN in host defence in lung cells (Shi *et al.*, 2018). Additionally, as role of PXDN in regulation of the ECM has been well established, it is reasonable to assume that it may be involved in matrix remodelling that allows for immune cells to migrate through tissues to reach and eliminate infected cells. The orientation and density of the ECM components control cell migration such that areas with looser collagen and fibronectin allow for cell mobility but areas where the ECM is more dense impedes migration therefore matrix remodelling allows for migration track for immune cells to navigate through and can recruit immune cells to affected areas (Bonnans, Chou, and Werb 2014). Notably, the study by You *et al.* (2018) demonstrates this potential mechanism by finding that PXDN mediates a pathway that promotes cell migration in pulmonary cells and is this is further validated by the involvement of NF-κB in this pathway. The potential function of PXDN (and PXDNL) in altering matrix architecture for migration of immune cells could be a further avenue to utilise in therapeutic intervention.

Furthermore, the association of PXDN and PXDNL to aspects of disease that are associated with COVID-19 would suggest that these proteins contribute to disease pathology. For example, the cytokine storm is seen to cause disseminated intravascular coagulation (DIC) leading to tissue ischemia and damage, and PXDN is activated by oxidative-stress pathways that contributes to ischemia-reperfusion injury (Mangalmurti and Hunter, 2020; Zhang *et al.*, 2012; Hanmer and Mavri-Damelin, 2018). Furthermore, a major physiological characteristic of ARDS is the upregulation of collagen in the alveolar space, which limits oxygenation (Y. Zhou et al. 2018). In progression to ARDS, the inflammatory response gradually increases over time to cause the severe illness as seen in **Figure 1.2** and therefore it stands to reason that if PXDN and PXDNL are transcriptionally mediated by cytokine stimulation then expression levels would be maintained through the inflammatory response. Since elevated levels of PXDN

and PXDNL have been linked to pathologies associated with severe COVID-19, such as tissue damage, ischemic reperfusion and fibrosis (Zhang *et al.*, 2012, You *et al.*, 2018) it implicates the putative role these proteins have in disease progression of COVID-19.

It has been observed that multisystemic conditions arise following a SARS-CoV-2 infection. This is referred to has long COVID and occurs in 50-70% of patients who were hospitalised with COVID-19 and in 10-30% of people who had COVID-19 but were not hospitalised (Davis et al. 2023). One condition that is seen with long COVID is pulmonary fibrosis (Alrajhi 2023) and as PXDN has been associated with fibrosis (Cheng and Shi 2022), it could suggest PXDN as a contributor to this COVID-19 complication. Similarly, myocardial fibrosis has been found in patients with long COVID (Krishnan et al. 2022) and as PXDNL has been shown to have contributions to fibrosis in the heart (Péterfi *et al.*, 2014), elucidating PXDNL in possible disease progression, which are further avenues for exploration; indeed our lab has previously shown TGF-β to regulate PXDN expression (Sitole and Mavri-Damelin 2018) .

While the COVID-19 pandemics has inspired further research into cytokine storms, this aberrant expression of cytokines is not unique to the COVID-19 disease and can also be present in multiple upper respiratory infections, other respiratory disorders like asthma and lifestyle related conditions such as emphysema from smoking (Barnes 2012; Morello Gearhart et al. 2017; Barnes 2018). Therefore, building from this research could bring forward implications of PXDN and PXDNL expression in more diseases of the lung.

5. Conclusion

PXDN and PXDNL are expressed in lung tissue and this is seen to be upregulated in the presence of specific cytokines namely IFN-γ and IL-6. PXDN is likely upregulated by NF-κB in response to IFN-γ, and by STAT3 in response to IFN-γ and IL-6, while PXDNL expression in response to IL-6 is likely caused by STAT3. These findings imply that PXDN and PXDNL are regulated as part of the immune response and therefore in the case of an aberrant immune response such as a cytokine storm, their expression would subsequently be dysregulated and their abnormal expression could contribute to clinical manifestations of disease such as tissue damage and fibrosis. This would make PXDN and PXDNL suitable targets for therapeutic intervention or biomarkers to indicate diagnosis and prognosis for COVID-19.

6. References

Akamatsu, Milena Apetito, Júlia Tavares de Castro, Carolina Yumi Takano, and Paulo Lee Ho. 2021. "Off Balance: Interferons in COVID-19 Lung Infections." *EBioMedicine* 73 (November). https://doi.org/10.1016/j.ebiom.2021.103642.

Alrajhi, Nuha Nasser. 2023. "Post-COVID-19 Pulmonary Fibrosis: An Ongoing Concern." *Annals of Thoracic Medicine* 18 (4): 173. https://doi.org/10.4103/ATM.ATM_7_23.

Andersen, Kristian G., Andrew Rambaut, W. Ian Lipkin, Edward C. Holmes, and Robert F. Garry. 2020. "The Proximal Origin of SARS-CoV-2." *Nature Medicine* 26 (4): 450–52. https://doi.org/10.1038/S41591-020-0820-9.

Bar-On, Yinon M., Avi Flamholz, Rob Phillips, and Ron Milo. 2020. "SARS-CoV-2 (COVID-19) by the Numbers." *ELife* 9 (March): e57309. https://doi.org/10.7554/ELIFE.57309.

Barnes, Peter J. 2012. "The Cytokine Network in Chronic Obstructive Pulmonary Disease." *Https://Doi.Org/10.1165/Rcmb.2009-0220TR* 41 (6): 631–38. https://doi.org/10.1165/RCMB.2009-0220TR.

Barnes, Peter J.. 2018. "Targeting Cytokines to Treat Asthma and Chronic Obstructive Pulmonary Disease." *Nature Reviews Immunology 2018 18:7* 18 (7): 454–66. https://doi.org/10.1038/s41577-018-0006-6.

Bass, J. J., D. J. Wilkinson, D. Rankin, B. E. Phillips, N. J. Szewczyk, K. Smith, and P. J. Atherton. 2016. "An Overview of Technical Considerations for Western Blotting Applications to Physiological Research." *Scandinavian Journal of Medicine & Science in Sports* 27 (1): 4. https://doi.org/10.1111/SMS.12702.

Bhave, Gautam, Christopher F. Cummings, Roberto M. Vanacore, Chino Kumagai-Cresse, Isi A. Ero-Tolliver, Mohamed Rafi, Jeong Suk Kang, et al. 2012. "Peroxidasin Forms Sulfilimine Chemical Bonds Using Hypohalous Acids in Tissue Genesis." *Nature Chemical Biology* 8 (9): 784–90. https://doi.org/10.1038/NCHEMBIO.1038.

Bonnans, Caroline, Jonathan Chou, and Zena Werb. 2014. "Remodelling the Extracellular Matrix in Development and Disease." *Nature Reviews. Molecular Cell Biology* 15 (12): 786. https://doi.org/10.1038/NRM3904.

Boost, Kim A., Christian D. Sadik, Malte Bachmann, Bernhard Zwissler, Josef Pfeilschifter, and Heiko Mühl. 2008. "IFN-Gamma Impairs Release of IL-8 by IL-1beta-Stimulated A549 Lung Carcinoma Cells." *BMC Cancer* 8 (1): 1–8. https://doi.org/10.1186/1471-2407-8-265/FIGURES/3.

Bordallo, Bruno, Mozart Bellas, Arthur Fernandes Cortez, Matheus Vieira, and Marcelo Pinheiro. 2020. "Severe COVID-19: What Have We Learned with the Immunopathogenesis?" *Advances in Rheumatology* 60 (1): 1–13. https://doi.org/10.1186/S42358-020-00151-7/FIGURES/3.

Bramhall, S., N. Noack, M. Wu, and J. R. Loewenberg. 1969. "A Simple Colorimetric Method for Determination of Protein." *Analytical Biochemistry* 31 (C): 146–48. https://doi.org/10.1016/0003-2697(69)90251-6.

Cascella, Marco, Michael Rajnik, Arturo Cuomo, Scott C. Dulebohn, and Raffaela Di Napoli. 2023. "Features, Evaluation, and Treatment of Coronavirus (COVID-19)." *StatPearls*,

August. https://www.ncbi.nlm.nih.gov/books/NBK554776/.

Castelli, Vanessa, Annamaria Cimini, and Claudio Ferri. 2020. "Cytokine Storm in COVID-19: 'When You Come Out of the Storm, You Won't Be the Same Person Who Walked in.'" *Frontiers in Immunology* 11 (September): 2132. https://doi.org/10.3389/FIMMU.2020.02132/BIBTEX.

Castro-Mondragon, Jaime A., Rafael Riudavets-Puig, Ieva Rauluseviciute, Roza Berhanu Lemma, Laura Turchi, Romain Blanc-Mathieu, Jeremy Lucas, et al. 2022. "JASPAR 2022: The 9th Release of the Open-Access Database of Transcription Factor Binding Profiles." *Nucleic Acids Research* 50 (D1): D165–73. https://doi.org/10.1093/NAR/GKAB1113.

Chen, Li Da, Zhen Yu Zhang, Xiao Jie Wei, Yu Qing Cai, Weng Zhen Yao, Ming Hui Wang, Qiu Fen Huang, and Xiao Bin Zhang. 2020. "Association between Cytokine Profiles and Lung Injury in COVID-19 Pneumonia." *Respiratory Research* 21 (1): 1–8. https://doi.org/10.1186/S12931-020-01465-2/FIGURES/3.

Cheng, Guangjie, and Ruizheng Shi. 2022. "Mammalian Peroxidasin (PXDN): From Physiology to Pathology." *Free Radical Biology & Medicine* 182 (March): 100. https://doi.org/10.1016/J.FREERADBIOMED.2022.02.026.

Choi, Alex, Richard Lao, Paul Ling-Fung Tang, Eunice Wan, Wasima Mayer, Tanya Bardakjian, Gary M. Shaw, Pui Yan Kwok, Adele Schneider, and Anne Slavotinek. 2015. "Novel Mutations in PXDN Cause Microphthalmia and Anterior Segment Dysgenesis." *European Journal of Human Genetics* 23 (3): 337–41. https://doi.org/10.1038/ejhg.2014.119.

Colon, Selene, Patrick Page-McCaw, and Gautam Bhave. 2017. "Role of Hypohalous Acids in Basement Membrane Homeostasis." *Antioxidants & Redox Signaling* 27 (12): 839–54. https://doi.org/10.1089/ARS.2017.7245.

Corbière, Véronique, Violette Dirix, Sarah Norrenberg, Mattéo Cappello, Myriam Remmelink, and Françoise Mascart. 2011. "Phenotypic Characteristics of Human Type II Alveolar Epithelial Cells Suitable for Antigen Presentation to T Lymphocytes." *Respiratory Research* 12 (1). https://doi.org/10.1186/1465-9921-12-15.

Davis, Hannah E., Lisa McCorkell, Julia Moore Vogel, and Eric J. Topol. 2023. "Long COVID: Major Findings, Mechanisms and Recommendations." *Nature Reviews Microbiology 2023 21:3* 21 (3): 133–46. https://doi.org/10.1038/s41579-022-00846-2.

Declercq, Jozefien, Elisabeth De Leeuw, and Bart N. Lambrecht. 2022. "Inflammasomes and IL-1 Family Cytokines in SARS-CoV-2 Infection: From Prognostic Marker to Therapeutic Agent." *Cytokine* 157 (September): 155934. https://doi.org/10.1016/J.CYTO.2022.155934.

Dougan, Jodi, Ohuod Hawsawi, Liza J. Burton, Gabrielle Edwards, Kia Jones, Jin Zou, Peri Nagappan, et al. 2019. "Proteomics-Metabolomics Combined Approach Identifies Peroxidasin as a Protector against Metabolic and Oxidative Stress in Prostate Cancer." *International Journal of Molecular Sciences* 20 (12). https://doi.org/10.3390/ijms20123046.

Dutta, Pranabananda, Nafiseh Sabri, Jinghong Li, and Willis X Li. 2015. "Role of STAT3 in Lung Cancer." *JAK-STAT* 3 (4): e999503. https://doi.org/10.1080/21623996.2014.999503.

Eda, Hiroyuki, Barry L. Burnette, Hideaki Shimada, Heidi R. Hope, and Joseph B. Monahan. 2011. “Interleukin-1β-Induced Interleukin-6 Production in A549 Cells Is Mediated by Both Phosphatidylinositol 3-Kinase and Interleukin-1 Receptor-Associated Kinase-4.” *Cell Biology International* 35 (4): 355–58. https://doi.org/10.1042/CBI20100247.

Fathima, Tahreem, M. P. Brundha, and D. Ezhilarasan. 2020. “Role of Interferon Gamma in COVID-19 Prevention - A Review.” *International Journal of Current Research and Review* 12 (21 Special Issue): 91–96. https://doi.org/10.31782/IJCRR.2020.SP42.

Gleeson, Tara A, Erik Nordling, Christina Kaiser, Catherine B Lawrence, David Brough, Jack P Green, and Stuart M Allan. 2022. “Looking into the IL-1 of the Storm: Are Inflammasomes the Link between Immunothrombosis and Hyperinflammation in Cytokine Storm Syndromes?” *Discovery Immunology* 1 (1). https://doi.org/10.1093/DISCIM/KYAC005.

Gopallawa, Indiwari, Li Eon Kuek, Nithin D. Adappa, James N. Palmer, and Robert J. Lee. 2021. “Small-Molecule Akt-Activation in Airway Cells Induces NO Production and Reduces IL-8 Transcription through Nrf-2.” *Respiratory Research* 22 (1): 1–17. https://doi.org/10.1186/S12931-021-01865-Y/FIGURES/7.

Gudowska-Sawczuk, Monika, and Barbara Mroczko. 2022. “The Role of Nuclear Factor Kappa B (NF-KB) in Development and Treatment of COVID-19: Review.” *International Journal of Molecular Sciences* 23 (9): 5283. https://doi.org/10.3390/IJMS23095283.

Guo, Yan Rong, Qing Dong Cao, Zhong Si Hong, Yuan Yang Tan, Shou Deng Chen, Hong Jun Jin, Kai Sen Tan, De Yun Wang, and Yan Yan. 2020. “The Origin, Transmission and Clinical Therapies on Coronavirus Disease 2019 (COVID-19) Outbreak – an Update on the Status.” *Military Medical Research* 7 (1): 11. https://doi.org/10.1186/S40779-020-00240-0.

Guo, Yi, Ke Hu, Yuxuan Li, Chanjun Lu, Ken Ling, Chuanqi Cai, Weici Wang, and Dawei Ye. 2022. “Targeting TNF-α for COVID-19: Recent Advanced and Controversies.” *Frontiers in Public Health* 10 (February): 153. https://doi.org/10.3389/FPUBH.2022.833967/BIBTEX.

Han, Xiao, Yuxi Wang, Hailong Chen, Jingwen Zhang, Caiming Xu, Jian Li, and Mingyue Li. 2016. “Enhancement of ICAM-1 via the JAK2/STAT3 Signaling Pathway in a Rat Model of Severe Acute Pancreatitis-Associated Lung Injury.” *Experimental and Therapeutic Medicine* 11 (3): 788. https://doi.org/10.3892/ETM.2016.2988.

Hanmer, Kerry L., and Demetra Mavri-Damelin. 2018. “Peroxidasin Is a Novel Target of the Redox-Sensitive Transcription Factor Nrf2.” *Gene* 674 (October): 104–14. https://doi.org/10.1016/j.gene.2018.06.076.

Haring, Max, Sascha Offermann, Tanja Danker, Ina Horst, Christoph Peterhansel, and Maike Stam. 2007. “Chromatin Immunoprecipitation: Optimization, Quantitative Analysis and Data Normalization.” *Plant Methods* 3 (1): 11. https://doi.org/10.1186/1746-4811-3-11.

Hayden, M. S., A. P. West, and S. Ghosh. 2006. “NF-KappaB and the Immune Response.” *Oncogene* 25 (51): 6758–80. https://doi.org/10.1038/SJ.ONC.1209943.

Hillmer, Emily J., Huiyuan Zhang, Haiyan S. Li, and Stephanie S. Watowich. 2016. “STAT3 Signaling in Immunity.” *Cytokine & Growth Factor Reviews* 31 (October): 1. https://doi.org/10.1016/J.CYTOGFR.2016.05.001.

Holden, Neil S., Matthew C. Catley, Lisa M. Cambridge, Peter J. Barnes, and Robert Newton. 2004. “ICAM-1 Expression Is Highly NF-KB-Dependent in A549 Cells.” *European Journal of Biochemistry* 271 (4): 785–91. https://doi.org/10.1111/J.1432-1033.2004.03982.X.

Hopewell, Emily L., Weipeng Zhao, William J. Fulp, Crystina C. Bronk, Alexis S. Lopez, Michael Massengill, Scott Antonia, et al. 2013. “Lung Tumor NF-KB Signaling Promotes T Cell–Mediated Immune Surveillance.” *The Journal of Clinical Investigation* 123 (6): 2509. https://doi.org/10.1172/JCI67250.

Hu, Xiaoyi, Jing li, Maorong Fu, Xia Zhao, and Wei Wang. 2021. “The JAK/STAT Signaling Pathway: From Bench to Clinic.” *Signal Transduction and Targeted Therapy 2021 6:1* 6 (1): 1–33. https://doi.org/10.1038/s41392-021-00791-1.

Im, Kyuseok, Sergey Mareninov, M. Fernando Palma Diaz, and William H. Yong. 2019. “An Introduction to Performing Immunofluorescence Staining.” *Methods in Molecular Biology (Clifton, N.J.)* 1897: 299. https://doi.org/10.1007/978-1-4939-8935-5_26.

Jafarzadeh, Abdollah, Maryam Nemati, and Sara Jafarzadeh. 2021. “Contribution of STAT3 to the Pathogenesis of COVID-19.” *Microbial Pathogenesis* 154 (May): 104836. https://doi.org/10.1016/J.MICPATH.2021.104836.

Jafarzadeh, Abdollah, Maryam Nemati, and Sara Jafarzadeh. 2021. 2021. “Contribution of STAT3 to the Pathogenesis of COVID-19.” *Microbial Pathogenesis* 154 (May): 104836. https://doi.org/10.1016/J.MICPATH.2021.104836.

Jang, Dan In, A. Hyeon Lee, Hye Yoon Shin, Hyo Ryeong Song, Jong Hwi Park, Tae Bong Kang, Sang Ryong Lee, and Seung Hoon Yang. 2021. “The Role of Tumor Necrosis Factor Alpha (TNF-α) in Autoimmune Disease and Current TNF-α Inhibitors in Therapeutics.” *International Journal of Molecular Sciences* 22 (5): 2719. https://doi.org/10.3390/IJMS22052719.

Joseph, Adrien, Lara Zafrani, Asma Mabrouki, Elie Azoulay, and Michael Darmon. 2020. “Acute Kidney Injury in Patients with SARS-CoV-2 Infection.” *Annals of Intensive Care* 10 (1): 1–8. https://doi.org/10.1186/S13613-020-00734-Z/TABLES/2.

Kaneko, Naoe, Mie Kurata, Toshihiro Yamamoto, Shinnosuke Morikawa, and Junya Masumoto. 2019. “The Role of Interleukin-1 in General Pathology.” *Inflammation and Regeneration 2019 39:1* 39 (1): 1–16. https://doi.org/10.1186/S41232-019-0101-5.

Kesanakurti, D., C. Chetty, D. Rajasekhar Maddirela, M. Gujrati, and J. S. Rao. 2012. “Essential Role of Cooperative NF-KB and Stat3 Recruitment to ICAM-1 Intronic Consensus Elements in the Regulation of Radiation-Induced Invasion and Migration in Glioma.” *Oncogene* 32 (43): 10.1038/onc.2012.546. https://doi.org/10.1038/ONC.2012.546.

Kesanakurti, D., C. Chetty, D. Rajasekhar Maddirela, M. Gujrati, and J. S. Rao.. 2012. “Essential Role of Cooperative NF-KB and Stat3 Recruitment to ICAM-1 Intronic Consensus Elements in the Regulation of Radiation-Induced Invasion and Migration in Glioma.” *Oncogene* 32 (43): 10.1038/onc.2012.546. https://doi.org/10.1038/ONC.2012.546.

Khan, Kamron, Adam Rudkin, David A. Parry, Kathryn P. Burdon, Martin McKibbin, Clare V. Logan, Zakia I.A. Abdelhamed, et al. 2011. “Homozygous Mutations in PXDN Cause Congenital Cataract, Corneal Opacity, and Developmental Glaucoma.” *American*

Journal of Human Genetics 89 (3): 464–73. https://doi.org/10.1016/j.ajhg.2011.08.005.

Kokkotis, Georgios, Konstantina Kitsou, Ioannis Xynogalas, Vana Spoulou, Gkikas Magiorkinis, Ioannis Trontzas, Panagiotis Trontzas, Garyphallia Poulakou, Konstantinos Syrigos, and Giorgos Bamias. 2022. "Systematic Review with Meta-Analysis: COVID-19 Outcomes in Patients Receiving Anti-TNF Treatments." *Alimentary Pharmacology & Therapeutics* 55 (2): 154–67. https://doi.org/10.1111/APT.16717.

Krishnan, A., K. A. Ellenberger, C. Phetsouphanh, A. P. Kelleher, G. V. Matthews, D. R. Darley, and C. J. Holloway. 2022. "Myocardial Fibrosis Occurs in Non-Hospitalised Patients with Chronic Symptoms after COVID-19." *International Journal of Cardiology. Heart & Vasculature* 39 (April): 100964. https://doi.org/10.1016/J.IJCHA.2022.100964.

Kumar, Manish, Nitin Dhaka, Tahseen Raza, Prikshat Dadhwal, Hanudatta S. Atreya, and Sulakshana P. Mukherjee. 2021. "Domain Stability Regulated through the Dimer Interface Controls the Formation Kinetics of a Specific NF-KB Dimer." *Biochemistry* 60 (7): 513–23. https://doi.org/10.1021/ACS.BIOCHEM.0C00837/SUPPL_FILE/BI0C00837_SI_001.PDF.

Lampi, Marsha C., and Cynthia A. Reinhart-King. 2018. "Targeting Extracellular Matrix Stiffness to Attenuate Disease: From Molecular Mechanisms to Clinical Trials." *Science Translational Medicine* 10 (422). https://doi.org/10.1126/SCITRANSLMED.AAO0475.

Lázár, Eniko, Zalán Péterfi, Gábor Sirokmány, Hajnal A. Kovács, Eva Klement, Katalin F. Medzihradszky, and Miklós Geiszt. 2015. "Structure-Function Analysis of Peroxidasin Provides Insight into the Mechanism of Collagen IV Crosslinking." *Free Radical Biology and Medicine* 83 (June): 273–82. https://doi.org/10.1016/j.freeradbiomed.2015.02.015.

Li, Chaofan, Wei Qian, Xiaoqin Wei, Harish Narasimhan, Yue Wu, Mohd Arish, In Su Cheon, et al. 2024. "Comparative Single-Cell Analysis Reveals IFN-γ as a Driver of Respiratory Sequelae after Acute COVID-19." *Science Translational Medicine* 16 (756). https://doi.org/10.1126/SCITRANSLMED.ADN0136/SUPPL_FILE/SCITRANSLMED.ADN0136_MDAR_REPRODUCIBILITY_CHECKLIST.PDF.

Li, Hong, Zehong Cao, Guogang Zhang, Victor J. Thannickal, and Guangjie Cheng. 2012. "Vascular Peroxidase 1 Catalyzes the Formation of Hypohalous Acids: Characterization of Its Substrate Specificity and Enzymatic Properties." *Free Radical Biology and Medicine* 53 (10): 1954–59. https://doi.org/10.1016/J.FREERADBIOMED.2012.08.597.

Li, Jie, and Jian Gao Fan. 2020. "Characteristics and Mechanism of Liver Injury in 2019 Coronavirus Disease." *Journal of Clinical and Translational Hepatology* 8 (1): 13. https://doi.org/10.14218/JCTH.2020.00019.

Li, Li, and Peter E. Shaw. 2004. "A STAT3 Dimer Formed by Inter-Chain Disulphide Bridging during Oxidative Stress." *Biochemical and Biophysical Research Communications* 322 (3): 1005–11. https://doi.org/10.1016/J.BBRC.2004.08.014.

Li, Yanqing, Yan Jiao, Zhangping Luo, Yang Li, and Yanan Liu. 2019. "High Peroxidasin-like Expression Is a Potential and Independent Prognostic Biomarker in Breast Cancer." *Medicine* 98 (44): e17703. https://doi.org/10.1097/MD.0000000000017703.

Liu, Jia, Yufeng Li, Qian Liu, Qun Yao, Xi Wang, Huanyu Zhang, Rong Chen, et al. 2021.

"SARS-CoV-2 Cell Tropism and Multiorgan Infection." *Cell Discovery 2021 7:1* 7 (1): 1–4. https://doi.org/10.1038/s41421-021-00249-2.

Liu, Ting, Lingyun Zhang, Donghyun Joo, and Shao Cong Sun. 2017. "NF-KB Signaling in Inflammation." *Signal Transduction and Targeted Therapy 2017 2:1* 2 (1): 1–9. https://doi.org/10.1038/sigtrans.2017.23.

Liu, Ting, Lingyun Zhang, Donghyun Joo, and Shao Cong Sun. 2017. 2017. "NF-KB Signaling in Inflammation." *Signal Transduction and Targeted Therapy 2017 2:1* 2 (1): 1–9. https://doi.org/10.1038/sigtrans.2017.23.

Liu, Zhaoya, Qian Xu, Qixin Yang, Jing Cao, Cong Wu, Huihui Peng, Xinyi Zhang, et al. 2019. "Vascular Peroxidase 1 Is a Novel Regulator of Cardiac Fibrosis after Myocardial Infarction." *Redox Biology* 22 (April): 101151. https://doi.org/10.1016/J.REDOX.2019.101151.

Lu, Miaolong, Bolong Liu, Dongyang Li, Zhentao Gao, Wenbiao Li, Xiangfu Zhou, and Hailun Zhan. 2023. "PXDNL Activates the Motility of Urothelial Bladder Carcinoma Cells through the Wnt/β-Catenin Pathway and Has a Prognostic Value." *Life Sciences* 312 (January): 121270. https://doi.org/10.1016/J.LFS.2022.121270.

Lv, You, Jianxun Qi, Jeffrey J. Babon, Longxing Cao, Guohuang Fan, Jiajia Lang, Jin Zhang, Pengbing Mi, Bostjan Kobe, and Faming Wang. 2024. "The JAK-STAT Pathway: From Structural Biology to Cytokine Engineering." *Signal Transduction and Targeted Therapy 2024 9:1* 9 (1): 1–37. https://doi.org/10.1038/s41392-024-01934-w.

Mahmood, Tahrin, and Ping Chang Yang. 2012. "Western Blot: Technique, Theory, and Trouble Shooting." *North American Journal of Medical Sciences* 4 (9): 429. https://doi.org/10.4103/1947-2714.100998.

Mangalmurti, Nilam, and Christopher A. Hunter. 2020. "Cytokine Storms: Understanding COVID-19." *Immunity* 53 (1): 19–25. https://doi.org/10.1016/J.IMMUNI.2020.06.017.

Marshall, Jean S., Richard Warrington, Wade Watson, and Harold L. Kim. 2018. "An Introduction to Immunology and Immunopathology." *Allergy, Asthma and Clinical Immunology* 14 (2): 1–10. https://doi.org/10.1186/S13223-018-0278-1/TABLES/4.

Martincuks, Antons, Katarzyna Andryka, Andrea Küster, Hildegard Schmitz-Van de Leur, Michal Komorowski, and Gerhard Müller-Newen. 2017. "Nuclear Translocation of STAT3 and NF-KB Are Independent of Each Other but NF-KB Supports Expression and Activation of STAT3." *Cellular Signalling* 32 (April): 36–47. https://doi.org/10.1016/J.CELLSIG.2017.01.006.

Medfai, Hayfa, Alia Khalil, Alexandre Rousseau, Vincent Nuyens, Martina Paumann-Page, Benjamin Sevcnikar, Paul G. Furtmüller, et al. 2019. "Human Peroxidasin 1 Promotes Angiogenesis through ERK1/2, Akt, and FAK Pathways." *Cardiovascular Research* 115 (2): 463–75. https://doi.org/10.1093/cvr/cvy179.

Mitchell, Jane A, Maria G Belvisi, Tpravit Akarasereenont, Richard A Robbins, O.-Jung Kwon, Tjamie Croxtall, Peter J Barnes, and R Vane. 1994. "Induction of Cyclo-Oxygenase-2 by Cytokines in Human Pulmonary Epithelial Cells: Regulation by Dexamethasone." *Br. J. PharmacoL*. Vol. 113. https://doi.org/10.1111/j.1476-5381.1994.tb17093.x.

Mogensen, Trine H. 2009. "Pathogen Recognition and Inflammatory Signaling in Innate

Immune Defenses." *Clinical Microbiology Reviews* 22 (2): 240. https://doi.org/10.1128/CMR.00046-08.

Mohd Zawawi, Zarina, Jeevanathan Kalyanasundram, Rozainanee Mohd Zain, Ravindran Thayan, Dayang Fredalina Basri, and Wei Boon Yap. 2023. "Prospective Roles of Tumor Necrosis Factor-Alpha (TNF-α) in COVID-19: Prognosis, Therapeutic and Management." *International Journal of Molecular Sciences* 24 (7). https://doi.org/10.3390/IJMS24076142.

Montazersaheb, Soheila, Seyed Mahdi Hosseiniyan Khatibi, Mohammad Saeid Hejazi, Vahideh Tarhriz, Afsaneh Farjami, Faramarz Ghasemian Sorbeni, Raheleh Farahzadi, and Tohid Ghasemnejad. 2022. "COVID-19 Infection: An Overview on Cytokine Storm and Related Interventions." *Virology Journal 2022 19:1* 19 (1): 1–15. https://doi.org/10.1186/S12985-022-01814-1.

Morello Gearhart, Alessandra, Rodrigo Cavallazzi, Paula Peyrani, Timothy L. Wiemken, Stephen P. Furmanek, Andrea Reyes-Vega, Umair Gauhar, et al. 2017. "Lung Cytokines and Systemic Inflammation in Patients with COPD." *The University of Louisville Journal of Respiratory Infections* 1 (4): 4. https://doi.org/10.18297/jri/vol1/iss4/4.

Morris, Rhiannon, Nadia J. Kershaw, and Jeffrey J. Babon. 2018. "The Molecular Details of Cytokine Signaling via the JAK/STAT Pathway." *Protein Science : A Publication of the Protein Society* 27 (12): 1984. https://doi.org/10.1002/PRO.3519.

Morris, Rhiannon, Nadia J. Kershaw, and Jeffrey J. Babon. 2018. "The Molecular Details of Cytokine Signaling via the JAK/STAT Pathway." *Protein Science : A Publication of the Protein Society* 27 (12): 1984. https://doi.org/10.1002/PRO.3519.

Nelson, Robert E., Liselotte I. Fessler, Yasumitsu Takagi, Bruce Blumberg, Douglas R. Keene, Pamela F. Olson, Carol G. Parker, and John H. Fessler. 1994. "Peroxidasin: A Novel Enzyme-matrix Protein of Drosophila Development." *The EMBO Journal* 13 (15): 3438–47. https://doi.org/10.1002/J.1460-2075.1994.TB06649.X.

Papageorgiou, Anna Pia, and Stephane Heymans. 2014. "Peroxidasin-like Protein: Expanding the Horizons of Matrix Biology." *Cardiovascular Research*. Oxford Academic. https://doi.org/10.1093/cvr/cvu017.

Péterfi, Zalán, Ágnes Donkó, Anna Orient, Adrienn Sum, Ágnes Prókai, Beáta Molnár, Zoltán Veréb, et al. 2009. "Peroxidasin Is Secreted and Incorporated into the Extracellular Matrix of Myofibroblasts and Fibrotic Kidney." *The American Journal of Pathology* 175 (2): 725. https://doi.org/10.2353/AJPATH.2009.080693.

Péterfi, Zalán, Ágnes Donkó, Anna Orient, Adrienn Sum, Ágnes Prókai, Beáta Molnár, Zoltán Veréb, et al.. 2009. "Peroxidasin Is Secreted and Incorporated into the Extracellular Matrix of Myofibroblasts and Fibrotic Kidney." *American Journal of Pathology* 175 (2): 725–35. https://doi.org/10.2353/ajpath.2009.080693.

Péterfi, Zalán, and Miklós Geiszt. 2014. "Peroxidasins: Novel Players in Tissue Genesis." *Trends in Biochemical Sciences* 39 (7): 305–7. https://doi.org/10.1016/J.TIBS.2014.05.005.

Péterfi, Zalán, Zsuzsanna E. Tóth, Hajnal A. Kovács, Enik Lázár, Adrienn Sum, Ágnes Donkó, Gábor Sirokmány, Ajay M. Shah, and Miklós Geiszt. 2014. "Peroxidasin-like Protein: A Novel Peroxidase Homologue in the Human Heart." *Cardiovascular Research* 101 (3): 393–99. https://doi.org/10.1093/CVR/CVT256.

Péterfi, Zalán, Zsuzsanna E. Tóth, Hajnal A. Kovács, Enik Lázár, Adrienn Sum, Ágnes Donkó, Gábor Sirokmány, Ajay M. Shah, and Miklós Geiszt.. 2014. “Peroxidasin-like Protein: A Novel Peroxidase Homologue in the Human Heart.” *Cardiovascular Research* 101 (3): 393–99. https://doi.org/10.1093/cvr/cvt256.

Potere, Nicola, Evan Garrad, Yogendra Kanthi, Marcello Di Nisio, Gilles Kaplanski, Aldo Bonaventura, Jean Marie Connors, Raffaele De Caterina, and Antonio Abbate. 2023. “NLRP3 Inflammasome and Interleukin-1 Contributions to COVID-19-Associated Coagulopathy and Immunothrombosis.” *Cardiovascular Research* 119 (11): 2046. https://doi.org/10.1093/CVR/CVAD084.

Purbey, Prabhat K., Koushik Roy, Sandeep Gupta, and Manash K. Paul. 2023. “Mechanistic Insight into the Protective and Pathogenic Immune-Responses against SARS-CoV-2.” *Molecular Immunology* 156 (April): 111. https://doi.org/10.1016/J.MOLIMM.2023.03.009.

Qi, Yun feng, Yan xin Huang, Hong yan Wang, Y. Zhang, Yong li Bao, Lu guo Sun, Yin Wu, et al. 2013. “Elucidating the Crosstalk Mechanism between IFN-Gamma and IL-6 via Mathematical Modelling.” *BMC Bioinformatics* 14 (1): 41. https://doi.org/10.1186/1471-2105-14-41/FIGURES/9.

Queiroz, Maria Alice Freitas, Pablo Fabiano Moura das Neves, Sandra Souza Lima, Jeferson da Costa Lopes, Maria Karoliny da Silva Torres, Izaura Maria Vieira Cayres Vallinoto, Carlos David Araújo Bichara, et al. 2022. “Cytokine Profiles Associated With Acute COVID-19 and Long COVID-19 Syndrome.” *Frontiers in Cellular and Infection Microbiology* 12 (June). https://doi.org/10.3389/FCIMB.2022.922422.

Ragab, Dina, Haitham Salah Eldin, Mohamed Taeimah, Rasha Khattab, and Ramy Salem. 2020. “The COVID-19 Cytokine Storm; What We Know So Far.” *Frontiers in Immunology* 11 (June): 1446. https://doi.org/10.3389/FIMMU.2020.01446/BIBTEX.

Riss, Terry L, Richard A Moravec, Andrew L Niles, Sarah Duellman, Hélène A Benink, Tracy J Worzella, and Lisa Minor. 2016. “Cell Viability Assays.” *Assay Guidance Manual*, July. https://www.ncbi.nlm.nih.gov/books/NBK144065/.

Saitoh, Yasunori, Vicente Javier Martínez Bruyn, Shin Uota, Atsuhiko Hasegawa, Naoki Yamamoto, Issei Imoto, Johji Inazawa, and Shoji Yamaoka. 2010. “Overexpression of NF-KB Inducing Kinase Underlies Constitutive NF-KB Activation in Lung Cancer Cells.” *Lung Cancer (Amsterdam, Netherlands)* 70 (3): 263–70. https://doi.org/10.1016/J.LUNGCAN.2010.03.001.

Sapir, Tzuriel, Zaelig Averch, Brian Lerman, Abraham Bodzin, Yeshaya Fishman, and Radhashree Maitra. 2022. “COVID-19 and the Immune Response: A Multi-Phasic Approach to the Treatment of COVID-19.” *International Journal of Molecular Sciences* 23 (15): 8606. https://doi.org/10.3390/IJMS23158606.

Schütz, Alexander, Katrin Röser, Jana Klitzsch, Franziska Lieder, Fritz Aberger, Wolfgang Gruber, Kristina M. Mueller, Alexander Pupyshev, Richard Moriggl, and Karlheinz Friedrich. 2015. “Lung Adenocarcinomas and Lung Cancer Cell Lines Show Association of MMP-1 Expression With STAT3 Activation.” *Translational Oncology* 8 (2): 97–105. https://doi.org/10.1016/J.TRANON.2015.02.002.

Sharma, Anshika, Isra Ahmad Farouk, and Sunil Kumar Lal. 2021. “COVID-19: A Review on the Novel Coronavirus Disease Evolution, Transmission, Detection, Control and

Prevention." *Viruses* 13 (2): 202. https://doi.org/10.3390/V13020202.

Shcherbak, Sergey G., Anna Yu Anisenkova, Sergei V. Mosenko, Oleg S. Glotov, Alexander N. Chernov, Svetlana V. Apalko, Stanislav P. Urazov, et al. 2021. "Basic Predictive Risk Factors for Cytokine Storms in COVID-19 Patients." *Frontiers in Immunology* 12 (November): 745515. https://doi.org/10.3389/FIMMU.2021.745515/FULL.

Shi, Ruizheng, Zehong Cao, Hong Li, Jochen Graw, Guogang Zhang, Victor J. Thannickal, and Guangjie Cheng. 2018. "Peroxidasin Contributes to Lung Host Defense by Direct Binding and Killing of Gram-Negative Bacteria." *PLoS Pathogens* 14 (5). https://doi.org/10.1371/journal.ppat.1007026.

Shi, Ruizheng, Zehong Cao, Hong Li, Jochen Graw, Guogang Zhang, Victor J. Thannickal, and Guangjie Cheng. 2018. "Peroxidasin Contributes to Lung Host Defense by Direct Binding and Killing of Gram-Negative Bacteria." *PLoS Pathogens* 14 (5): e1007026. https://doi.org/10.1371/JOURNAL.PPAT.1007026.

Sitole, Boitumelo Nonhlanhla, and Demetra Mavri-Damelin. 2018. "Peroxidasin Is Regulated by the Epithelial-Mesenchymal Transition Master Transcription Factor Snai1." *Gene* 646 (March): 195–202. https://doi.org/10.1016/j.gene.2018.01.011.

Soudi, Monika, Marcel Zamocky, Christa Jakopitsch, Paul G. Furtmüller, and Christian Obinger. 2012. "Molecular Evolution, Structure, and Function of Peroxidasins." *Chemistry & Biodiversity* 9 (9): 1776. https://doi.org/10.1002/CBDV.201100438.

Stringer, Bradley, and Lester Kobzik. 2010. "Environmental Particulate-Mediated Cytokine Production in Lung Epithelial Cells (A549): Role Of Preexisting Inflammation and Oxidant Stress." *Http://Dx.Doi.Org/10.1080/009841098158601* 55 (1): 31–44. https://doi.org/10.1080/009841098158601.

Swift, Joseph, and Gloria M. Coruzzi. 2016. "A Matter of Time - How Transient Transcription Factor Interactions Create Dynamic Gene Regulatory Networks." *Biochimica et Biophysica Acta* 1860 (1): 75. https://doi.org/10.1016/J.BBAGRM.2016.08.007.

Tamanini, Anna, Rossella Rolfini, Elena Nicolis, Paola Melotti, and Giulio Cabrini. 2003. "MAP Kinases and NF-KB Collaborate to Induce ICAM-1 Gene Expression in the Early Phase of Adenovirus Infection." *Virology* 307 (2): 228–42. https://doi.org/10.1016/S0042-6822(02)00078-8.

Tang, Yixin, Qian Xu, Haiyang Peng, Zhaoya Liu, Tianlun Yang, Zaixin Yu, Guangjie Cheng, Xiaohui Li, Guogang Zhang, and Ruizheng Shi. 2015. "The Role of Vascular Peroxidase 1 in Ox-LDL-Induced Vascular Smooth Muscle Cell Calcification." *Atherosclerosis* 243 (2): 357–63. https://doi.org/10.1016/J.ATHEROSCLEROSIS.2015.08.047.

Vatansever, Hafize Seda, and Eda Becer. 2020. "Relationship between IL-6 and COVID-19: To Be Considered during Treatment." *Https://Doi.Org/10.2217/Fvl-2020-0168* 15 (12): 817–22. https://doi.org/10.2217/FVL-2020-0168.

Verma, Shrikant, Sushma Verma, Sheeba Afreen, Zeba Siddiqi, Faizan Haider Khan, Mohammad Abbas, and Farzana Mahdi. 2024. "Impact of Interleukin-1 Gene Polymorphisms on the Severity of COVID-19." *Human Gene* 41 (September): 201303. https://doi.org/10.1016/J.HUMGEN.2024.201303.

Visan, Ioana. 2015. “About STATs.” *Nature Immunology 2015 16:7* 16 (7): 688–688. https://doi.org/10.1038/ni.3220.

Wang, Weiyuan, Melanie Cristina Lopez McDonald, Christine Kim, Mirielle Ma, Zetao Pan, Charlotte Kaufmann, and David A. Frank. 2023. “The Complementary Roles of STAT3 and STAT1 in Cancer Biology: Insights into Tumor Pathogenesis and Therapeutic Strategies.” *Frontiers in Immunology* 14 (November): 1265818. https://doi.org/10.3389/FIMMU.2023.1265818/BIBTEX.

Wei, Zheng, Wenjing Jiang, Hengzhen Wang, Hali Li, Bo Tang, Bing Liu, Hongchi Jiang, and Xueying Sun. 2018. “The IL-6/STAT3 Pathway Regulates Adhesion Molecules and Cytoskeleton of Endothelial Cells in Thromboangiitis Obliterans.” *Cellular Signalling* 44 (April): 118–26. https://doi.org/10.1016/J.CELLSIG.2018.01.015.

Wit, Emmie De, Neeltje Van Doremalen, Darryl Falzarano, and Vincent J. Munster. 2016. “SARS and MERS: Recent Insights into Emerging Coronaviruses.” *Nature Reviews Microbiology 2016 14:8* 14 (8): 523–34. https://doi.org/10.1038/nrmicro.2016.81.

Wyllie, Kaitlin, Vasilios Panagopoulos, and Thomas R. Cox. 2023. “The Role of Peroxidasin in Solid Cancer Progression.” *Biochemical Society Transactions* 51 (5): 1881. https://doi.org/10.1042/BST20230018.

Xue, Jiaping, Prabhakar B. Thippegowda, Guochang Hu, Kurt Bachmaier, John W. Christman, Asrar B. Malik, and Chinnaswamy Tiruppathi. 2009. “NF-KB Regulates Thrombin-Induced ICAM-1 Gene Expression in Cooperation with NFAT by Binding to the Intronic NF-KB Site in the ICAM-1 Gene.” *Physiological Genomics* 38 (1): 42. https://doi.org/10.1152/PHYSIOLGENOMICS.00012.2009.

Yang, Xiao Ping, Kaikobad Irani, Subhendra Mattagajasingh, Anthony Dipaula, Firdous Khanday, Michitaka Ozaki, Karen Fox-Talbot, William M. Baldwin, and Lewis C. Becker. 2005. “Signal Transducer and Activator of Transcription 3α and Specificity Protein 1 Interact to Upregulate Intercellular Adhesion Molecule-1 in Ischemic-Reperfused Myocardium and Vascular Endothelium.” *Arteriosclerosis, Thrombosis, and Vascular Biology* 25 (7): 1395–1400. https://doi.org/10.1161/01.ATV.0000168428.96177.24/SUPPL_FILE/ATVB6902_METHODS.PDF.

Yang, Youfeng, Zehong Cao, Ling Tian, W. Timothy Garvey, and Guangjie Cheng. 2013. “VPO1 Mediates ApoE Oxidation and Impairs the Clearance of Plasma Lipids.” *PLOS ONE* 8 (2): e57571. https://doi.org/10.1371/JOURNAL.PONE.0057571.

Ye, Jian, George Coulouris, Irena Zaretskaya, Ioana Cutcutache, Steve Rozen, and Thomas L. Madden. 2012. “Primer-BLAST: A Tool to Design Target-Specific Primers for Polymerase Chain Reaction.” *BMC Bioinformatics* 13: 134. https://doi.org/10.1186/1471-2105-13-134.

Yeh, Chia Chou, Shang Jyh Kao, Chih Che Lin, Shulhn Der Wang, Ching Ju Liu, and Shung Te Kao. 2007. “The Immunomodulation of Endotoxin-Induced Acute Lung Injury by Hesperidin in Vivo and in Vitro.” *Life Sciences* 80 (20): 1821–31. https://doi.org/10.1016/J.LFS.2007.01.052.

You, Baiyang, Yanbo Liu, Jia Chen, Xiao Huang, Huihui Peng, Zhaoya Liu, Yixin Tang, et al. 2018. “Vascular Peroxidase 1 Mediates Hypoxia-Induced Pulmonary Artery Smooth Muscle Cell Proliferation, Apoptosis Resistance and Migration.” *Cardiovascular*

Research 114 (1): 188–99. https://doi.org/10.1093/CVR/CVX234.

Yu, Hui, Liangbin Lin, Zhiqiang Zhang, Huiyuan Zhang, and Hongbo Hu. 2020. "Targeting NF-KB Pathway for the Therapy of Diseases: Mechanism and Clinical Study." *Signal Transduction and Targeted Therapy 2020 5:1* 5 (1): 1–23. https://doi.org/10.1038/s41392-020-00312-6.

Yuki, Koichi, Miho Fujiogi, and Sophia Koutsogiannaki. 2020. "COVID-19 Pathophysiology: A Review." *Clinical Immunology* 215 (June): 108427. https://doi.org/10.1016/J.CLIM.2020.108427.

Zanza, Christian, Tatsiana Romenskaya, Alice Chiara Manetti, Francesco Franceschi, Raffaele La Russa, Giuseppe Bertozzi, Aniello Maiese, Gabriele Savioli, Gianpietro Volonnino, and Yaroslava Longhitano. 2022. "Cytokine Storm in COVID-19: Immunopathogenesis and Therapy." *Medicina* 58 (2): 144. https://doi.org/10.3390/MEDICINA58020144.

Zanza, Christian, Tatsiana Romenskaya, Alice Chiara Manetti, Francesco Franceschi, Raffaele La Russa, Giuseppe Bertozzi, Aniello Maiese, Gabriele Savioli, Gianpietro Volonnino, and Yaroslava Longhitano. 2022. "Cytokine Storm in COVID-19: Immunopathogenesis and Therapy." *Medicina* 58 (2): 144. https://doi.org/10.3390/MEDICINA58020144.

Zhang, Jun Ming, and Jianxiong An. 2007. "Cytokines, Inflammation and Pain." *International Anesthesiology Clinics* 45 (2): 27. https://doi.org/10.1097/AIA.0B013E318034194E.

Zhang, Yi Shuai, Lan He, Bin Liu, Nian Sheng Li, Xiu Ju Luo, Chang Ping Hu, Qi Lin Ma, Guo Gang Zhang, Yuan Jian Li, and Jun Peng. 2012. "A Novel Pathway of NADPH Oxidase/Vascular Peroxidase 1 in Mediating Oxidative Injury Following Ischemia-Reperfusion." *Basic Research in Cardiology* 107 (3): 1–19. https://doi.org/10.1007/S00395-012-0266-4/METRICS.

Zhang, Yi Shuai, Lan He, Bin Liu, Nian Sheng Li, Xiu Ju Luo, Chang Ping Hu, Qi Lin Ma, Guo Gang Zhang, Yuan Jian Li, and Jun Peng. 2012. "A Novel Pathway of NADPH Oxidase/Vascular Peroxidase 1 in Mediating Oxidative Injury Following Ischemia-Reperfusion." *Basic Research in Cardiology* 107 (3): 1–19. https://doi.org/10.1007/S00395-012-0266-4/METRICS.

Zheng, Ying Ze, and Lei Liang. 2018. "High Expression of PXDN Is Associated with Poor Prognosis and Promotes Proliferation, Invasion as Well as Migration in Ovarian Cancer." *Annals of Diagnostic Pathology* 34 (June): 161–65. https://doi.org/10.1016/j.anndiagpath.2018.03.002.

Zhong, Jian, and John M. Kyriakis. 2007. "Dissection of a Signaling Pathway by Which Pathogen-Associated Molecular Patterns Recruit the JNK and P38 MAPKs and Trigger Cytokine Release *." *Journal of Biological Chemistry* 282 (33): 24246–54. https://doi.org/10.1074/JBC.M703422200.

Zhou, Qiaoqiao, Lei Zhang, Yanming Dong, Yuan Wang, Bin Zhang, Shiyi Zhou, Qing Huang, Tian Wu, and Gongxuan Chen. 2023. "The Role of SARS-CoV-2-Mediated NF-KB Activation in COVID-19 Patients." *Hypertension Research 2023 47:2* 47 (2): 375–84. https://doi.org/10.1038/s41440-023-01460-2.

Zhou, Yong, Jeffrey C. Horowitz, Alexandra Naba, Namasivayam Ambalavanan, Kamran

Atabai, Jenna Balestrini, Peter B. Bitterman, et al. 2018. “Extracellular Matrix in Lung Development, Homeostasis and Disease.” *Matrix Biology : Journal of the International Society for Matrix Biology* 73 (November): 77. https://doi.org/10.1016/J.MATBIO.2018.03.005.

Zhu, Na, Dingyu Zhang, Wenling Wang, Xingwang Li, Bo Yang, Jingdong Song, Xiang Zhao, et al. 2020. “Brief Report: A Novel Coronavirus from Patients with Pneumonia in China, 2019.” *The New England Journal of Medicine* 382 (8): 727. https://doi.org/10.1056/NEJMOA2001017.

Appendices

Appendix A

A

ANOVA Table

Source	SS	df	MS	F	Prob>F
Groups	0.01448	5	0.0029	0.55	0.7339
Error	0.06288	12	0.00524		
Total	0.07736	17			

B

ANOVA Table

Source	SS	df	MS	F	Prob>F
Groups	0.01	5	0.002	1.38	0.2991
Error	0.01741	12	0.00145		
Total	0.02741	17			

C

ANOVA Table

Source	SS	df	MS	F	Prob>F
Groups	0.03115	5	0.00623	2.4	0.0998
Error	0.03119	12	0.0026		
Total	0.06234	17			

D

ANOVA Table

Source	SS	df	MS	F	Prob>F
Groups	0.02256	5	0.00451	1.09	0.4132
Error	0.04957	12	0.00413		
Total	0.07213	17			

Figure A: Results of ANOVA analysis of MTT assay. *No significant change between groups* for *(A) treatment with TNF-α, (B) treatment with IL-1β, (C) treatment with IFN-γ and (D) treatment with IL-6.*

Appendix B

CAACTGGAGTGTGAACTGCACCCACTTGAGTGAGAGGTTGGGATGCTGCAGGTGGATGGCATTTGGAG
TGTGAACTGGACCCACTTGAGTGTATGGGTAGGGTCCTGCAGGAGAGATGGCAACTGGAGTGTGAACT
GGACCCACTGTTGTGCCTGGAGAGGATCCTGCAGAAGACAAGGCATCTGCAGTGTAAACTGGGCCACT
GGGGTGTGTAGCTAGAATCATGCTGGAGTAACGGCTTCTGGACTGTGAGCTGGCCCCATTAAAGTGTG
TGTATAGGATCCTGCAAAAGTGATAGCCTCTGGAGTGTGAATGGGACCCACTGAGGTGTGTGGATAGG
ATACTGCAGGGGTGATGGTGTCTGCAGTGTGAGCTGCAGCCCTGGGGCATGTGGATAGGACTCTGCAA
AGAGACAGCATCTGTGGTGTGAATGGCACCGGTGGAATGTGTAGAGAGGATCCTGCAAAAGTGATGT
CCTCTAGAGTGTGAACTGGACCCACTGGAGGGTGTGGACATCGTCCTGCAGGAGAGATGGCATCTAGA
GTGTGAATGGCACCTCCGGAGTGTGTGGATAGGAGCCCGCAGGAGAGAGCACATGTAGAGCGTGAAC
TGGACCCACTGAAATGTGTGGACAGGATTCTGCAGAAGATACGGCATCCGGAGTGTGAAATGCACC
ACTAGTGTGTGTGCATAGAATCCTGCATAAGTTTTGGCATCTACAGTGTGAACTGGAGTCACTGGAAT
GTGTGAATAGGATCTTGCAGGAGAGATGTCTGCAGTGTGAGCTGGACCCACTTCTGTGTGTGGATAGT
ATCCTGCAGGAGAGATGTTGTCTGCAGTGTGAGCTGGGCCCACCGGAGTGTGTGAATAGGATCCTGCA
GGAGAAATGGAATCCGGAGTGTGAGGTGCATCCGCTGTAGAGGGTGGATAAAATCCTGCAGGAAAG
ATGGCATCTGGAATGTCAGCGGGAGCCACCGACCTCTGAGGATGCACCCCGCAGGTGTGATGCGGGG
CCAGTTCCAAGGCTGGGTTAGGTTTTACCCTGGCTTCTGTGTTGTACTCTCATTCTCTTCCTCTTTCTTCT
AATACCTGCTCTGGGAGGCATCAGGCCATGTCCAGTGTGCAGGCCATGGAGACCCACACGGCAAGGA
ACTGGAACCCCCTGCCAGCAGCCTCGGGGGTCCAGTCCTTAGATGGTGCCCTGTGGTCAGCAATGCAC
CTGTGACCTCCGGGCTATGTCTCGTGGTAGTTGCTTTTGTGTTTTAACATAGCAACAGGAAACTAGCCT
ATTACCCACCAATCCCATTCCAGGCTGCTTTCAAACGCAGCTCAGGCTAGAACACCAGCACGGGGACA
CAGCTGAGACTTGGGGTTTGCGACGGGAACACGCCCATGCTGTGCCTCTGAATCTGGCACCGTCACCC
TGTGGCCTGGGTTCAGCAACTTGGCCTCACCTTCCTTGTCTGTGAAATTCAGACTGGGTCCTTGTGAGA
TGATTGGAGAGAATGTATGAACTATGTGAGAACGCCACCTTTGTGCGTATCTCACGCAGTGTCTTCCCT
CCTTTCCAAAGTCTTCTGCTGTCTCTAGACACACCCGACGTGGGGGGGGGGGGGTTCCCTGGGTCTCCTC
CTAGGTCTGTCCCAGGAGGGCACGCACTGAAGGCCGCGAGAATCCCGGGGGCTGCATTGCGCCGCGC
CAAGGACTCCACACAGGACCTTTCATTTTCCCAACTGTGCTGAGCCAGGCGGCCGGCAGAGAGCAGGT
GGCTGACAGGCCCCGGGGAGCCGGACCGCCTGGGTCTAATCTTCCCGCAGACTCCCTTGCTGTGCGCT
TTGGGGCTTGGGCCTCAGTTTCCTCAAAAGGAATGAGGGGCTTTTTTGGAACGTTAAATAATTTCCTAC
GTGGTTGCGGGTAGGGAGAAGGAGAAAGAGAGGAGCGCGCCTGCGCGCCTGGAATCGTGCCCGGATC
AGAGCAAGCGCTCTAAAAGTGTTACAAACATTAAGGCGCCAACTAAAAAACCCGTAGTGAGCGCAGG
CAGAAACCACGGGTAAGAGAAGTGGAGAAGCTTCGCGTAGGCCCCAGGGTCCCGAGCCCCGAGTCTC
GAGCGCAGAATCAGGGGTGCCAATGCTCTCCTCCGCGCCCCCGAGCGCTCGCCTTGGCCATGCGGGCC
GCCCCACCGGGATGAGGGCGCTCAGGCCGGACGCTGGGGCCCCGGGTTCTCGCCCCGCCCCGCCCTCG
GGGATTCAGAGGGGCCGGGAGGAGCCTCGCGCATGTGCACAGCTGGCGCCCCCCGCCCCCCGCGCACC
AGCTGGGACGTGGGCCGCGGCCGGGCGGGC**GCAGTCGGGAGCCGGCCGTGGTGGCTCCGTGCGTC**
CGAGCGTCCGTCCGCGCCGTCGGCCATGGCCAAGCGCTCCAGGGGCCCCGGGCGCCGCTGCCTGTT
GGCGCTCGTGCTGTTCTGCGCCTGGGGGACGCTGGCCGTGGTGGCCCAGAAGCCGGGCGCAGGGTGTC
CGAGCCGCTGCCTGTGCTTCCGCACCACCGTGCGCTGCATGCATCTGCTGCTGGAGGCCGTGCCCGCCG
TGGCGCCGCAGACCTCCATCCTgtgagtgccgcgggggacgccgggggcgcggggtccggggcttcgtggagatccgggagcgcagggggtg
atcggaggtgggggcgcggagggtggagggggcatcgggcgcgcgggggcctggggacttgggacgcagaagggaacctccgaaggggacgtggggg
gacctgggcgcggggacccgctgggcctttgttcgccctgcgggagacgccgaggggcggaacagagcgctgtgcgcgcggccttcgtagccgcctttgttcggaa
ctcggaatccccgcaggactgggaagttgttggagcctccggggctcccccgctcgcctcccgccgccccctctcatgctcc

Figure B-1: Full sequence of the *PXDN* promoter (5'-3') showing primer pairs and putative binding sites. *PXDN-A primer pairs (purple); PXDN-B primer pairs (brown); PXDN-C primer pairs (light blue); PXDN-D primer pairs (dark blue); PXDN-E primer pairs (dark green). STAT3 putative binding sites are marked in red text and NF-κB putative binding sites are marked with green text. Yellow highlighting indicated the putative binding sites with the highest binding affinities. The 5' UTR is in bold text, the first exon is in blue text and the first intron is in lowercase text.*

CTGAGCAGGGCCATGCCTTGCAGTTCTTAGTCCTGTACTGACAGTTGGTAATCAGTAGATTTTTTTTTC
ATTCAACATAAGTTTAGGTTTCTAAAGTGGAAAGTTTTTTGTATTTTTTTTTTCTGTAAAAAAAATGCTT
TATGGGCTGCGTGCGGTGGCTCACCCCTGTAATCCCAGCACTTTGGGAGGCCAGAGCGGGTAGATCA
CAAGGTCAGGAGATCGAGACCATCCTGGTCAACATGGTGAAACCCTGTCTCTACTAAAATACAAAAA
ATTAACCAGGTGTGGTGACAGGCACCTGTAATCCCAGCTACTCAGGAGGCTGAGGCAGGAGAATCGC
TTGAACCTGGAAGGCAGAGGTTGCAGTGAGCCAAGATTGCGCCATTGCACTCTAGCCTGGCAACAGA
GTGAGACTCCATCTCAAAAAAAAAAAAAAAAAAAGCTTTATGAATGCTAGATTTTTTTTTATAATTCG
AACTGAAAACAAGGCACAAAAACTTGCAGAATTTTTTTCCTTCGACCTAATTATTATACACCCTTAGC
TCAATGACTTTTAGAACCGCATGTCTTGCCTTTTTCTCCCTCCTGAACTTACATATTTCTGAGTCCCTAC
CCTTTTTAAGTCTACTTTATGAATGCAAGATATTTTTATATTTTTGTATTTTATATATTTTATATTATTT
ATATTTTTTGTATTTTATATTTTGAACTGCAAACAAGGCACAAACCTGCAGGTCTTGTCTATGTCCTCC
AAATCACAGGCACTGCCAAGAGCATAGTGATTGTTGGGATTTAAAGGAATAAATTTCGTTTTTTGGCT
TTATTGGTATACTTGGACAATAAAAGTCATGTGAACAATGTCAAATGTAAAGTTTAAAATAAATCATT
CTTGTTCATGGAGATTAGTTTTGTTTTTTAGATCTTTTTACATTTTAATCTCCCCAAAATCACATATTTA
GATATGAACATTTTGCCAAAAGAGGGCAGTATTCGCCTACAGTAGAATGTAAAGGGACTGAAACATT
TCTGCAGAGACAAGGATGAACTTATTTTCCTCTTAAGATTGGTCTACTAGTCTGATCATCTGGGATTG
ACCATGCAAGTTTTAATTTGTTTTCTATTACTTTTATGGATTTAAAACATTTTTGTTTGAAAATGTTAG
TCTTTAAAGATAAAGCCAAAAATCTGTTTAAAAATACCTGCTTACAGAATGACCAAAAAGTAGATGT
TTTCATATTTATTAAGTTTTTCAGACACGTCCTCAACGAGGTGCTGCTCACTTCAGGGAAAGATGGCCA
GTTCAAACTGCTGATGAAAAGTCTGCAACCAGCAAGACCACTGCTGCCAGTGTGTCCTGAGGGAGCT
TGCATCTGTTTGACTTTACATATACATACTTAGGTTTGTCCATCAGTTGTATCCTCTTGAAGGAGGTAT
GTGAGTTCATGGTTTTAAGCATATAAATTTAAACGTTAAAAGAAGAAATCAGAAGTAGCCCGTTTGA
GTCTTACATGAGTGAAATGTGTTGGGTTTCAGCAGCAGAATATATAGAAGGAAATGAAACAATTTTT
ATTAAAGAGCATAGTTTGGAATAAAGAAAGAATATGTGCACCTAGATGAACGAATTAGAACTCTGCC
TGCCCTTTAGGGTTTGGTAATGTTACCAGATAAAAAAGAAGAAAAGCTGTTCTGCATTGTTTCAATAC
ATTCTTAATCAACTTGGGCTTCAAGAGGACAGCTGGAGGCTAAGAGGTCGGGTTTTTCATCAAATGCG
CAGTGGAAGTAATTTTGGAAAAGTTTGTTTGCATTATGCTGCCTAAAACACGGTGTTTTAGAAAGAGG
CTTTTGCATTGAAAAGCTTCTCGTCCTCGCCTCTGGGAGTCTAGTGCTTCCTAGAGCTGCTTGTGCCCT
CAGCCCTGTAATGTGATATCCCTCCTCCTGGATTGGTCAGAGGGGTGTCCTTTCCCTGGGAGCTGCTTT
CCACCACGGCTCCCAAACTTGGCTC**AGTCCAGCAGCCACCATCACCACCACTGCGGTTGCTGCTG**
CAGCTGCAGCTGCTGCTCTCCCTCCGGCTGCTTCTTCGCGTGGCCAGCAGCGAATGGAGCGAT
GGAGCCCAGACTGTTCTGCTGGACCACTCTCTTTCTCCTGGCCGGGTGGTGCCTGCCAGGGTTGCCCT
GCCCCAGCCGGTGCCTTTGCTTTAAGAGCACCGTCCGCTGCATGCACTTGATGCTGGACCACATTCCT
CAGGTACCACAGCAGACCACAGTTCT

Figure B-2: Full sequence of the *PXDNL* promoter (5'-3') showing primer pairs and putative binding sites. *PXDNL-A primer pairs (light green); PXDNL-B primer pairs (light blue); PXDNL-C primer pairs (purple); PXDNL-D primer pairs (teal)). STAT3 putative binding sites are marked in red text and yellow highlighting indicated the putative binding sites with the highest binding affinities. The 5' UTR is in bold text and the first exon is in blue text.*

Appendix C

Figure C: Sequence alignment of peptides of the PXDNL isoform and canonical PXDNL. *Probable oxidoreductase PXDNL isoform X6 (XP_047277325.1) is conserved in the C-terminus of probable oxidoreductase PXDNL precursor (NP_653252.4)*

Table C: STAT1 putative binding sites in the *PXDNL* promoter region.

Predicted Sequence (5'-3')	Strand	Score	In which amplicon region
AGGAAATGAAACAA	Positive	14.407219	PXDNL-C
AGAAACCTAAACTT	Negative	12.316712	PXDNL-A
CTTCAGGGAAA	Positive	12.179675	PXDNL-C
AAAAAACAAAACTA	Negative	12.001695	PXDNL-B
TCTTTCCCTGAAGTG	Negative	11.619351	PXDNL-C
TTCAGGGAA	Positive	11.447477	PXDNL-C
AAAAAACGAAATTT	Negative	11.351869	PXDNL-A
GGGAAAGGACACCC	Negative	10.140842	PXDNL-D
CTCTAGGAA	Negative	9.411399	PXDNL-C
TTTAAAGGAAT	Positive	9.005268	PXDNL-B
GCTCTAGGAAG	Negative	8.888646	PXDNL-C
TTATTCCTTTAAATC	Negative	8.4397335	PXDNL-B
TTAAAGGAA	Positive	8.4105425	PXDNL-B
TTTACAGAAAA	Negative	8.1235485	PXDNL-A
CACTTCAGGGAAAGA	Positive	7.988001	PXDNL-C
TTTTTTCTGTAAAAA	Positive	7.496539	PXDNL-A
TTACAGAAA	Negative	6.1514516	PXDNL-A
TTAAAAGAA	Positive	4.121454	PXDNL-C
GTTAAAAGAAG	Positive	3.5987008	PXDNL-C
ATCTGGTAA	Negative	2.929893	PXDNL-C
TTTCTGTAAAA	Positive	2.9004097	PXDNL-A
TGCTGGGAT	Negative	2.333324	PXDNL-A
CTCCATGAA	Negative	1.9662061	PXDNL-B

Appendix D

Table D-1: Rel-A putative binding sites in the ICAM-1 NF-κB positive control region.

Predicted Sequence (5'-3')	Strand	Score
AGGAATTTCC	Negative	11.76209
TGGAAATTCC	Positive	11.220083
AGGATTTTCC	Positive	9.337831
GGGAAAATCC	Negative	8.623042
CTGAATTCCC	Negative	8.406022

Table D-2: STAT3 putative binding sites in the ICAM-1 STAT3 positive control region.

Predicted Sequence (5'-3')	Strand	Score
TTTATGGGAAG	Positive	11.750087
CTTCGGAGAAC	Negative	1.3740993

Table D-3: Putative binding sites in the ICAM-1 negative control region.

Transcription Factor	Predicted Sequence (5'-3')	Strand	Score
NF-κB	AGGGATTTCGA	Positive	5.3382735
STAT3	TCGCTGGGAAA	Negative	5.958692
STAT3	CGCTGGGAA	Negative	4.744717